2D MAGNETOTELLURIC MODELLING OF EARTH USING EXPONENTIAL FINITE DIFFERENCE METHOD

A DISSERTATION

Submitted in partial fulfillment of the requirements for the award of the degree of

MASTER OF TECHNOLOGY

in

GEOPHYSICAL TECHNOLOGY

By

PIYOOSH JAYSAVAL

DEPARTMENT OF EARTH SCIENCES
INDIAN INSTITUTE OF TECHNOLOGY ROORKEE
ROORKEE - 247 667 (INDIA)

JUNE, 2012

CANDIDATE'S DECLARATION

I hereby declare that the work which is being presented in this dissertation, entitled **'2D Magnetotelluric Modelling of Earth using Exponential Finite Difference Method'** in the partial fulfillment of the requirement for the award **Master of Technology** in **Geophysical Technology** submitted in **Department of Earth Sciences, Indian Institute of Technology, Roorkee**, carried out during a period of July 2011 to April 2012 under the supervision of **Dr. P. K. Gupta**, Professor, Department of the Earth Sciences, Indian Institute of Technology, Roorkee.

The matter embodied in this dissertation has not been submitted by me for the award of any other degree.

Dated: 15th June 2012
Place: IIT Roorkee

Piyoosh Jaysaval
Piyoosh Jaysaval

This is to certify that the above statement made by the candidate is correct to the best of my knowledge.

P.K. Gupta

Dr. P. K. Gupta
(Supervisor)
Professor of Geophysics
Department of Earth Sciences
Indian Institute of Technology
Roorkee-India

Dated: 12.6.12
Place: IIT Roorkee

ABSTRACT

This dissertation presents an efficient forward modelling algorithm MT_2D_EFDM based on Exponential Finite Difference Method (EFDM) for simulation of magnetotelluric response of 2D earth as a modification of Classical Finite Difference Method (CFDM). EFDM employs exponential basis functions whose exponent parameter μ must be chosen judiciously to obtain optimum results. The near optimal values of μ can be constructed using model parameters. Since the electromagnetic response has oscillatory behaviour, EFDM handles it better and gives more accurate results in comparison to the CFDM for a given grid. Alternatively, using EFDM we can choose coarser grids to obtain same accuracy of result as CFDM provides with a given finer grid. As a result EFDM reduces the time and cost of computation in comparison to CFDM.

LIST OF PUBLICATIONS

a) Journal

1. **Jaysaval, P.**, and Gupta, P. K., Khatri, V., 2D MT modelling using exponential finite difference method; *Journal of Earth System Science.* (communicated)

b) Conferences

1. **Jaysaval, P.**, and Gupta, P. K., 2012. Use of exponential finite difference method for simulation of EM response of layered Earth; 5th International Conference and Exhibitions, "Saint Petersburg 2012", Conference of European Association of Geoscientist and Engineers (EAGE), April, 02-05, 2012, Saint Petersburg-Russia, Expanded Abstracts. (Presented)

2. **Jaysaval, P.**, Ray, S., and Gupta, P. K., 2012. Exponential finite difference method for simulation of EM response of layered earth; 9th International Conference & Exposition on Petroleum Geophysics, "Hyderabad 2012", Biennial conference of Society of Petroleum Geophysicists (SPG), an affiliate society of SEG, Feb., 16-18, 2012, HICC Hyderabad, India, Expanded Abstract. (Presented)

3. **Jaysaval, P.**, Gupta, P. K., Khatri, V., Efficient computation of 2D MT Response using Exponential Finite Difference Method; 21st Electromagnetic Induction Workshop, July 25-31, 2012, Darwin, Australia, Extended Abstract. (Accepted)

4. **Jaysaval, P.**, Gupta, P. K., Khatri, V., Use of exponential finite difference method for efficient computation of 2D MT response; 82nd Annual Meeting Las Vegas 2012, Society of Exploration Geophysicist (SEG), Las Vegas-USA, Expanded Abstract. (communicated)

ACKNOWLEDGEMENTS

It is indeed a matter of great pleasure for me to submit this thesis on the topic '2D ***Magnetotelluric Modelling of Earth using Exponential Finite Difference Method'*** *as a part of my curriculum course ES-552 Dissertation, M. Tech. Geophysical Technology, Indian Institute of Technology Roorkee, Roorkee, India.*

First of all I would like to express my regards and heartily gratitude to my respectable and adorable father, ***Shri Rajendra Jaysaval*** *and mother,* ***Smt. B. D. Jaysaval,*** *for their endless motivation and unconditional love, encouragement and blessings which gave me necessary energy and happiness to work hard throughout this dissertation.*

I would like to thank my learned supervisor ***Prof. P. K. Gupta,*** *Professor, Department of Earth Sciences, IIT Roorkee, for introducing me the topic of this dissertation that allowed me to develop a sound concept and understanding in numerical modelling. I wish to express my deep sense of gratitude and appreciation to him for his stimulating supervision with invaluable suggestions, keen interest, constructive criticisms and constant encouragement during the period of this dissertation. I wholeheartedly acknowledge his full cooperation that I received from the very beginning of this work till the completion in the form of this thesis.*

I would also like to thank ***Prof. M. Israil,*** *Professor, Department of Earth Sciences, IIT Roorkee, for his invaluable help and advice from time to time as when needed.*

I express my heartily thanks to ***Prof. H. Sinvhal, Prof. M. Israil and Dr. Kamal,*** *Officers in-Charge Dissertation, Department of Earth Sciences, IIT-Roorkee, for providing all the academic and administrative support necessary for this dissertation.*

The enthusiastic help of my sisters, ***Simmi Jaiswal, Smrita Jaiswal*** *and* ***Priyanka Jaiswal,*** *who were distant to me but were always by their side whenever the need so arrived and accompany for me to work peacefully during the study period. I am in lack of proper words to express my abounding feelings and affection for my lovely Jiju* ***Ravi N. Mishra.*** *I deeply thank to* ***Akansha Khanna*** *for her love and excellent support during the course of dissertation.*

I sincerely acknowledge the contributions of ***Vishal Khatri****, Ph. D. Scholar, Department of Earth Sciences, for his help in programing to develop this forward modelling algorithm and* ***Sohom Ray****, CMPDI for his help to understand the topic during initial period of dissertation.*

I would also like thank to my batch-mates at IIT Roorkee, for their wonderful support and lovely moments which made this journey really pleasurable.

Finally thanks to the almighty god who has given me the spiritual support and courage to carry out this work.

Dated: 15th June 2012
Place: IIT-Roorkee

Piyoosh Jaysaval
(Piyoosh Jaysaval)

CONTENTS

LIST OF FIGURES

LIST OF TABLES

CHAPTER 1

INTRODUCTION

Forward modeling is an essential part in all geophysical problems. Using trial and error method, forward modeling itself can be used to find the solution for given field data. It is also prime requirements for inversion. The present work deals with the development of a new forward modeling algorithm for Magnetotelluric problems. Logical flow diagram of forward problem can be sketched as given below in Figure 1.1.

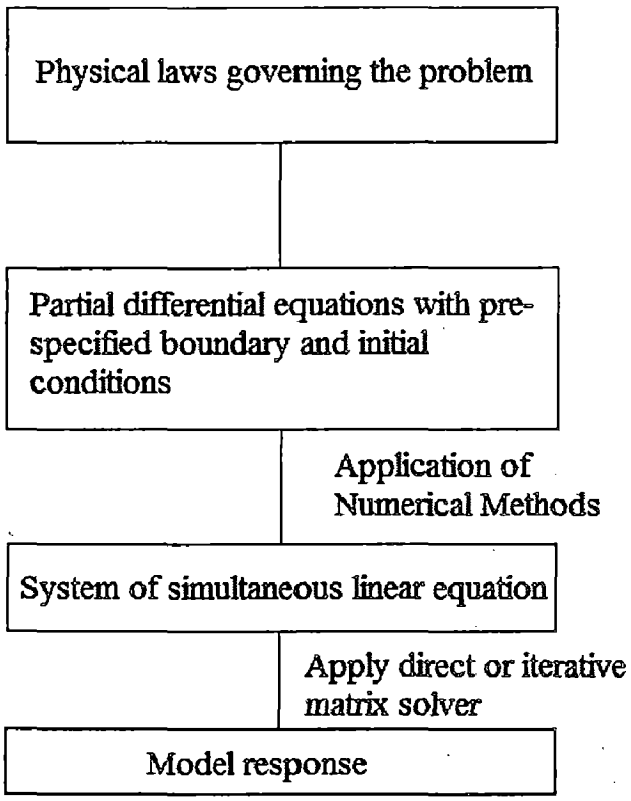

Figure 1.1: Logic diagram for numerical solution of forward problem.

As mentioned above, in geophysical forward problems generally we encounter partial differential equations (PDEs). For an inhomogeneous earth model (2D or 3D), numerical methods such as Finite Difference Method (FDM), Finite Element Method (FEM) or Integral Equation Method (IEM) (Wannamaker, 1991; Weaver, 1994; Gupta et al., 1999; Mitsuhata and Uchida, 2004) are applied to get solutions of these PDEs. In general, these numerical methods transform the governing differential equation into a matrix equation which is then solved. The quality of solution depends on the numerical methods employed for such a

transformation and efficiency of the method is judged by the factors like time of computation, accuracy of solution, memory of computer used. The first two factors are complementary. The numerical scheme that optimizes these factors is the best one to use.

In these mentioned numerical methods, Classical Finite Difference Method (CFDM) is one of the most widely used methods because it is easily implemented in comparison to FEM and IEM. The first CFDM-based 2D forward modelling program was developed by Jones and Pascoe (1971). Since then, several researchers have contributed to the refinement of the finite difference solution of 2D induction problems. But there are certain limitations of CFDM, implicitly it assumes that unknown field, to be solved for, does not have oscillating character within the cell and behaves as a low degree polynomial. However, when field has oscillating or hyperbolic behavior (as in the case of electromagnetic or seismic) then accuracy of the solution obtained using CFDM is not very good unless finely discretized grid is used so that within each cell field can be assumed as a low degree polynomial. Thus it leads to a large coefficient matrix and will take quite an amount of time to solve.

In this dissertation, we present a new algorithm MT_2D_EFDM using the Exponential Finite Difference Method (EFDM) based on the work of Ixaru (1997), Ixaru and Berghe (2004), Ray (2011), where the function is approximated by considering the exponential basis function like $\{1, \exp(\pm\mu x), x\exp(\pm\mu x), \ldots\}$ rather than monomials. EFDM can handle oscillating nature of field and we can discretize domain of interest with coarser grid to get same accuracy of result as with the CFDM in significantly less time and cost of computations.

EFDM requires the exponent parameter μ that need be chosen properly in accordance with the characteristics of field. Estimator of near optimum μ is constructed using model parameters so that it will result in small relative errors.

After presenting the results validating the EFDM algorithm, we present comparison of CFDM and EFDM results of different 2D earth models highlighting the efficiency of proposed method.

1.1 Plan of thesis

The thesis is composed of seven Chapters. The first four chapters are devoted to make the theory very clear and to develop understanding about the work. Fifth chapter deals with

development of algorithms. The later chapters deal with results and conclusions. The subsequent chapters are;

- Chapter 2 deals with basic theory of Magnetotelluric and its application in geophysics.

- Chapter 3 deals with CFDM where basic understanding about numerical solution of differential equations is developed. It also explains the limitations of CFDM that leads to the development of proposed EFDM.

- Chapter 4 deals with Exponential Finite Difference Method (EFDM) where theory of exponential fitting is given.

- Chapter 5 deals with development and details of algorithms MT_2D_CFDM and MT_2D_EFDM.

- Chapter 6 produces the application part of EFDM and results are obtained. First the algorithm is validated on different standard 2D earth models then experiments are performed on various standard 2D earth models to established efficiency of EFDM in comparison to CFDM.

- Chapter 7 presents the conclusions and scope of future work of this dissertation work.

- Appendix A.1 deals with the generation of input files for a given 2D earth model.

- Appendix A.2 deals with details of sample output files.

- Appendix A.3 deals with details of BiCG method of solving Matrix equations.

CHAPTER 2

THEORY OF MAGNETOTELLURIC

Electromagnetic methods are techniques of applied geophysics to obtain information about subsurface which are not directly accessible for probing. In particular, frequency domain EM measurements are commonly employed to explore the subsurface. The parameter of investigation is the distribution of electric conductivity in the earth.

Using conductivity, one can deduce information about the properties of the subsurface rock. Even though there is no non-ambiguous attribution of a conductivity value to a single earth materials, one can make advantage of the fact that the electric resistivity of different earth material varies over many order of magnitude. This was initially used in mineral exploration to locate very conductive ore bodies in their usually much more resistive host rock.

Electromagnetic methods can be used in two forms as Controlled source EM (CSEM) and natural source EM i.e. MT. In CSEM applications, an active source is used while in magnetotelluric method, naturally generated EM waves are used. MT is primarily used to delineate the crustal structure of the earth as in MT we can get information upto several hundreds of kilometres. EM method is used to map aquifers due to their contrast to the less conductive surroundings dry sand and rock, what significantly eases the search for drinking water in arid areas. In addition, the conductivity parameter allows distinguishing between fresh water and the more conductive saline water (Petrick, 2005; Rao, 2008). Now a days MT along with CSEM method is widely applied in marine environment for oil and gas explorations (Rao et al., 2003). MT method is also widely used in crustal studies like determination of depth of crust and different tectonic features (Adam, 1997; Wei et al., 2001; Pous et al., 2007; Tyagi, 2007; Israil et al., 2008). MT method is also applied for geothermal studies (Hoover et al., 1978; Pellerin et al., 1996; Harinarayana, 2002; Lee et al., 2007). Marin Magnetotellurics (MMT) is mainly used as a complement to MCSEM (Marine Controlled Source Electromagnetic) to provide the background resistivity of the sub-bottom sediments, that is, to constrain the inversions (resistivity vs. depth models) produced from MCSEM data. MCSEM has shown great potential in hydrocarbon exploration to detect thin resistive layers at depth below the sea floor (MacGreger and Sinha, 2000; Kong et al., 2002, Johansen et al., 2005; Weitemeyer, 2006; Fox and Ingerov, 2007).

The principle of electromagnetic measurement is based on Maxwell's equations. According to these, an EM source induces secondary currents in conductive materials, which themselves again generates secondary magnetic fields. The observed field observed as total field that can be viewed as a superposition of the primary and secondary fields. Primary fields are generated by an external source, while the secondary fields are generated by the induced secondary currents in the earth. If the Earth model is a uniform half space, then the induced currents and the resulting secondary fields follow a regular pattern. Inhomogeneities present in the real earth invariably disturb this regular pattern of secondary currents and of the secondary fields leading to perturbation of the total EM fields. These perturbed fields, measured on the earth surface, provide an insight into the resistivity distribution within the earth. This provides information about the structure of the earth and also helps in understanding the ongoing physical processes.

The mechanism of perturbed fields can be understood only when the capability of generating responses of arbitrary resistivity distributions is fully developed. The computation of EM response of a given earth model, with prescribed resistivities, is known as the forward problem of EM induction.

A comprehensive knowledge of EM theory, based on the fundamental Maxwell's equations, is essential for solving the forward problem. In literature there exists a vast pool of texts on EM theory differing in their emphasis on mathematical background, computational aspects and applications. One can refer to Smythe (1950), Morse and Feshbach (1953), Jackson (1975), Born and Wolf (2005, 7th edition) for fundamentals, to Mitra (1973, 1975), Morgan (1990), Zhou (1993) and Taflove (1995) for computational aspects and to Grant and West (1965), Rikitake (1966), Ward (1967), Porstendorfer (1975), Wait (1982), Kaufman and Keller (1981), Berdichevsky and Zhdanov (1984), and Nabighian (1988, 1991, 2000) for geophysical applications. A brief description of EM theory is presented here.

2.1 Electromagnetic waves in earth

In simple words the electrical properties of subsurface can be studied by introducing electromagnetic waves inside the earth by some source configuration. The problem deals in this dissertation work assumes source to be plane wave generator, which is usually the case in magnetotelluric where source is natural and very far from earth surface. Meteorological

activities and interaction of solar wind with earth's outer atmosphere serve as sources of primary èlectromagnetic field.

The EM phenomenon is governed by Gauss law for electrostatics, Gauss law for magnetostatics (i.e. non-existence of monopoles), Faraday's law of induction and Ampere's law for magnetic induction. Maxwell's equations are the mathematical forms of these laws and are given below for a source free case,

a) $\nabla . \mathbf{d} = q_f ,$ (2.1)

b) $\nabla . \mathbf{b} = 0 ,$ (2.2)

c) $\nabla \times \mathbf{e} = -\frac{\partial \mathbf{b}}{\partial t},$ (2.3)

d) $\nabla \times \mathbf{b} = \mu \mathbf{j} + \mu \frac{\partial \mathbf{d}}{\partial t}.$ (2.4)

Here, $\mathbf{d}$ is dielectric displacement vector in coulomb/meter^2 (C/m^2), $\mathbf{b}$ is magnetic induction vector in tesla (T), $\mathbf{e}$ is the electric field intensity vector in volt/meter (V/m) and $\mathbf{j}$ is the electric current density vector in ampere/meter^2 (A/m^2). q_f is the free electric charge density in Coulomb/meter^3 (C/m^3) and μ is the magnetic permeability in henry/meter (H/m).

If time dependence is $exp(-\omega t)$ then the corresponding frequency domain Maxwell's equations are,

i. $\nabla . \mathbf{D} = q_f ,$ (2.5)

ii. $\nabla . \mathbf{B} = 0 ,$ (2.6)

iii. $\nabla \times \mathbf{E} = i\omega \mathbf{B} ,$ (2.7)

iv. $\nabla \times \mathbf{B} = \mu \mathbf{J} - i\mu\omega \mathbf{D}.$ (2.8)

Equations 2.1 and 2.4 lead to the equation of continuity,

$$\nabla . \mathbf{J} + \frac{\partial q_f}{\partial t} = 0. \quad (2.9)$$

Equations 2.7 and 2.8 involve five vectors, making it an underdetermined system. To make the system of vector equations deterministic, the following constitutive relations are employed,

$$\mathbf{J} = \sigma \mathbf{E}, \quad (2.10)$$

$$\mathbf{D} = \varepsilon \mathbf{E}, \quad (2.11)$$

and

$$\mathbf{H} = \frac{1}{\mu}\mathbf{B}. \tag{2.12}$$

Here, σ is the electrical conductivity in Siemens/meter (S/m) and ε is the medium dielectric permittivity in Farad/meter (F/m). **H** is the magnetic field intensity vector in ampere/meter (A/m). Equation 2.10 may be recognized as Ohm's law. The μ and ε can be respectively expressed as,

$$\mu = \mu_r \mu_0 \text{ and } \varepsilon = \varepsilon_r \varepsilon_0 .$$

Here μ_r is the relative permeability and ε_r is relative electrical permittivity. Since the primary physical property of interest in magnetotelluric is conductivity σ, the magnetic permeability and dielectric permittivity of the medium are assumed to be equal to corresponding free space values μ_0 and ε_0 as;

$$\mu_0 = 4\pi \times 10^{-7} \text{ H/m},$$

and

$$\varepsilon_0 = \frac{10^{-9}}{36\mu} \text{ F/m}.$$

In above Equation 2.8 the first term is conduction current (σE) and the second term is displacement current ($-i\varepsilon_0\omega$E) which plays a fundamental role in propagation of electromagnetic field. The ratio between the two terms in case of magnetotelluric is very small. So, displacement current term can be drooped in comparison to conduction current. This can be shown as follows:

$$\frac{\varepsilon_0\omega}{\sigma} = \frac{2\pi\rho}{T}.\frac{1}{36\pi} \times 10^{-9} = \frac{\rho}{2T}.10^{-10},$$

where T is the time period of the signal used and ρ is the resistivity. The range of periods used in MT is from 0.001 to 1000 seconds. So, the first term in fourth Maxwell's equation (Equation 2.8) can be neglected which in turn means that in magnetotelluric sounding, k^2 is purely imaginary which immediately implies that magnetotelluric deals with purely diffusion phenomenon. (Nabighian, 2000)

Now if we take curl of equation fourth Maxwell's equation in time domain and substituting Equations 2.2, diffusive wave equation is obtained as shown below

$$\nabla \times \nabla \times \mathbf{b} = \mu_0 \nabla \times \mathbf{j} + \mu_0 \varepsilon_0 \nabla \times \frac{\partial \mathbf{e}}{\partial t},$$

$$\nabla(\nabla . \mathbf{b}) - \nabla^2 \mathbf{b} = \mu_0 \nabla \times (\sigma \mathbf{e}) + \mu_0 \varepsilon_0 \frac{\partial(\nabla \times \mathbf{e})}{\partial t},$$

$$\nabla^2 \mathbf{b} = \mu_0 \sigma \frac{\partial(\mathbf{b})}{\partial t} + \mu_0 \varepsilon_0 \frac{\partial^2(\mathbf{b})}{\partial t^2}. \tag{2.13}$$

Similarly,

$$\nabla^2 \mathbf{e} = \mu_0 \sigma \frac{\partial(\mathbf{e})}{\partial t} + \mu_0 \varepsilon_0 \frac{\partial^2(\mathbf{e})}{\partial t^2}. \tag{2.14}$$

If the conductivity of the medium is zero (medium is highly resistive) then Equations 2.13 and 2.14 reduce to pure wave equation, otherwise wave propagation is diffusive. Transforming above equations in frequency domain by taking Fourier transform following result is obtained:

$$\nabla^2 \mathbf{E} = \mu_0 \sigma (-i\omega)\mathbf{E} - \mu_0 \varepsilon_0 \omega^2 \mathbf{E},$$
$$\nabla^2 \mathbf{E} = -(\mu_0 \varepsilon_0 \omega^2 + i\omega \mu_0 \sigma)\mathbf{E},$$

$$\nabla^2 \mathbf{E} + k^2 \mathbf{E} = 0. \tag{2.15}$$

Similarly,

$$\nabla^2 \mathbf{B} + k^2 \mathbf{B} = 0. \tag{2.16}$$

Where,

$$k^2 = \mu_0 \varepsilon_0 \omega^2 + i\omega \mu_0 \sigma.$$

Equations 2.15 or 2.16 are known as Helmholtz equation. When k is purely real then it becomes wave equation, otherwise if imaginary part is too dominating then it behaves as diffusion equation. As mention above for magnetotelluric, k is pure imaginary and given by $k^2 = i\omega \mu_0 \sigma$.

2.1.1 Electromagnetic waves in layered earth

In this model for subsurface is assumed to be layered earth model where resistivity of different layers is different but within a particular layer resistivity does not vary. Medium is assumed to be linear, isotropic, homogeneous and electrical properties are independent of time, temperature or pressure. This is shown in Figure 2.1.

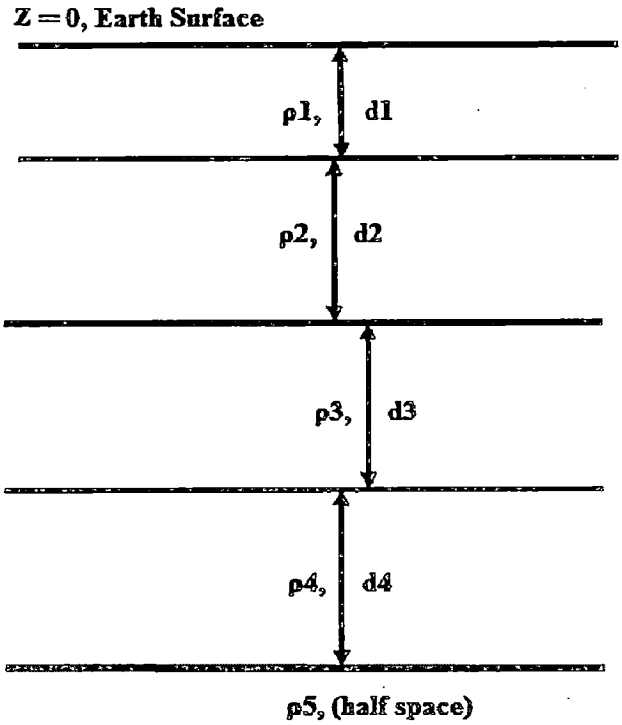

Figure 2.1: Layered earth model

The primary electromagnetic field is assumed to be varying only with depth axis (i.e. z- axis) and does not depend on horizontal coordinates (i.e. x and y axes). The primary electric and magnetic field are assumed to be oriented along x and y axes respectively as shown in Figure 2.2. The primary electric field causes current in the conducting medium which serves as the source of secondary EM field. Density of induced current does not change over horizontal plane so secondary field components do not vary along horizontal coordinates. So total field is: $E = (E_x, 0, 0)$ and $H = (0, H_y, 0)$. Another assumption is taken that fields are linearly polarised. This means that direction of electric and magnetic field does not change with time. In this dissertation it is assumed that depth is along z-axis and z=0 corresponds to earth's surface. Electric field is polarised along x-axis and magnetic field is polarised along y-axis.

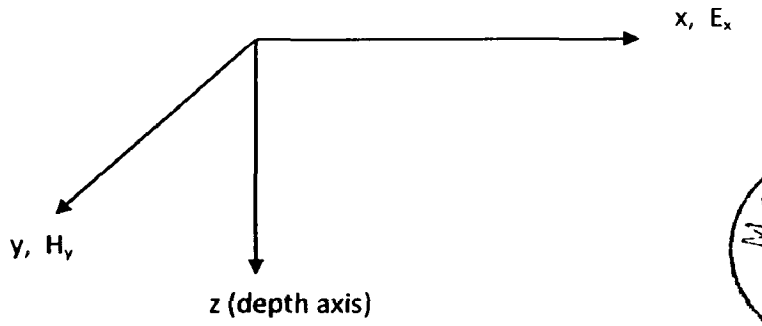

Figure 2.2 Coordinate axes orientation and direction of field

Therefore for layered Earth with field components (E_x, 0, 0) and (0, H_y, 0), Helmholtz Equation 2.15 becomes, (Kaufman and Keller, 1981)

$$\frac{d^2E_x}{dz^2} + k^2E_x = 0\,, \tag{2.17}$$

$$\frac{d^2H_y}{dz^2} + k^2H_y = 0\,, \tag{2.18}$$

where,

$$k^2 = i\mu\omega\sigma\,. \tag{2.19}$$

The above three Equations 2.17, 2.18 and 2.19 are written assuming uniform half space but in case of layered earth the above set of equations are valid for each layer. The solution for uniform half-space assumes following form

$$E_x(z) = Aexp(-ikz) + Bexp(ikz)\,. \tag{2.20}$$

Since for homogenous Earth, there is no boundary hence no field is propagate in upward direction therefore the coefficient A has to be zero. Applying boundary condition at $z = 0, E(z) = E_o$ coefficient B turns out to be E_o . So, the solution for half space is

$$E_{uniform}(z) = E_o \exp(ikz)\,. \tag{2.21}$$

When medium is layered as shown in Figure 2.1, then Equations 2.17 and 2.18 is obeyed by each layer, which has a solution as in Equation 2.20. For two layer earth model with interface at depth d_1 the solution looks like: (Kaufman and Keller, 1981)

$$E(z) = \begin{cases} A_1 exp(-ik_1 z) + B_1 exp(ik_1 z), & z < d_1 \\ A_2 exp(-ik_2 z), & z \geq d_1 \end{cases}, \quad (2.22)$$

$$where,\ A_1 = \frac{E_0 (k_1+k_2)}{(k_1+k_2)+(k_1-k_2)\exp(2ik_1 d_1)},$$

$$B_1 = \frac{(k_1-k_2)\exp(2ik_1 d_1)}{(k_1+k_2)} A_1 ,$$

$$A_2 = A_1 \exp(ik_1 d_1) + B_1 \exp(-ik_1 d_1).$$

Similarly we can solve Helmholtz equation for three layers but for more than three layers obtaining analytical solution is very difficult or not possible at all. In such situations numerical methods are applied to get a solution. Chapter 3 explains this in detail.

2.1.2 Attenuation of electromagnetic waves in subsurface

Electromagnetic waves get attenuated with depth in the subsurface due to finite resistivity of the earth materials. This can be easily seen from the uniform half space solution and complex nature of k. Assuming $k = k_r + ik_m$ and substituting in half space solution following result is obtained:

$$E(z) = E_o \exp(i(k_r + ik_m)z) ,$$

$$E(z) = E_o \exp(-k_m z).\exp(ik_r z). \quad (2.23)$$

The second factor in Equation 2.23 which depends on imaginary part of k is responsible for amplitude decay of EM waves inside the surface. The depth at which the amplitude becomes 1/e (nearly one third) times the maximum amplitude is called as skin depth (δ). The skin depth is an important parameter in electromagnetic wave propagation. It depends on the frequency of incident signal and on the medium resistivity. In magnetotelluric, $k = k_m = \sqrt{i\omega\mu\sigma}$. Skin depth is given by $\delta = \sqrt{\frac{2}{\omega\mu\sigma}}$. It is related with k as

$$k = \frac{1+i}{\delta} . \quad (2.24)$$

Also, skin depth can be expressed in terms of time period of signal and resistivity of the medium. Taking permeability equal to that of free space, skin depth comes out to be:

$$\delta = \sqrt{\frac{2}{\omega\mu\sigma}} \approx 503 \times \sqrt{\rho T}\,. \tag{2.25}$$

Equation 2.25 shows that with increasing period of oscillations (decreasing frequency), the depth of investigation increases. Also, signals decay faster when it encounters layer with low resistivity and goes almost unattenuated when skin depth is very high compared to depth of the layer. If Equation 2.20 is substituted in half space solution it can be seen that it is the ratio of thickness and skin depth of the layer which determines the fate of the signal. Following equation explains it:

$$E(z) = E_o\, exp\left(\frac{i(1+i)}{\delta} z\right) = E_o\, exp\left(-\frac{z}{\delta}\right) exp\left(\frac{iz}{\delta}\right). \tag{2.26}$$

2.1.3 Electromagnetic waves in 2D earth

This model of subsurface assumes that inhomogeneity presents in layered earth or half space as shown in Figure 2.3.

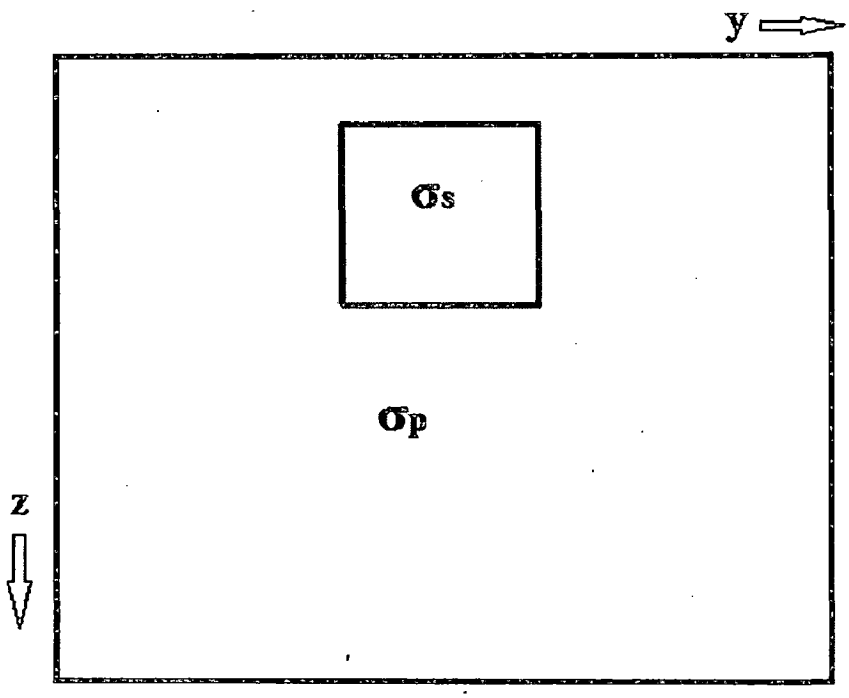

Figure 2.3: Anomalous conductive block in a half space

Consider Helmholtz Equation 2.15 for 2D Earth models,

$$\nabla^2 \mathbf{E} + \mathrm{k}^2 \mathbf{E} = \mathbf{0}. \tag{2.27}$$

Figure 2.3 shows 2D inhomogeneity present in the half space. σ_P and σ_S respectively are the conductivities of half space and anomalous region present in it. Thus, the total conductivity is defined as sum,

$$\sigma_T = \sigma_P + \sigma_S. \tag{2.28}$$

So in wave number domain one can define k_T^2 as

$$k_T^2 = k_P^2 + k_S^2, \tag{2.29}$$

where $k^2 = i\omega\mu_0\sigma$

similarly, total field $\boldsymbol{E_T} = \boldsymbol{E_P} + \boldsymbol{E_S}$. (2.30)

Substituting Equations 2.28, 2.29 and 2.30 into 2.27, we get

$$\nabla^2(\boldsymbol{E_P} + \boldsymbol{E_S}) + (k_P^2 + k_S^2)(\boldsymbol{E_P} + \boldsymbol{E_S}) = \mathbf{0},$$

$$\nabla^2 \boldsymbol{E_P} + \nabla^2 \boldsymbol{E_S} + k_P^2 \boldsymbol{E_P} + k_P^2 \boldsymbol{E_S} + k_S^2 \boldsymbol{E_P} + k_S^2 \boldsymbol{E_S} = \mathbf{0}. \tag{2.31}$$

Primary field $\boldsymbol{E_P}$ satisfies following equation

$$\nabla^2 \boldsymbol{E_P} + k_P^2 \boldsymbol{E_P} = \mathbf{0}. \tag{2.32}$$

Using Equation 2.31 and 2.32, we get

$$\nabla^2 \boldsymbol{E_S} + (k_P^2 + k_S^2)\boldsymbol{E_S} = -k_S^2 \boldsymbol{E_P},$$

$$\nabla^2 \boldsymbol{E_S} + k_T^2 \boldsymbol{E_S} = -k_S^2 \boldsymbol{E_P}. \tag{2.33}$$

Since host model is either layered earth model or half space thus E_P can be easily obtained from 1D formulation of Equation 2.32 i.e.,

$$\frac{d^2E_P}{dz^2} + k_P^2 E_P = 0 . \tag{2.34}$$

Having obtained E_P, secondary field E_S can be obtained using 2D Helmholtz Equation 2.33.

In this dissertation all fields E_P, E_S and E_T are obtained using both the method Classical Finite Difference Method as well as Exponential Finite Difference Method. The CFDM and EFDM used for obtaining these fields are discussed in subsequent chapters.

However, these field component values do not directly reflect the effect of changes in the subsurface resistivity in a perceptible manner. So, more representative response function, derived from these field values are discussed in the following sections.

2.2 MT Response Functions

Although the response functions derived from the fields values also do not present a direct functional relationship with the subsurface resistivity yet these reflect the bulk information about the resistivity distribution.

The appropriate choice of response function is governed by the objective of the study, whether lateral or vertical variation in resistivity is desired. The spatial variation can be studied in two modes, (i) profiling mode, for a given frequency, the observations are taken at points along a profile, and (ii) sounding mode, the observations are taken at a single point for different frequencies. Profiling delineates the lateral variations while sounding helps in deciphering the vertical variation of resistivity.

2.2.1 MT apparent resistivity and phase

The magnetotelluric method was first described by Tikhonov in 1950 and Cagniard in 1953 independently (Kaufman and Keller, 1981). Using the assumption of a plane wave source, the

ratio of observed horizontal electric field (E_x or E_y) and the orthogonal magnetic field component ($H_y or H_x$), is called the impedance;

$$Z = \frac{E_x}{H_y} = -\frac{E_y}{H_x}. \tag{2.35}$$

H-field can be easily computed from E-field using third Maxwell's equation (2.7) as;

$$\nabla \times E = i\omega\mu_0 H.$$

Since $E = (E_x, 0, 0)$ and $H = (0, H_y, 0)$ thus

$$H_y = \frac{1}{i\omega\mu_0}\frac{\partial E_x}{\partial z}. \tag{2.36}$$

Using Equation 2.36 we can compute H-field from calculated E-field. Once the E-fields and H-fields are obtained we can easily compute impedance from Equation 2.35 and other MT responses apparent resistivity and phase can be computed from impedance in following ways.

The impedance values are used to define the commonly used MT response function as apparent resistivity, which may be defined as the resistivity of equivalent fictitious half space. The apparent resistivity, ρ_a, and the impedance phase, $\emptyset$, are respectively given by the relation

$$\rho_a = \frac{1}{\mu\omega}|Z|^2, \tag{2.37}$$

and $$\emptyset = tan^{-1}\left[\frac{Im\,(Z)}{Re\,(Z)}\right], \tag{2.38}$$

where $-90^0 \leq \emptyset \leq 0^0$

For a homogeneous half space, phase will always be -45^0. For a conductive body in half space phase varies from -45^0 to -90^0, while for a resistive body it varies from 0^0 to -45^0.

The variation of resistivity in the earth is rarely one-dimensional, therefore above definition of apparent resistivity and phase has only limited utility. To describe higher dimensionality or anisotropy, we have a rank 2 impedance tensor $\mathbf{Z}$;

$$\begin{bmatrix} E_x \\ E_y \end{bmatrix} = \begin{bmatrix} Z_{xx} & Z_{xy} \\ Z_{yx} & Z_{yy} \end{bmatrix} \begin{bmatrix} H_x \\ H_y \end{bmatrix}, \tag{2.39}$$

where Z_{xy}, Z_{yx} are principal impedances and Z_{xx}, Z_{yy} are additional impedances. For a 1D Earth,

$$Z_{xy} = Z_{yx},$$
$$Z_{xx} = Z_{yy} = 0.$$

In case of 2D, we have TE and TM mode,

$$E_{TE} = (E_x, 0, 0), \ and \ H_{TE} = (0, H_y, H_z), \tag{2.40}$$

and

$$E_{TM} = (0, E_y, E_z), \ and \ H_{TE} = (H_x, 0, 0). \tag{2.41}$$

For Epol (2D TE), the impedance and apparent resistivity and phase are defined as

$$Z_{xy} = \frac{E_x}{H_y}, \qquad \rho_{xy} = \frac{1}{\mu_0 \omega}|Z_{xy}|^2, \quad \emptyset_{xy} = tan^{-1}\left[\frac{Im\,(Z_{xy})}{Re\,(Z_{xy})}\right], \tag{2.42}$$

Similarly for Hpol (2D TM)

$$Z_{yx} = -\frac{E_y}{H_x}, \qquad \rho_{yx} = \frac{1}{\mu_0 \omega}|Z_{yx}|^2, \quad \emptyset_{yx} = tan^{-1}\left[\frac{Im\,(Z_{yx})}{Re\,(Z_{yx})}\right] \tag{2.43}$$

and $Z_{xx} = Z_{yy} = 0$.

In this dissertation E-field, H-fields and apparent resistivities are computed for different 2D earth models using both CFDM and EFDM to observe the efficiency of proposed EFDM in comparison to CFDM.

CHAPTER 3

CLASSICAL FINITE DIFFERENCE METHOD (CFDM)

Classical Finite difference method (CFDM) is widely used methods to approximate the derivative of a function. CFDM is broadly used to solve partial differential equations by replacing derivatives by finite difference equations. In CFDM, the derivatives are approximated by finite difference and the partial differential equation is converted into a large algebraic system of equations (matrix equation) to be solved simultaneously in place of differential equation. For detailed description of CFDM, one can refer to standard texts like Forsythe and Wasow (1964), Hildebrand (1974), Mitchell and Griffiths (1980) and Taflove (1995).

3.1 FD Approximation of first order derivative

First order derivative of u(x) i.e. $u'(x)$ can be approximated using finite difference approximation. This can be done in following ways,

The Taylor's series expansion of $u(x)$ is given as,

$$u(x+h) = u(x) + hu'(x) + \frac{h^2}{2}u''(x) + \frac{h^3}{3!}u'''(x) + \ldots\ldots \quad (3.1)$$

$$u(x-h) = u(x) - hu'(x) + \frac{h^2}{2}u''(x) - \frac{h^3}{3!}u'''(x) + \ldots. \quad (3.2)$$

If we neglect higher order term then we can write,

$$u'(x)_f \approx \frac{u(x+h)-u(x)}{h}, \text{ (Forward difference)} \quad (3.3)$$

$$u'(x)_b \approx \frac{u(x)-u(x-h)}{h}, \text{ (Backward difference)} \quad (3.4)$$

$$u'(x)_c \approx \frac{u(x+h)-u(x-h)}{2h} = \frac{1}{2}\left(u'(x)_f + u'(x)_b\right). \text{ (Central difference)} \quad (3.5)$$

Forward difference and backward difference formulas are first order approximation of derivative of u. On the other hand, central difference formula of $u'(x)$ is second order approximation (Press et al., 1993).

Equation 3.3 is obtained by truncating Taylor series after first two terms and hence truncation error is of the order $O(h)$. Same argument holds for Equation 3.4. But central difference formula Equation 3.5 is obtained by subtracting Equations 3.1 and 3.2 and hence truncation error is of the order $O(h^2)$.

3.2 FD approximation of second order derivatives

If we add Equations 3.1 and 3.2 then we get finite difference approximation for double derivative of u(x);

$$u''(x) \approx \frac{u(x-h)-2u(x)+u(x+h)}{h^2}. \tag{3.6}$$

This result can be achieved in other way like taking forward difference of $u'(x)_b$ that is taking forward difference of backward difference formula of first derivative (Press et al., 1993). This is three point formula of second derivative. The truncation error is of the order of $o(h^2)$.

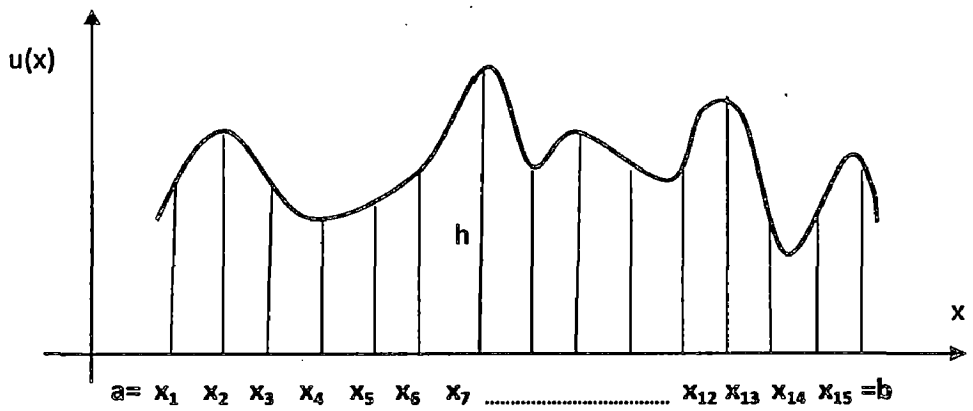

Figure 3.1 Grid discretization of interval h for an oscillating function.

The important assumption in evaluating derivative of a function using n-point finite difference formula is that the function to be differentiated should behave as a polynomial of degree at most (n-1), between n nodes. Therefore to get the derivative of a function at a point x by three point finite difference formula, it should behave as a quadratic function between (x - h), x and (x + h). Expressing in more appropriate terms: "to get derivative of a function at a point $x = x_o$, the interval size 'h' should be chosen in such a manner, that the function behaves as a second degree polynomial between (x_o - h), x_o and (x_o + h)". This shows that most crucial part in FDM is the choice of interval length 'h'. If the chosen interval size is too

coarse the result may not be faithful. Grid size should be selected in accordance with the nature of the function to be differentiated. If the function happens to be rapidly oscillating throughout the domain and second order derivative is to be taken, then grid size required to be small enough, so that the function behaves as a second degree polynomial between any three grids.

3.2.1 FD approximation of derivatives using non-uniform grid system

There are situation which demand finer grid alignment in certain part compared to grids in other parts of the domain. In such a case finite difference method is to be formulated for non-uniform grid spacing. Again from Taylor series expansion of u(x):

$$u(x_{i-1}) = u(x_i) + (x_{i-1} - x_i)u'(x_i) + \frac{(x_{i-1}-x_i)^2}{2}u''(x_i) + \frac{(x_{i-1}-x_i)^3}{3!}u'''(x_i) + \cdots,$$

$$u(x_{i-1}) = u(x_i) - (h_{i-1})u'(x_i) + \frac{(h_{i-1})^2}{2}u''(x_i) - \frac{(h_{i-1})^3}{3!}u'''(x_i) + \cdots, \quad (3.7)$$

$$u(x_{i+1}) = u(x_i) + (x_{i+1} - x_i)u'(x_i) + \frac{(x_{i+1}-x_i)^2}{2}u''(x_i) + \frac{(x_{i+1}-x_i)^3}{3!}u'''(x_i) + \ldots$$

$$u(x_{i+1}) = u(x_i) + (h_i)u'(x_i) + \frac{(h_i)^2}{2}u''(x_i) + \frac{(h_i)^3}{3!}u'''(x_i) + \ldots. \quad (3.8)$$

Using Equation 3.7 and 3.8;

$$\frac{u(x_{i-1})}{h_{i-1}} + \frac{u(x_{i+1})}{h_i} = \left(\frac{u(x_i)}{h_{i-1}} + \frac{u(x_i)}{h_i}\right) + \frac{(h_{i-1}+h_i)}{2}u''(x_i),$$

$$\frac{u(x_{i-1})}{h_{i-1}} - \left(\frac{1}{h_{i-1}} + \frac{1}{h_i}\right)u(x_i) + \frac{u(x_{i+1})}{h_i} = \frac{(h_{i-1}+h_i)}{2}u''(x_i),$$

$$h_i u(x_{i-1}) - (h_{i-1} + h_i)u(x_i) + h_{i-1}u(x_{i+1}) = \frac{h_i.h_{i-1}\,(h_{i-1}+h_i)}{2}u''(x_i).$$

Let $(h_{i-1} + h_i) = n_i$ which is length of the neighbourhood about point $x = x_i$. The double derivative $u''(x)$ becomes:

$$u''(x_i) = \frac{2}{h_{i-1}.h_i}\left[\frac{h_i}{n_i}u(x_{i-1}) - u(x_i) + \frac{h_{i-1}}{n_i}u(x_{i+1})\right], \quad (3.9)$$

$$u''(x_i) = \frac{1}{H_i^2}\left[\frac{h_i}{n_i}u(x_{i-1}) - u(x_i) + \frac{h_{i-1}}{n_i}u(x_{i+1})\right], \quad (3.10)$$

$where\ H_i^2 = \frac{1}{2}(h_{i-1} \times h_i)$

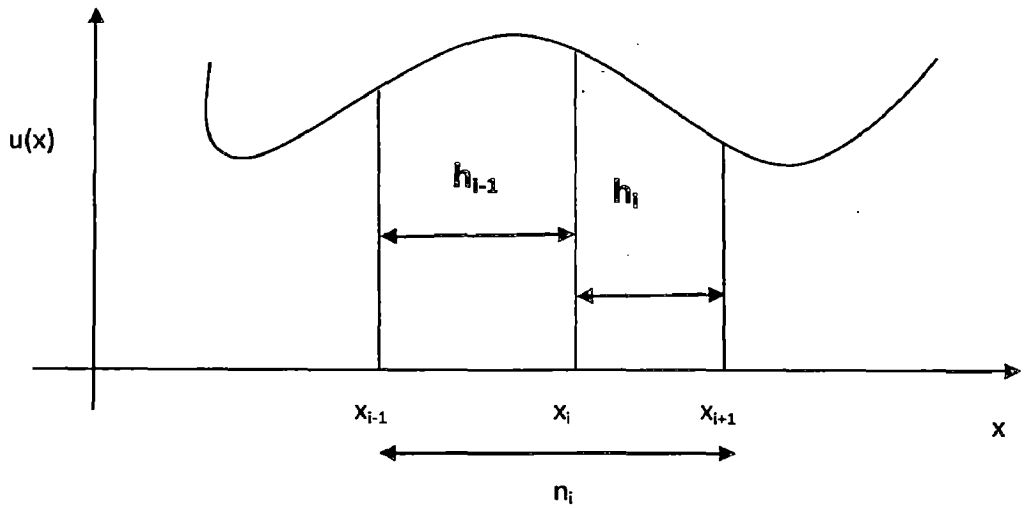

Figure 3.2 Non uniform grid around x_i with length of neighbourhood n_i.

The Equation 3.10 is used for classical finite difference approximation of second derivative with non-uniform discretization. This is substituted in Helmholtz equation to solve for fields as discussed in following section.

3.3 Solving partial differential equations (PDEs) using Classical Finite Difference Method (CFDM)

In this dissertation, both one dimensional Helmholtz equation as well as 2D Helmholtz equation needed to be solved using CFDM and EFDM. The details of CFDM are discussed below and, of EFDM are discussed in Chapter 4;

Referring to chapter 2, the primary field E_P can be obtained by solving 1D Helmholtz Equation 2.34;

$$\frac{d^2u_P(z)}{dz^2} + k^2u_P(z) = 0. \tag{3.11}$$

Having obtained E_P, secondary field E_S can be obtained using 2D Helmholtz Equation 2.33;

$$\nabla^2 u_S + k^2 u_S = -k_S^2 u_P, \tag{3.12}$$

The details of solving these differential equations using CFDM are as follows.

3.3.1 Solving 1D Helmholtz equation with CFDM using uniform grids for primary field

First the domain is discretized as shown in the Figure 3.3 such that $(z_{i+1} - z_i) = h$, is constant throughout.

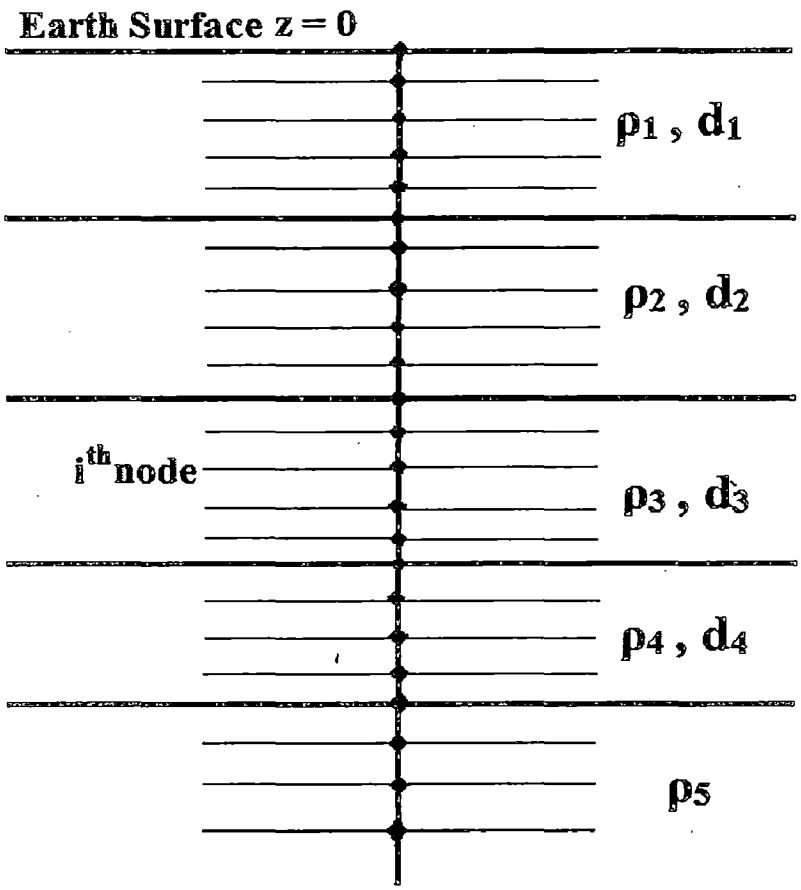

Figure 3.3: Layered earth model and grid generation. Thin lines show nodal line, thick lines show layer interfaces and points show the nodes.

The task is to obtain $u(z_i)$ for i=1,2, ... n. The boundary condition is $u_P(z_o) = u_o$ and $u_P(z_{n+1}) = u_{n+1}$. At i^{th} nodes Equation 3.11 can be written as:

$$\frac{1}{h^2}[u_P(z_i - h) - 2u_P(z_i) + u_P(z_i + h)] + k_i{}^2 u_P(z_i) = 0,$$

$$\frac{1}{h^2}[u_{P_{i-1}} - 2u_{P_i} + u_{P_{i+1}}] + k_i{}^2 u_{P_i} = 0,$$

$$u_{P_{i-1}} + (k_i{}^2 h^2 - 2)u_{P_i} + u_{P_{i+1}} = 0. \qquad (3.13)$$

Equation 3.13 is to be solved simultaneously for i=1 to nz which reduces to solving a matrix equation as shown in the below:

$$\begin{bmatrix} (k_1{}^2h^2-2) & 1 & 0 & 0 & 0 & 0 \dots\dots\dots\dots & 0 \\ 1 & (k_2{}^2h^2-2) & 1 & 0 & 0 & 0 \dots\dots\dots & 0 \\ 0 & 1 & (k_3{}^2h^2-2) & 1 & 0 & \dots\dots\dots & 0 \\ 0 & 0 & 1 & (k_4{}^2h^2-2) & 1 & 0 \dots\dots & 0 \\ & & & \vdots & & & \\ & & & \vdots & & & \\ & & & \vdots & & & \\ 0 & 0 & 0 & 0 \dots\dots\dots & 0 & 1 & (k_n{}^2h^2-2) \end{bmatrix} \begin{bmatrix} u_{P_1} \\ u_{P_2} \\ u_{P_3} \\ u_{P_4} \\ \vdots \\ \vdots \\ \vdots \\ u_{P_n} \end{bmatrix} = \begin{bmatrix} u_0 \\ 0 \\ 0 \\ 0 \\ \vdots \\ \vdots \\ \vdots \\ u_{n+1} \end{bmatrix} \tag{3.14}$$

$$\mathbf{M}.\boldsymbol{u_P} = \mathbf{b}, \tag{3.15}$$

where M is an *nz-by-nz* tridiagonal matrix. The point to be noted is that k_i is a medium property, and its value depends on the layer where i^{th} node is located if it is located on interface its value is taken as weighted average of k of surrounding layers. The matrix equation can be solved by LU decomposition method or any other matrix equation solver methods.

3.3.2 Solving 1D Helmholtz equation with CFDM using non-uniform grids for primary field

Figure 3.4 shows the layered earth model and its discretization with non-uniform grid. Helmholtz equation will be written at each point including at layer interfaces. Having the information about resistivity (ρ) and layer thickness grids are generated. Grid generation is an important task because it is the grid size which determines the quality of the solution. If grids are too fine then the size of matrix M (Equation 3.14 or 3.15) will be very large and hence will require more time to solve for field vector, though large M will give a very accurate solution vector. The Figure 3.4 shows a coarse grid system and size of matrix M will be very small. Positions of grids along x axis are determined by the skin depth of each layer. The grids are placed about an interface at a distance of one fourth of skin depth.

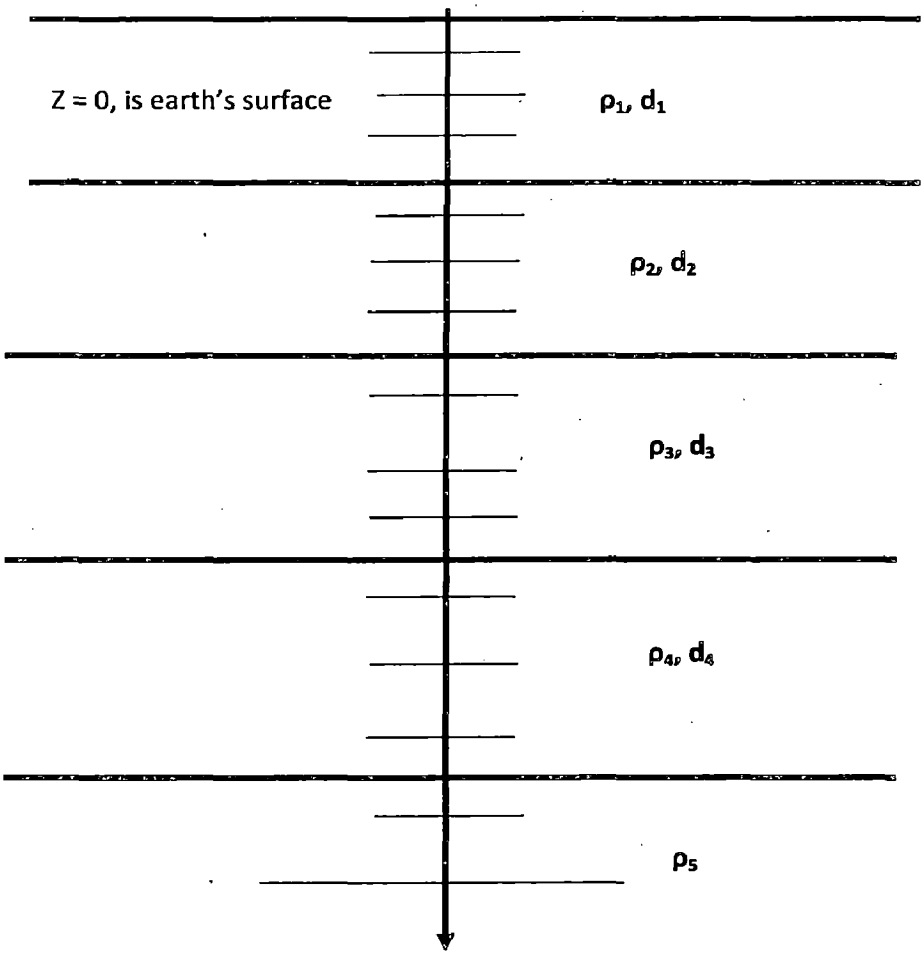

Figure 3.4: Layered earth model and non-uniform grid generation. Thin lines show grid points and thick lines are layer interfaces.

For i^{th} nodes Equation 3.11 with non-uniform grid can be written with the help of Equation 3.10 as follows;

$$\frac{1}{H_i^2}\left[\frac{h_{i+1}}{n_i}u_P(z_{i-1}) - u_P(z_i) + \frac{h_i}{n_i}u_P(z_{i+1})\right] + k_i^2 u_P(z_i) = 0\,,$$

$$\frac{h_{i+1}}{n_i}u_{P_{i-1}} + (k_i^2 H_i^2 - 1)^2 u_{P_i} + \frac{h_i}{n_i}u_{P_{i+1}} = 0\,, \qquad (3.16)$$

where $h_i = (z_{i+1} - z_i)$, $H_i^2 = \frac{1}{2}(h_{i+1}.h_i)$ and $n_i = (h_i + h_{i+1})$

In Equation 3.16 above i run from 1 to n. So, u_0 and u_{n+1} act as boundary conditions which are needed to be supplied to solve system of Equations 3.16 which is a matrix equation as follows;

$$\begin{bmatrix} (k_1^2H_1^2-1) & \frac{h_1}{n_1} & 0 & 0 & 0 & 0 \dots\dots\dots\dots\dots\dots\dots & 0 \\ \frac{h_3}{n_2} & (k_2^2H_2^2-1) & \frac{h_2}{n_2} & 0 & 0 & 0 \dots\dots\dots\dots\dots\dots & 0 \\ 0 & \frac{h_4}{n_3} & (k_3^2H_3^2-1) & \frac{h_3}{n_3} & 0 & 0 \dots\dots\dots\dots\dots & 0 \\ & & & \vdots & & & \\ 0 & 0 & 0 & \dots & \frac{h_{i+1}}{n_i} & (k_i^2H_i^2-1) \quad \frac{h_i}{n_i} \quad 0 \dots\dots & 0 \\ & & & & \vdots & & \\ 0 & 0 & 0 & \dots\dots & \frac{h_n}{n_{n-1}} & (k_{n-1}^2H_{n-1}^2-1) & \frac{h_{n-1}}{n_{n-1}} \\ 0 & 0 & 0 & 0 & 0 \dots\dots & \frac{h_{n+1}}{n_n} & (k_n^2H_n^2-1) \end{bmatrix} \begin{bmatrix} u_{P_1} \\ u_{P\ 2} \\ u_{P_3} \\ \vdots \\ u_{P_i} \\ \vdots \\ u_{P_{n-1}} \\ u_{P_n} \end{bmatrix} = \begin{bmatrix} \frac{h_2}{n_1}u_0 \\ 0 \\ 0 \\ \vdots \\ 0 \\ \vdots \\ 0 \\ \frac{h_n}{n_n}u_{n+1} \end{bmatrix} \tag{3.17}$$

$$\mathbf{M}.\boldsymbol{u_P} = \mathbf{b}\,, \tag{3.18}$$

M is an *nz*-by-*nz* matrix and has a tridiagonal structure. Size of matrix depends on the number of grids generated. The situation where analytical solution is not available or cumbersome to get one (e.g. over four layered earth model) then very fine grid structure is used, so that obtained field vector E is very close to analytical result.

3.3.3 Solving 2D Helmholtz equation with CFDM using non-uniform grids for secondary field

From Equation 3.12;

$$\nabla^2 u_S + k^2 u_S = -k_S^2 u_P\,,$$

$$\frac{\partial^2 u_S(y,z)}{\partial y^2} + \frac{\partial^2 u_S(y,z)}{\partial z^2} + k^2 u_S(y,z) = -k_S^2 u_P\,, \tag{3.19}$$

where $u_S(y,z)$ is secondary field value we seek to obtain.

The first step of solving 2D PDEs is discretization of domain of interest as shown in Figure 3.5. Then the field is computed at all nodes (shown in Figure 3.5 as solid black points).

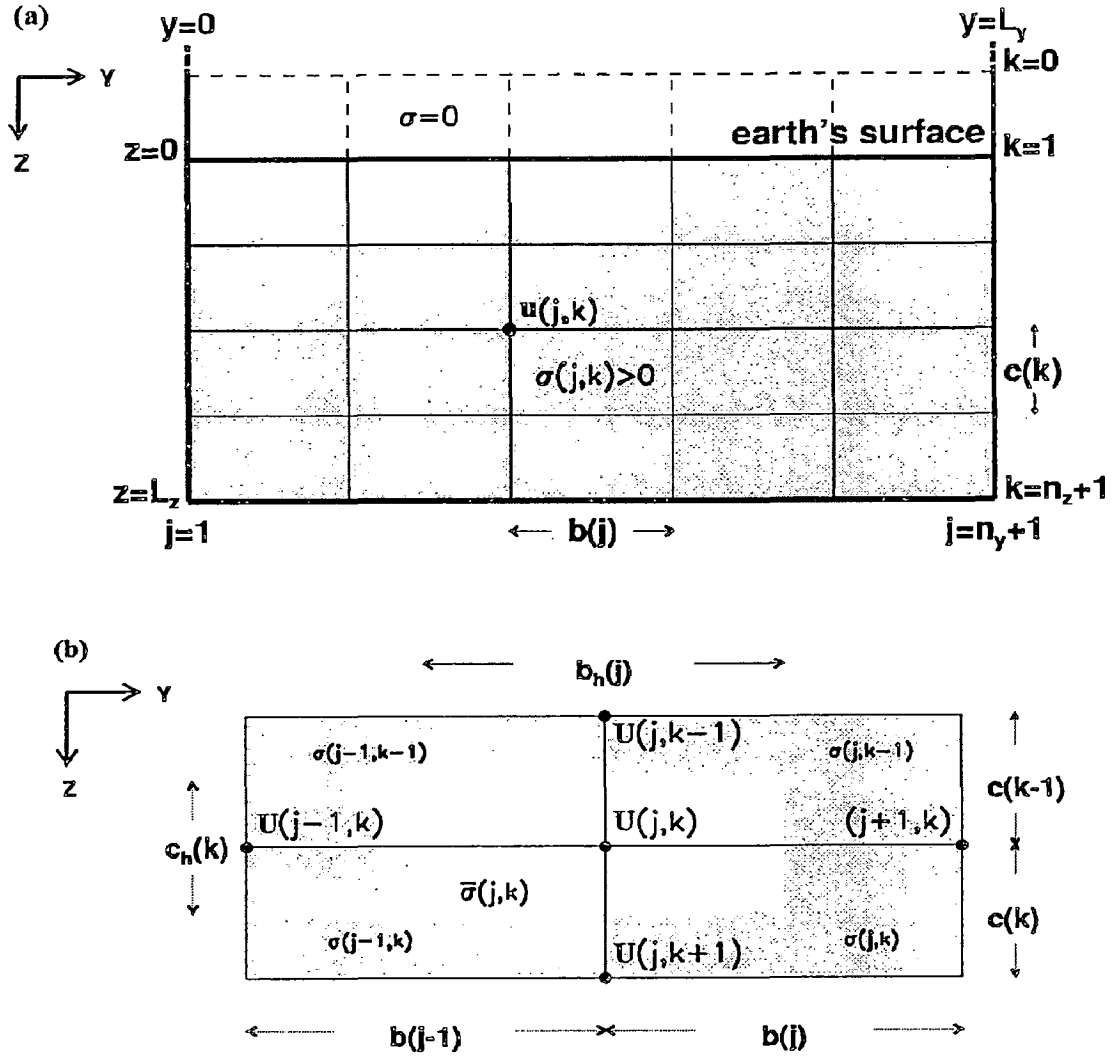

Figure 3.5(a) Schematic 2D grid used for finite difference. (b) FD situation at node (j, k) with its area of averaged conductivity $\bar{\sigma}$(j, k).

Let we consider a 2D conducting box in the region $0 \leq y \leq L_y$ and $0 \leq z \leq L_z$ with perfectly conducting ($\sigma = \infty$) bounding wall except at z = 0, shown in Figure 3.5.

The box is divided into $(n_y \times n_z)$ regular cells of size $b(j) \times c(j)$ and with conductivity σ(j,k), for j= 1,.... n_y, k= 1,2,3... n_z.

The conductivity at each node (j, k) is obtained from the area weighted average of the conductivity of four surrounding cells, (j-1, k), (j+1, k), (j, k-1) and (j, k+1); (Brewitt-Taylor and Weaver, 1976) as,

$$\overline{\sigma}(j,k) = \frac{1}{4bh_j ch_k}\{b_j c_k \sigma_{j,k} + b_{j-1} c_k \sigma_{j-1,k} + b_{j-1} c_{k-1} \sigma_{j-1,k-1} + b_j c_{k-1} \sigma_{j,k-1}\},$$

where, $bh_j = \frac{1}{2}[b_{j-1} + b_j]$ and $ch_k = \frac{1}{2}[c_{k-1} + c_k]$.

Utilizing the Equation 3.10, the central difference formula for second derivative is,

$$\frac{\partial^2 u}{\partial y^2} = \frac{1}{B_j^2}\left[\frac{b_{j-1}}{2bh_j} u_{j+1,k} - u_{j,k} + \frac{b_j}{2bh_j} u_{j-1,k}\right], \tag{3.20}$$

where $b_j = (y_j - y_{j-1})$, $B_j^2 = \frac{1}{2}(b_{j-1}.b_j)$ and $bh_j = \frac{1}{2}(b_{j-1} + b_j)$.

Similarly,

$$\frac{\partial^2 u}{\partial z^2} = \frac{1}{C_k^2}\left[\frac{c_{k-1}}{2ch_k} u_{j,k+1} - u_{j,k} + \frac{c_k}{2ch_k} u_{j,k-1}\right], \tag{3.21}$$

where $c_k = (z_k - z_{k-1})$, $C_k^2 = \frac{1}{2}(c_{k-1}.c_k)$ and $ch_k = \frac{1}{2}(c_{k-1} + c_k)$.

Using Equations 3.19, 3.20 and 3.21

$$\frac{1}{B_j^2}\left[\frac{b_{j-1}}{2bh_j} u_{j+1,k} - u_{j,k} + \frac{b_j}{2bh_j} u_{j-1,k}\right] + \frac{1}{C_k^2}\left[\frac{c_{k-1}}{2ch_k} u_{j,k+1} - u_{j,k} + \frac{c_k}{2ch_k} u_{j,k-1}\right] + {k_{j,k}}^2 u_{j,k} = -k_S^2 u_P,$$

$$\frac{2}{b_{j-1}b_j}\left[\frac{b_{j-1}}{2bh_j} u_{j+1,k} - u_{j,k} + \frac{b_j}{2bh_j} u_{j-1,k}\right] + \frac{2}{c_{k-1}c_k}\left[\frac{c_{k-1}}{2ch_k} u_{j,k+1} - u_{j,k} + \frac{c_k}{2ch_k} u_{j,k-1}\right] + {k_{j,k}}^2 u_{j,k} = -k_S^2 u_P, \tag{3.22}$$

$$\frac{bh_j}{c_{k-1}} u_{j,k-1} + \frac{ch_k}{b_{j-1}} u_{j-1,k} + \frac{ch_k}{b_j} u_{j+1,k} + \frac{bh_j}{c_k} u_{j,k+1} + \left(-\frac{bh_j}{c_{k-1}} - \frac{ch_k}{b_{j-1}} - \frac{ch_k}{b_j} - \frac{bh_j}{c_k} + {k^2}_{j,k}.bh_j.ch_j\right) u_{j,k} = -k_S^2 u_P. \tag{3.23}$$

This equation can be written as,

$$Au_{j,k-1} + Bu_{j-1,k} + Cu_{j+1,k} + Du_{j,k+1} + Pu_{j,k} = 0. \tag{3.24}$$

In Equation 3.24, j= 1, 2, ..., n_y and, k= 1, 2, 3,...n_z and this gives system of equations,

$$M_{cl}.u_{S_{cl}} = b_{cl}, \tag{3.25}$$

where M_{cl} is an n_y-by-n_z pentadiagonal matrix of following form,

$$\begin{bmatrix} P_1 & C_1 & 0 & 0 & D_1 & 0 & 0 & 0 & 0 \\ B_2 & P_2 & C_2 & 0 & 0 & D_2 & 0 & 0 & 0 \\ 0 & B_3 & P_3 & C_3 & 0 & 0 & D_3 & 0 & 0 \\ 0 & 0 & B_4 & P_4 & C_4 & 0 & 0 & D_4 & 0 \\ A_5 & 0 & 0 & B_5 & P_5 & C_5 & 0 & 0 & D_5 \\ 0 & A_6 & 0 & 0 & B_6 & P_6 & C_6 & 0 & 0 \\ 0 & 0 & A_7 & 0 & 0 & B_7 & P_7 & C_7 & 0 \\ 0 & 0 & 0 & A_8 & 0 & 0 & B_8 & P_8 & C_8 \\ 0 & 0 & 0 & 0 & A_9 & 0 & 0 & B_9 & P_9 \end{bmatrix} \begin{bmatrix} u_1 \\ u_2 \\ u_3 \\ u_4 \\ u_5 \\ u_6 \\ u_7 \\ u_8 \\ u_9 \end{bmatrix} = \begin{bmatrix} -A_1 u_0 - B_1 u_0 \\ 0 \\ 0 \\ 0 \\ 0 \\ 0 \\ 0 \\ 0 \\ -C_9 u_{10} - D_9 u_{10} \end{bmatrix}$$

This pentadiagonal matrix equation is to be solved to get fields at all nodes using CFDM. Size of matrix depends on the number of nodes generated, more is the number of nodes large is the size of matrix and requires large amount of time and cost of computations. The situation where analytical solution is not available or cumbersome to get then very fine grid structure is used, so that obtained field vector u is very close to analytical result.

3.4 Limitation of CFDM

The main problem with CFDM is its assumption that field to be solved does not have oscillating character and behaves as low degree polynomial within each cell. However, when field has very oscillating nature (as in the case of Electromagnetic or Seismic) then accuracy of the solution obtained using CFDM is not very good. It will give good result only when domain of interest is very finely discretized so that within each cell field can be assumed as low degree polynomial. Therefore if we have field like Figure 3.6 then CFDM requires very fine discretization so that within each cell field behaves as low degree polynomial.

Thus it leads to large number of nodes as a result a coefficient matrix of very large size and will take quite an amount of time to solve. As in the case of geophysical problems we are dealing with several kilometre of depth and on surfaces therefore size of matrix will become enormous and CFDM requires huge amount of time and cost to solve. Therefore Classical Finite Difference Method is not expected to handle oscillating functions with coarse grid system.

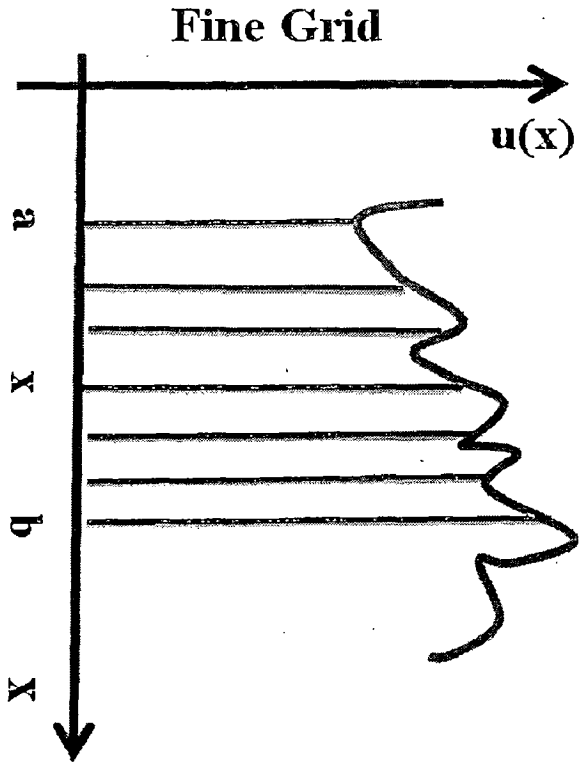

Figure 3.6: Fine discretization required for CFDM to get better results.

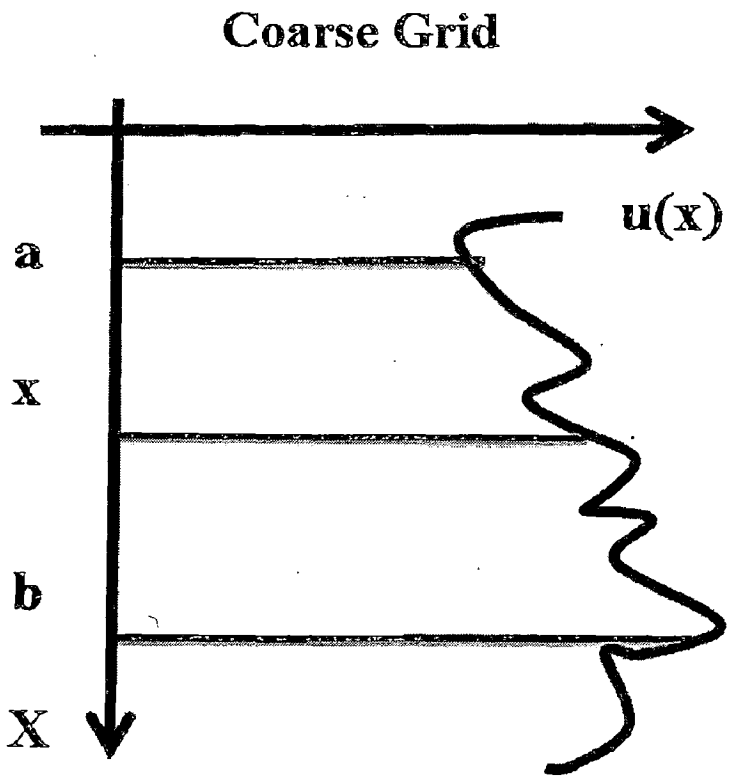

Figure 3.7: Coarse discretization for EFDM to get better results.

This dissertation aims to answer the question that: **"Can a coarse grid system be used to evaluate double derivative of a function with oscillating behaviour (as in Figure 3.7)?"** Here comes exponential fitting technique (Ixaru, 1997; Ixaru and Berghe, 2004), where it is assumed that between any three nodes the function is exponential in nature i.e. $exp(\pm\mu x)$ where μ may be imaginary, real or complex. Choosing basis $\{1, exp(\mu x), exp(-\mu x)\}$ instead of $\{1, x, x^2\}$ between three nodes can allow working with coarse grid with a different formulation of finite difference method known as Exponential Finite Difference scheme. Details of Exponential Finite Difference technique is dealt in detail in Chapter 4.

CHAPTER 4

EXPONENTIAL FINITE DIFFERENCE METHOD (EFDM)

The CFDM formulation derived in Chapter 3 holds good only when $u(x)$ can be approximated by a low degree polynomial within cells. The situation where $u(x)$ is a weighted sum of exponential or trigonometric or hyperbolic functions, it will give approximate results only when nodes are very closely spaced. This implies that size of matrix will increase by many times and in the case of 2D/3D, this problem will become more severe. Exponential fitting approach deals with such a class of functions that have oscillatory or hyperbolic behavior.

The central difference formula for second order derivative can be written as:

$$u''(x) \approx \frac{1}{h^2}[Au(x-h) + Bu(x) + Cu(x+h)]. \quad (4.1)$$

In CFDM, u(x) is assumed to be low degree polynomial with basis $\{1, x, x^2, ..\}$ while in Exponential Finite Difference Method (EFDM) the basis functions on which u(x) is expressed are $\{x^m . \exp(\pm\mu_i x), where\ m = 0,1,2,3 \ldots and\ i = 1,2,3..\}$ (Ixaru and Berghe, 2004). To obtain the dimensionless coefficients $\{\boldsymbol{a} \equiv [A, B, C]\}$ in Equation 4.1 an operator $\mathcal{L}[h, \boldsymbol{a}]$ is defined as follows (Ixaru, 1997);

$$\mathcal{L}[h, a]u(x) = u''(x) - \frac{1}{h^2}[Au(x-h) + Bu(x) + Cu(x+h)]. \quad (4.2)$$

Here operator $\mathcal{L}[h, \boldsymbol{a}]$ measures the misfit between approximations in Equation 4.1. Our main objective is to find out a set of coefficients $\{\boldsymbol{a} \equiv [A, B, C]\}$ such that $\mathcal{L}[h, \boldsymbol{a}]u(x) = 0$, it means approximation in 4.1 will be appropriate.

4.1 Classical Finite difference method revisited

For CFDM, $u(x)$ is considered to be some combination of $\{1, x, x^2, x^3..\}$ and we want to find such a set $\mathbf{a}=\mathbf{a}^*$, so that $\mathcal{L}[h, \boldsymbol{a}]u(x)$ is equal to zero. Following equations show how application of operator $\mathcal{L}$ on different monomials yield;

$$\mathcal{L}[h, \boldsymbol{a}]1 = -\frac{1}{h^2}(A + B + C)$$

$$\mathcal{L}[h, a]x = -\frac{x}{h^2}(A + B + C) + \frac{1}{h}(A - C),$$

$$\mathcal{L}[h, a]x^2 = -\frac{x^2}{h^2}(A + B + C) + \frac{2x}{h}(A - C) + (2 - A - C),$$

$$\mathcal{L}[h, a]x^3 = -\frac{x^3}{h^2}(A + B + C) + \frac{3x^2}{h}(A - C) - 3x(2 - A - C) - h(A - C)$$

$$\ldots\ldots \; etc \qquad (4.3)$$

The expressions in set of Equations 4.3 is also required to be evaluated at x=0 and, are known as moments of operator $\mathcal{L}[h, a]x^m$. These will be denoted as $\mathcal{L}_m$ (h, a) which is equal to $\mathcal{L}[h, a]x^m \; at \; x = 0, where \; m = 1,2,3, \ldots$

$$\mathcal{L}_0(h, a) = -\frac{1}{h}(A + B + C),$$

$$\mathcal{L}_1(h, a) = \frac{1}{h}(A - C),$$

$$\mathcal{L}_2(h, a) = (2 - A - C),$$

$$\mathcal{L}_3(h, a) = -h(A - C), \qquad \text{etc.} \qquad (4.4)$$

If $u(x) = (u_o + u_1x^1 + u_2x^2 + u_3x^3 + \cdots\ldots\ldots)$

Then, $\mathcal{L}[h, a]u(x) = \sum_{m=0}^{\infty} \frac{1}{m!} \mathcal{L}_m(\mathrm{h}, \mathrm{a}) \mathrm{D}^{\mathrm{m}} u(x)$. (4.5)

Equation 4.5 is derived in Ixaru and Berghe (2004). From Equations 4.3 and 4.5 it can be verified that making $\mathcal{L}[h, a]u(x)$=0 is equivalent to making;

$$\mathcal{L}_m(\mathrm{h}, \mathrm{a}) = 0, \qquad (4.6)$$

for $\mathrm{m} = 0,1,2,3, \ldots., (\mathrm{M} - 1)$ *and* $\mathcal{L}_M$ $(\mathrm{h}, \mathrm{a}) \neq 0$, which is a set of M linear equations for three unknowns.

Equation 4.6 gives us a maximum number of equations for which condition $\mathcal{L}_m$ $(\mathrm{h}, \mathrm{a}) = 0$ is valid. The task is now to find the biggest M for which system of Equations 4.6 is compatible. For uniform h, it can be verified that condition (4.6) is satisfied only for first four equations i.e. M = 4 (Ixaru, 2004). This is obtained by solving first three equations ($\mathcal{L}_m(\mathrm{h}, \mathrm{a}) =$

0, for m = 0,1,2) which gives A = C = 1 and B = - 2.This is in accordance with the result as derived in previous section for CFDM. The values of A, B and C satisfies the fourth equation (m = 3) but does not satisfy the equations beyond m = 3.

4.2 Theory of Exponential Finite Difference Method (EFDM)

As in previous section, first an operator $\mathcal{L}[h, a]$ is defined as in Equation 4.2;

$$\mathcal{L}[h, a]u(x) = u''(x) - \frac{1}{h^2}[Au(x - h) + Bu(x) + Cu(x + h)]. \quad (4.7)$$

In exponential fitting procedure, the basis functions are $\{x^m \exp(\mu_i x), where\ m = 0,1,2..\ and\ i = 1,2,3 ...\}$ and u(x) is a linear combination of these basis functions. In exponential fitting method the application of operator $\mathcal{L}$ on functions of the form $u(x) = x^m \exp(\mu x)$, for m=0, 1, 2, 3.. plays a central role. A quantity is define as;

$$E_m(h, \mu, a) = \mathcal{L}[h, a]x^m \exp(\mu x) \mid_{x=0}. \quad (4.8)$$

This expression is known as μ-moment of order m of operator $\mathcal{L}$ in Ixaru and Berghe (2004). The classical moment $\mathcal{L}_m$is a particular case with μ=0 (Ixaru, 1997). If m=0 is put in the Equation 4.8 then

$$E_0(h, \mu, a) = \mathcal{L}[h, a]\ \exp(\mu x) \mid_{x=0}. \quad (4.9)$$

It is shown in Ixaru and Berghe (2004) that higher order μ-moments can be derived from $E_0(h, \mu, a)$ by the following expression:

$$E_m = \frac{\partial^m E_0}{\partial \mu^m}. \quad (4.10)$$

The expression (4.8) can be expressed in more compact form with the help of dimensional analysis. Dimensional consistency demands that:

$$\dim\{E_m(h, \mu, a)\} = \dim\{\mathcal{L}[h, a]\}.\ dim\{x^m \exp(\mu x)\}.$$

If the definition of operator $\mathcal{L}[h, \boldsymbol{a}]$ (Equation 4.7) is viewed carefully, then it can be figured out that $\dim\{\mathcal{L}[h, \boldsymbol{a}]\}$ is h^l where, l is the negative of the order of derivative (Ixaru and Berghe, 2004). The second factor in above equation has the dimension of h^m. The final expression for $E_m(h, \mu, \boldsymbol{a})$ can be written as:

$$E_m(h, \mu, a) = h^{l+m} E_m^*(z, a). \tag{4.11}$$

Where z = μh, a dimensionless quantity.

Similar result can be derived for classical moment $\mathcal{L}_m(\mathrm{h}, \mathbf{a})$ which can be written as:

$$\mathcal{L}_m(\mathrm{h}, \mathbf{a}) = h^l L_m^*(\boldsymbol{a}). \tag{4.12}$$

Starred moments are $E_m^*(z, \boldsymbol{a})$ *and* $L_m^*(\boldsymbol{a})$ are equivalent to $E_m(h, \mu, \boldsymbol{a})$ *and* $\mathcal{L}_m(h, \boldsymbol{a})$ respectively.

4.2.1 Method to determine coefficients for EFDM

In section (4.1) we have seen how CFDM coefficients can be derived by the application of operator $\mathcal{L}$ on different monomials. Now we assume that, we have a hybrid set of basis functions, and u(x) can be expressed as linear combination of these functions. The set of functions which is assumed to be appropriate for given form of u(x) is;

$$\{1, x, x^2, x^3, \ldots\ldots, x^K, \exp(\pm\mu x), x\exp(\pm\mu x), x^2\exp(\pm\mu x) \ldots\ldots x^P \exp(\pm\mu x)\} \tag{4.13}$$

Having seen the application of operator $\mathcal{L}$ on classical set, let us see what operator $\mathcal{L}[h, \boldsymbol{a}]$ with definition as in Equation 4.7 yields when applied on exp(±μx).

$$\mathcal{L}[h, a]\exp(\pm\mu x) = \mu^2 \exp(\mu x) - \frac{1}{h^2}[Aexp(\mu x).exp(\mp\mu h)Bexp(\mu x) + Cexp(\mu x).exp(\pm\mu h)],$$

$$\mathcal{L}[h, a]\exp(\pm\mu x) = \frac{1}{h^2}\exp(\mu x)\,[\mu^2 h^2 - A\exp(\mp\mu h) - B - Cexp(\pm\mu h)] \tag{4.14}$$

If we see definition (4.9) and compare expressions in Equation 4.11 and Equation 4.14 we get that:

$$E_0^*(\pm z, \boldsymbol{a}) = z^2 - Aexp(\mp z) - B - Cexp(\pm z),$$
$$where\ z = \pm\mu h \tag{4.15}$$

The higher order μ-moments can be obtained by the help of Equation 4.10. In the frame of the general exponential fitting procedure, the coefficients to be determined for a problem have to satisfy the system;

$$E_p^*(\pm z, \boldsymbol{a}) = 0, for\ p = 0,1, \dots, P$$

There is an equivalent representation of above expression. In Ixaru (1997), two functions $G^{\pm}(Z, \boldsymbol{a})$ are introduced which are defined as follows ($Z = z^2$);

$$G^{+}(Z, \boldsymbol{a}) = \frac{1}{2}[E_0^*(z, \boldsymbol{a}) + E_0^*(-z, \boldsymbol{a})],$$
$$G^{-}(Z, \boldsymbol{a}) = \frac{1}{2z}[E_0^*(z, \boldsymbol{a}) - E_0^*(-z, \boldsymbol{a})]. \tag{4.16}$$

Then p[th] derivative with respect to Z of $G^{\pm}(Z, \boldsymbol{a})$ is denoted as $G^{\pm p}(Z, \boldsymbol{a})$. It has been showed in Ixaru and Berghe (2004) that system of equations represented by

$$E_p^*(\pm z, \boldsymbol{a}) = 0, for\ p = 0,1, \dots, P$$

is system equivalent to the of equations;

$$G^{\pm p}(Z, a) = 0, for\ p = 0,1,2, \dots P \tag{4.17}$$

Now the task is to find maximal P such that Equation 4.17 is valid. This will give us the coefficients $\{\boldsymbol{a} \equiv [A, B, C]\}$. However there is a condition on the maximal P, this is called as self consistency condition (Ixaru and Berghe, 2004). This is explained as follows:

Firstly, classical moments are solved and maximum number of equations M is found for which Equation 4.6 is compatible. The basis set (4.13) then must satisfy following condition:

$$(K + 1) + 2(\mathrm{P} + 1) = \mathrm{M}$$
$$K + 2P = M - 3 \tag{4.18}$$

The reference set is thus characterized by two integer parameters K and P. The set in which there is no classical component is identified by K = -1 while the set in which there is no exponential fitting component is identified by P = -1. Once K and P are decided, then Equations 4.6 and 4.17 are solved simultaneously to get the coefficients $\{\boldsymbol{a} \equiv [A, B, C]\}$.

It has been showed at the end of section (4.1) that maximum number of equations satisfied by classical moment is M = 4. This is obtained by solving $\mathcal{L}_m(h, a) = 0,\ for\ m = 0,1,2$. Also, $\mathcal{L}_3(h, a) = 0\ but\ \ \mathcal{L}_4(h, a) \neq 0$. So M = 4 is the maximum number of compatible equations satisfying Equation 4.6. From self-consistency relation (4.18) we get that, K+2P = 1. Thus there are three possible integer solutions of this equation,

1. K=3 and P= -1. This means we do not have any exponential component in our basis i.e., set is purely classical$\equiv\{1, x, x^2, x^3\}$. Hence to obtain coefficients, only $\mathcal{L}_m(h, a) = 0,\ for\ m = 0,1,2$, are needed to be solved. This gives A=C=1 and B= -2 which is in accordance with CFDM result.

2. K = 1 and P = 0. This means we have a hybrid set containing both classical and exponential terms $\{1,\ x,\ \exp(\mu x),\ \exp(-\mu x)\}$. Hence to obtain the coefficients we need to solve $\mathcal{L}_m(h, a) = 0,\ for\ m = 0,1$ and $G^{\pm}(Z, a) = 0$. The expression for $G^{\pm}(Z, a)$ can be easily obtained from Equations 4.16 and 4.17. The coefficients obtained have the form,

$$A = C = \frac{Z}{2(\eta_{-1}(Z) - 1)},$$

$$B = \frac{-Z}{(\eta_{-1}(Z) - 1)},$$

$$where\ \ Z = z^2 = \mu^2 h^2\ \ and\ \ \eta_{-1}(Z) = \frac{1}{2}\left[\exp\left(Z^{\frac{1}{2}}\right) + \exp\left(-Z^{\frac{1}{2}}\right)\right]. \qquad (4.19)$$

3. K= -1 and P = 1. This suggests that basis set does not have any classical component and is given by $\{exp(\mu x), exp(-\mu x),\ xexp(\mu x),\ xexp(-\mu x)\}$. The coefficients are obtained by solving $G^{\pm}(Z, a) = 0$ and $G^{\pm 1}(Z, a) = 0$. And this is given by following expressions,

$$A = C = \frac{1}{\eta_0(Z)} \quad and\ B = \frac{Z\eta_0(Z) - 2\eta_{-1}(Z)}{\eta_0(Z)},$$

$$where\ \ Z = z^2 = \mu^2 h^2\ \ and\ \ \eta_0(Z) = \frac{1}{2z}\left[\exp\left(Z^{\frac{1}{2}}\right) - \exp\left(-Z^{\frac{1}{2}}\right)\right] \tag{4.20}$$

This means that if u(x) is known to have either oscillatory or hyperbolic character, then above expressions in (Equations 4.19 and 4.20) yield coefficients which better approximate second order derivative of u(x). Depending upon whether u(x) is oscillatory or hyperbolic, μ will be either an imaginary or a real quantity. If u(x) has both the characteristics μ should be chosen as a complex number. The above coefficients are derived in Ixaru and Berghe (2004).

4.2.2 Expressions for coefficients using non-uniform grid spacing

In section 4.2.1, the coefficients are derived assuming uniform grid spacing h. But in many situations we actually work with non-uniform grid spacing. For instance, in case of solving one dimensional Helmholtz equation for layered earth model using CFDM, grid spacing required to be finer near the interfaces compared to other parts. So it requires evaluating the coefficients occurring in second order derivative for exponential FDM with non-uniform grid system. From our discussion in section (3.2.1) and Equation 3.10 we can approximate second order derivative for non-uniform grid system as:

$$u''(x_i) \approx \frac{1}{H^2}\ [Au(x_i - h_{i-1}) + Bu(x_i) + C\,u(x_i + h_i)]\,,$$

$$where\ H^2 = \frac{1}{2}(h_{i-1}.h_i) \tag{4.21}$$

To evaluate the coefficients $\{\boldsymbol{a} \equiv [A, B, C]\}$ we follow the steps mentioned in section (4.2.1). First an operator $\mathcal{L}[h_{i-1}, h_i, \boldsymbol{a}]u(x_i)$ is defined as follows;

$$\mathcal{L}[h_{i-1}, h_i, \boldsymbol{a}]u(x_i) = u''(x_i) - \frac{1}{H^2}[Au(x_i - h_{i-1}) + Bu(x_i) + C\,u(x_i + h_i)]\,. \tag{4.22}$$

Now we apply operator $\mathcal{L}[h_{i-1}, h_i, \boldsymbol{a}]$ on different terms of classical basis $\{1, x, x^2, x^3, \ldots\}$ to get expressions for classical moments. (Ray, 2011)

$$\mathcal{L}[h_{i-1}, h_i, a]1 = -\frac{1}{H^2}(A + B + C),$$

$$\mathcal{L}[h_{i-1}, h_i, a]x = -\frac{x}{H^2}(A + B + C) + \frac{1}{H^2}(Ah_{i-1} - Ch_i),$$

$$\mathcal{L}[h_{i-1}, h_i, a]x^2 = -\frac{x^2}{H^2}(A + B + C) + \frac{2x}{H^2}(Ah_{i-1} - Ch_i) + \frac{1}{H^2}(2H^2 - Ah_{i-1}^2 - Ch_i^2),$$

$$\mathcal{L}[h_{i-1}, h_i, a]x^3 = -\frac{x^3}{H^2}(A + B + C) + \frac{3x^2}{H^2}(Ah_{i-1} - Ch_i) + \frac{3x}{H^2}(2H^2 - Ah_{i-1}^2 - Ch_i^2) + \frac{1}{H^2}(Ah_{i-1}^3 - Ch_i^3).$$

(4.23)

Using definition for classical moments we get:

$$\mathcal{L}_0(h_{i-1}, h_i, a) = -\frac{1}{H^2}(A + B + C),$$

$$\mathcal{L}_1(h_{i-1}, h_i, a) = \frac{1}{H^2}(Ah_{i-1} - Ch_i),$$

$$\mathcal{L}_2(h_{i-1}, h_i, a) = \frac{1}{H^2}(2H^2 - Ah_{i-1}^2 - Ch_i^2),$$

$$\mathcal{L}_3(h_{i-1}, h_i, a) = \frac{1}{H^2}(Ah_{i-1}^3 - Ch_i^3), \quad \text{etc} \qquad (4.24)$$

Solving first three equations above for A, B and C we get $A = \frac{h_i}{n_i}$, $B = -1$, *and* $C = \frac{h_{i-1}}{n_i}$ which is in well accordance with the CFDM with non-uniform grid spacing (Equation 3.10). The solution obtained does not satisfy the fourth equation of set of equations (4.24). This means maximum number of equations satisfied by classical moments is M = 3. But as shown in previous section that M = 4 for uniform grids. So, results of uniform grids and non-uniform grids are expected to be different. So from self-consistency equation we get K+2P=0 which has only two sets of integer solution (K=2, P= -1) and (K=0, P=0). The first set will give classical solution with no exponential component whose solution we found already.

The second solution with K=P=0 constitutes a hybrid basis {1, $\exp(\mu x)$, $\exp(-\mu x)$}. It implies that we have to solve three simultaneous equations to get the coefficients. These are $\mathcal{L}_0(h_{i-1}, h_i, a) = 0$ and $G^{\pm}(Z, a) = 0$. To construct $G^{\pm}(Z, a) = 0$ we operate $\mathcal{L}(h_{i-1}, h_i, a)$ on $\exp(\pm\mu x)$ to get $E_0^*(z, a)$. This is shown in following steps:

$$\mathcal{L}[h_{i-1}, h_i, \boldsymbol{a}] \exp(\pm\mu x_i) = \mu^2 \exp(\pm\mu x_i) - \frac{1}{H^2}[A \exp(\pm\mu x_i) . exp(\mp\mu h_{i-1}) + Bexp(\pm\mu x_i) + Cexp(\pm\mu x_i). exp(\pm\mu h_i)],$$

$$\mathcal{L}[h_{i-1}, h_i, \boldsymbol{a}] \exp(\pm\mu x_i) = \frac{1}{H^2} \exp(\pm\mu x_i) [\mu^2 H^2 - Aexp(\mp\mu h_{i-1}) - B - C\, exp(\pm\mu h_i)].$$

Assuming $z^2 = \mu^2 H^2$, $z_i = \mu h_i$, $z_{i-1} = \mu h_{i-1}$ we get

$$E_0^*(z_{i-1}, z_i, \boldsymbol{a}) = z^2 - Aexp(-z_{i-1}) - B - Cexp(z_i),$$

$$E_0^*(-z_{i-1}, -z_i, \boldsymbol{a}) = z^2 - Aexp(z_{i-1}) - B - Cexp(-z_i).$$

Now we can construct $G^{\pm}(\hat{Z}, \boldsymbol{a})$ from above two expressions and using $\hat{Z} = z^2 = \mu^2 H^2$

$$G^{+}(\hat{Z}, a) = \frac{1}{2}[E_0^*(z_{i-1}, z_i, a) + E_0^*(-z_{i-1}, -z_i, a)],$$

$$G^{+}(\hat{Z}, a) = Z - A\eta_{-1}(Z_{i-1}) - C\eta_{-1}(Z_i) - B. \quad (4.25)$$

Similarly,

$$G^{-}(\hat{Z}, a) = \frac{1}{2z}[E_0^*(z_{i-1}, z_i, a) - E_0^*(-z_{i-1}, -z_i, a)],$$

$$G^{-}(\hat{Z}, a) = \frac{z_{i-1}}{z} A.\eta_0(Z_{i-1}) - \frac{z_i}{z} C.\eta_0(Z_i). \quad (4.26)$$

From first expression in Equation 4.24 we have;

$$\mathcal{L}_0(h_{i-1}, h_i, a) = -\frac{1}{H^2}(A + B + C). \quad (4.27)$$

Here $\eta_{-1}(Z_i)$ *and* $\eta_0(Z_i)$ are defined earlier in Equations 4.19 and 4.20. After constructing expressions for $G^{\pm}(\hat{Z}, \boldsymbol{a})$, we solve $\mathcal{L}_0(h_{i-1}, h_i, \boldsymbol{a}) = 0$ and $G^{\pm}(\hat{Z}, \boldsymbol{a}) = 0$ using Equations 4.25,4.26, and 4.27. The coefficients obtained are given below (Ray, 2011)

$$C = \frac{\hat{Z}}{\left[(\eta_{-1}(Z_i) - 1) + (\eta_{-1}(Z_{i-1}) - 1)\frac{\eta_0(Z_i)}{\eta_0(Z_{i-1})}\sqrt{\frac{Z_i}{Z_{i-1}}}\right]},$$

$$A = \frac{\eta_0(Z_i)}{\eta_0(Z_{i-1})}\sqrt{\frac{Z_i}{Z_{i-1}}}\,C\,,$$

$$B = -C\left[1 + \frac{\eta_0(Z_i)}{\eta_0(Z_{i-1})}\sqrt{\frac{Z_i}{Z_{i-1}}}\right] = -A - C\,. \tag{4.28}$$

The set of Equation 4.28 is an important development which was obtained in Ray (2011); it extends the existing results of EFDM for uniform grid, to non-uniform grid system. When grid spacing is made equal throughout the domain, then it matches existing result of Ixaru and Berghe (2004). The above Equation set (4.28) gives the coefficients for exponential finite difference method with non-uniform grid system.

4.2.3 Exponential Finite Difference Method for 2D case

In section 4.2.1 and 4.2.2, the coefficients are derived for 1D case but for 2D case basis functions are $[(y.z)^i \exp\{\mu(y+z)\}$, where i=0,1,2.....] and coefficients can be obtained in following manners,

The central difference formula for partial derivative for non-uniform gridding can be approximated as,

$$\frac{\partial^2 u}{\partial y^2}(y_j, z_k) \approx \frac{1}{B_j^2}\left[a_1 u_{j-1,k} + a_2 u_{j,k} + a_3 u_{j+1,k}\right]. \tag{4.29}$$

As in the previous sections, to evaluate the coefficients a= $[a_1, a_2, a_3]$ an operator $\mathcal{L}_y[b_{j-1}, b_j, \boldsymbol{a}]$ is defined as follows,

$$\mathcal{L}_y[b_{j-1}, b_j, \boldsymbol{a}]u(y_j, z_k) = \frac{\partial^2 u}{\partial y^2}(y_j, z_k) - \frac{1}{B_j^2}\left[a_1 u_{j-1,k} + a_2 u_{j,k} + a_3 u_{j+1,k}\right]. \tag{4.30}$$

Now we apply this operator $\mathcal{L}_y[b_{j-1}, b_j, \boldsymbol{a}]$on different terms of classical basis $\{1, (yz), (yz)^2\}$ to get expressions for classical moments.

$$\mathcal{L}_y[b_{j-1}, b_j, \boldsymbol{a}]1 = -\frac{1}{B_j{}^2}(a_1 + a_2 + a_3),$$

$$\mathcal{L}_y[b_{j-1}, b_j, \boldsymbol{a}](y_j z_k) = -\frac{y_j z_k}{B_j{}^2}(a_1 + a_2 + a_3) + \frac{z_k}{B_j{}^2}(a_1 b_{j-1} - a_3 b_j),$$

$$\mathcal{L}_y[b_{j-1}, b_j, \boldsymbol{a}](y_j z_k)^2 = -\frac{y_j{}^2 z_k{}^2}{B_j{}^2}(a_1 + a_2 + a_3) + \frac{2y_j z_k^2}{B_j{}^2}(a_1 b_{j-1} - a_3 b_j) + \frac{z_k^2}{B_j{}^2}(2B_j{}^2 - a_1 b_{j-1}^2 - a_3 b_j^2).$$

(4.31)

Using definition for classical moments at $y_j = 0$, we get:

$$\mathcal{L}_0[b_{j-1}, b_j, \boldsymbol{a}] = -\frac{1}{B_j{}^2}(a_1 + a_2 + a_3),$$

$$\mathcal{L}_1[b_{j-1}, b_j, \boldsymbol{a}] = \frac{z_k}{B_j{}^2}(a_1 b_{j-1} - a_3 b_j),$$

$$\mathcal{L}_2[b_{j-1}, b_j, \boldsymbol{a}] = \frac{z_k^2}{B_j{}^2}(2B_j{}^2 - a_1 b_{j-1}^2 - a_3 b_j^2), \quad \text{etc.} \tag{4.32}$$

Since for 2D case the exponential basis functions are $[1, exp\{\mu(y+z)\}, exp\{-\mu(y+z)\}]$ therefor let $u(y_j, z_k) = exp\{\pm\mu(y_j + z_k)\}$;

$$\mathcal{L}_y[b_{j-1}, b_j, \boldsymbol{a}] \exp\{\pm\mu(y_j + z_k)\} = \mu^2 \exp\{\pm\mu(y_j + z_k)\} - \frac{1}{B_j{}^2}[a_1 \exp\{\pm\mu(y_j + z_k)\} \exp(\mp\mu b_{j-1}) + a_2 \exp\{\pm\mu(y_j + z_k)\} + a_3 \exp\{\pm\mu(y_j + z_k)\} \exp(\pm\mu b_j)],$$

$$\mathcal{L}_y[b_{j-1}, b_j, \boldsymbol{a}] \exp\{\pm\mu(y_j + z_k)\} = \frac{1}{B_j{}^2} \exp\{\pm\mu(y_j + z_k)\}[\mu^2 B_j{}^2 - a_1 \exp(\mp\mu b_{j-1}) - a_2 - a_3 \exp(\pm\mu b_j)].$$

(4.33)

Assuming $\widehat{Y}_j = \mu^2 B_j{}^2$, $Y_j = \mu^2 b_j{}^2$, $Y_{j-1} = \mu^2 b^2{}_{j-1}$ we get

$$E_0^*(Y_{j-1}, Y_j, \boldsymbol{a}) = \widehat{Y}_j - a_1 exp(-\sqrt{Y_{j-1}}) - a_2 - a_3 exp(\sqrt{Y_j}),$$

$$E_0^*(-Y_{j-1}, -Y_j, \boldsymbol{a}) = \widehat{Y}_j - a_1 exp(\sqrt{Y_{j-1}}) - a_2 - a_3 exp(-\sqrt{Y_j}).$$

Now we can construct $G^{\pm}(\widehat{Y}_j, \boldsymbol{a})$ from above two expressions;

$$G^{+}(\hat{Y}_j, \boldsymbol{a}) = \frac{1}{2}\left[E_0^*(Y_{j-1}, Y_j, \boldsymbol{a}) + E_0^*(-Y_{j-1}, -Y_j, \boldsymbol{a})\right],$$

$$G^{+}(\hat{Y}_j, \boldsymbol{a}) = \hat{Y}_j - a_1\eta_{-1}(Y_{j-1}) - a_3\eta_{-1}(Y_j) - a_2 . \tag{4.34}$$

where, $\eta_{-1}(Y) = \frac{1}{2}\left[\exp\left(Y^{\frac{1}{2}}\right) + \exp\left(-Y^{\frac{1}{2}}\right)\right]$.

Similarly,

$$G^{-}(\hat{Y}_j, \boldsymbol{a}) = \frac{1}{2\sqrt{\hat{Y}_j}}\left[E_0^*(Y_{j-1}, Y_j, \boldsymbol{a}) - E_0^*(-Y_{j-1}, -Y_j, \boldsymbol{a})\right],$$

$$G^{-}(\hat{Y}_j, \boldsymbol{a}) = \frac{\sqrt{Y_{j-1}}}{\sqrt{\hat{Y}_j}} a_1 . \eta_0(Z_{i-1}) - \frac{\sqrt{Y_j}}{\sqrt{\hat{Y}_j}} a_3 . \eta_0(Z_i) . \tag{4.35}$$

where, $\eta_0(Y) = \frac{1}{2\sqrt{Y}}\left[\exp\left(Y^{\frac{1}{2}}\right) - \exp\left(-Y^{\frac{1}{2}}\right)\right]$.

After constructing expressions for $G^{\pm}(\hat{Y}_j, \boldsymbol{a})$, we solve $\mathcal{L}_0[b_{j-1}, b_j, \boldsymbol{a}] = 0$ and $G^{\pm}(\hat{Y}_j, \boldsymbol{a}) = 0$ using Equations 4.31,4.34, and 4.35. The coefficients obtained are given below,

$$a_3 = \frac{\hat{Y}_j}{\left[\{\eta_{-1}(Y_j)-1\}+\{\eta_{-1}(Y_{j-1})-1\}\frac{\eta_0(Y_j)}{\eta_0(Y_{j-1})}\sqrt{\frac{Y_j}{Y_{j-1}}}\right]},$$

$$a_1 = \frac{\eta_0(Y_j)}{\eta_0(Y_{j-1})}\sqrt{\frac{Y_j}{Y_{j-1}}}\, a_3 ,$$

$$a_2 = -\left[1 + \frac{\eta_0(Y_j)}{\eta_0(Y_{j-1})}\sqrt{\frac{Y_j}{Y_{j-1}}}\right] a_3 = -a_3 - a_1 . \tag{4.36}$$

where, $Y_j = \mu^2 b_j^2$, $\quad \hat{Y}_j = \mu^2 B_j^{\,2}$, $\quad B_j^{\,2} = \frac{1}{2}\left(b_{j-1} \times b_j\right)$,

$\eta_0(Y) = \frac{1}{2\sqrt{Y}}\left[\exp\left(Y^{\frac{1}{2}}\right) - \exp\left(-Y^{\frac{1}{2}}\right)\right]$ and

$\eta_{-1}(Y) = \frac{1}{2}\left[\exp\left(Y^{\frac{1}{2}}\right) + \exp\left(-Y^{\frac{1}{2}}\right)\right]$.

Similarly, we can approximate $\frac{\partial^2 u}{\partial z^2}(y_j, z_k)$ using EFDM

$$\frac{\partial^2 u}{\partial z^2}(y_j, z_k) \approx \frac{1}{c_k^2}\left[a_4 u_{j,k-1} + a_5 u_{j,k} + a_6 u_{j,k+1}\right], \tag{4.37}$$

$$a_6 = \frac{2_k}{\left[\{\eta_{-1}(z_k)-1\}+\{\eta_{-1}(z_{k-1})-1\}\frac{\eta_0(z_k)}{\eta_0(z_{k-1})}\sqrt{\frac{z_k}{z_{k-1}}}\right]},$$

$$a_4 = \frac{\eta_0(z_k)}{\eta_0(z_{k-1})}\sqrt{\frac{z_k}{z_{k-1}}}a_6 \text{ , and } a_5 = -a_6 - a_4 . \tag{4.38}$$

The above Equations 4.36 and 4.38 give the coefficient for EFDM with non-uniform grid system. These coefficients are required to be placed in the 2D Helmholtz equation to obtain fields $u(y, z)$ using EFDM,

Using Equations 3.11, 4.29, 4.36, 4.37 and 4.38

$$A_e u_{j+1,k} + B_e u_{j,k+1} + C_e u_{j,k-1} + D_e u_{j-1,k} + P_e u_{j,k} = 0 .$$

This results in following matrix equation similar to the case of CFDM,

$$\mathbf{M_{ex}}.\mathbf{u_{ex}} = \mathbf{b}_{ex}, \tag{4.39}$$

The structure of this matrix is also pentadiagonal (as in CFDM) and bands will contain coefficients [A_e, B_e, C_e, D_e, P_e] corresponding to different nodes. The pentadiagonal matrix Equation 4.39 needs to be solved to get field values at all nodes using EFDM. Time and cost of computations depend on the size of matrices $\mathbf{M_{cl}}$ and $\mathbf{M_{ex}}$ which in turn depend on number of nodes taken. Large is the number of nodes more will be the time and cost.

CHAPTER 5

DEVELOPMEMNT AND DETAILS OF ALGORITHMS

5.1 Introduction

In this dissertation we have developed two forward modeling algorithms (i) MT_2D_CFDM based on Classical Finite Difference Method and (ii) MT_2D_EFDM based on Exponential Finite Difference Method using Fortran 90. Integral boundary condition is applied at the air-earth interface (Stuntebeck, 2003) and asymptotic boundary conditions (Weaver and Brewitt-Taylor, 1978) are applied at the vertical sides of model. The bottom boundary is assumed to be perfectly conducting. Both the algorithms are used for solving 1D and 2D Helmholtz equation as applied to simulate MT response of 2D earth models. First, both the algorithms are used to solve Helmholtz equation to synthesize the electric field vector which, in turn, is used to obtain the magnetic field vector and the derived MT response functions impedance, apparent resistivity and phase. The details of development of algorithm are presented below.

5.2 Salient Features of MT_2D_CFDM and MT_2D_EFDM Algorithms

The developed algorithms have a compact modular structure; any subroutine can be plugged in or taken out easily without affecting the remaining program. The features to enhance versatility or efficiency are discussed below.

5.2.1 Grid generation

The algorithm is developed to generate uniform grids as well as manual grid. Skin depth based automatic grid generator is also used in this algorithm which was developed by Weaver (1994). The subroutine *gridgen* is used for generating automatic grid points.

5.2.2 Response functions

These algorithms are presently developed to get the responses for magnetotelluric profiling. The responses are computed at the surface for a single frequency. The algorithms are developed to compute response functions like impedance, apparent resistivity and phase, for

2D-TE mode only. The response functions apparent resistivity and phase are computed in subroutine *output2*.

5.2.3 Source term

The algorithms are so structured that the computations are carried out in terms of secondary fields. Later on, for total field computations, the primary fields are added to these secondary fields. Thus, in order to incorporate the source effect, only a subroutine computing the responses of primary layered earth model in the presence of given source, is added in lieu of the existing subroutines *primary* which compute the 1D field due to a plane wave source.

5.2.4 Tridiagonal Method

The subroutine *tridag* given in Numerical Recipes by Press et al. (1993) is used to solve tridigonal system of matrix equation encountered for 1D computation of primary fields.

5.2.5 BiCGStab Method

Bi Conjugate Gradient Stabilized (BiCGStab) is used to solve pentadiagonal equation encountered for computation of secondary fields because with appropriate preconditioner it provides the solution in optimal time and best one to use. The subroutine *bicgstab* developed by Rastogi, A. (1997) and Krishna Kumar (2009) is used in these algorithms for this purpose. Appendix A.3 explains the details of BiCGStab method.

5.3 Description of MT_2D_CFDM and MT_2D_EFDM Algorithms

The algorithm, MT_2D_CFDM, employs Classical Finite Difference Method for solving the EM field vectors to compute the 2D MT responses while MT_2D_EFDM, employs Exponential Finite Difference Method for the same. The MT_2D_CFDM algorithm comprises 3936 lines and 14 subroutines while MT_2D_EFDM algorithm comprises 4082 lines and 14 subroutines. The basic statistics and salient features are emphasised in the Figure 5.1.

Total five I/O units; one input unit and four output units are opened in the program. The parameters and data controls are read from the input file. The remaining four output files are used for different outputs helpful in analysing the results. All the descriptions about how to generate input file are given in the Appendix A.1.

Basic Algorithm Statistics

MT_2D_CFDM - 3936 Lines

Main program - 241 Lines

CFDM Algorithm

Subroutines - 3695 Lines

14= (8+6*)

* Adapted from other program

Methodology

Classical Finite Difference Method to transform the Helmholtz equation to matrix equation

Bi-CGStab method to solve above transformed matrix equation.

Field continuation at air-earth interface

Basic Algorithm Statistics

MT_2D_EFDM - 4082 Lines

Main program - 253 Lines

EFDM Algorithm

Subroutines - 3829 Lines

14= (8+6*)

* Adapted from other program

Methodology

Exponential Finite Difference Method to transform the Helmholtz equation to matrix equation

Bi-CGStab method to solve above transformed matrix equation.

Field continuation at air-earth interface

Figure 5.1: MT_2D_CFDM and MT_2D_EFDM Algorithms in nutshell.

5.4 Structure of MT_2D_CFDM and MT_2D_EFDM Algorithms

In the main program the control parameters are defined, input and output files are opened and the subroutines are called as shown in Figure 5.2. Input data and other parameters are reads in the subroutine *input*.

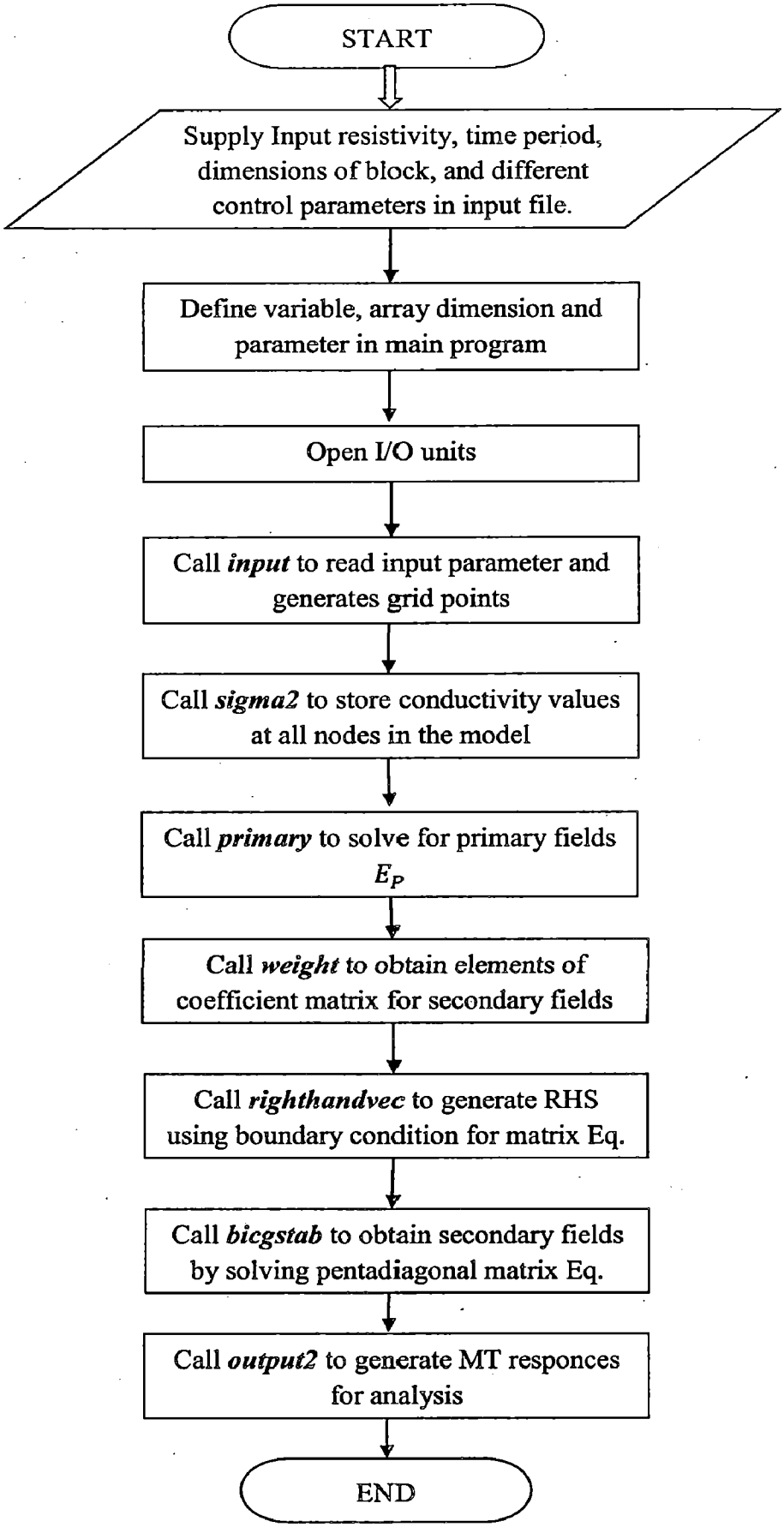

Figure 5.2: Flow chart of main program for both MT_2D_CFDM and MT_2D_EFDM.

The grid can be generated in three ways. First, by reading manually generated grid values, second by uniform grid generator by giving the values of uniform nodes spacing in y and z directions, third by using automatic grid generator based on skin depth developed by Weaver (1994). The counter *gridcount* is used to control the choice of grid generation.

The resistivity values are read for the half space and for the anomalous body from *input* file (see appendix A.1 for details) and finally stored in conductivity array *sx* using subroutine *sigma2*. Calculations of the elements of coefficient matrix, for all primary electric field components E_P, are carried out in subroutine *lanczos1*. This subroutine *lanczos1* is also used for solving primary fields E_P for layered earth model.

Subroutine *weight* is used to generate elements of coefficient matrix for all secondary field components E_S. The only difference in algorithms MT_2D_CFDM and MT_2D_EFDM is in the subroutine *weight*. Subroutine *weight* in MT_2D_CFDM employs classical finite difference approximation while subroutine *weight* in MT_2D_EFDM employs exponential finite difference approximation.

Subroutine *righthandvec* is used to generate the right hand side array using boundary condition for matrix equation to compute secondary fields. Subroutine *bicgstab* is used to solve pentadiagonal matrix equation to get secondary field values E_S. Finally subroutine *output2* is used to generate the MT response like total electric fields E_T, magnetic fields, apparent resistivities and phase responses. Figure 5.2 shows flow charts for main program.

The control parameters and their purpose and numerical value for different options are listed in Table A.1.1 of Appendix A.1. The remaining input parameters used in different subprograms are described in Table A.1.2 of Appendix A.1. The description of development of algorithm is completed. The results of experiments performed for checking and validation of MT_2D_CFDM and MT_2D_EFDM are presented in the succeeding chapter.

CHAPTER 6

RESULTS AND APPLICATIONS

This dissertation work is principally based on numerical simulation of 2D Helmholtz equation as appears in Magnetotelluric. As mentioned earlier the main aim of this dissertation is to develop algorithms for two numerical schemes employed namely Exponential Finite Difference Method (MT_2D_EFDM) and Classical Finite Difference Method (MT_2D_CFDM) to solve 2D Helmholtz equation and then, to test these algorithms in order to observe efficiency of proposed EFDM algorithm in comparison to CFDM. After development of EFDM algorithm, a question is raised what value of exponent μ is to be chosen to get optimum results since μ is prime requirement for the development of EFDM algorithm. Following section explains the estimation of near optimal μ.

6.1 Estimation of optimum value of μ

A significant point of discussion in EFDM is the exponent μ which is hidden in $Y = \mu^2 b^2$ or $Z = \mu^2 c^2$. The coefficients $[A_e, B_e, C_e, D_e, P_e]$ depend on Y or Z (Equations 4.36 or 4.38), hence these, in turn, depend on μ. Let the electromagnetic field is assumed to be a linear combination of basis functions $[1, exp\{\pm\mu(y+z)\}]$. Now, if field has some other frequency μ_1 ($\mu_1 \neq \mu$) then coefficients will not give the best response. So, the choice of μ is a crucial in EFDM. If we have prior knowledge about field then μ can be chosen accordingly.

After conducting exhaustive experiments on random 2D earth models, an estimator for μ through model parameters is defined as follows,

$$\mu = (1+i)\frac{\left(\sum_{j=1}^{n}(-1+i)\times\frac{real\{k(j)\}}{dy(j)dz(j)}\right)}{\sum_{j=1}^{n}\frac{1}{dy(j)dz(j)}}. \tag{6.1}$$

Here, $i = \sqrt{-1}$ and j runs from 1st conductivity block to nth conductivity block (Appendix A.1), k(j) is wave number of j^{th} block, dy(j) is width of j^{th} block and dz(j) is thickness of j^{th} block. It can be noted that the μ is some sort of area weighted average of k.

This estimator of μ is used in all the 2D models to solve the 2D Helmholtz equation using MT_2D_EFDM algorithm. Same formula is also used to find out near optimum value of μ for layered earth to find out primary fields. For this we have to put dy(j)=1 and each layer is taken as a block of thickness dz(k).

After developing MT_2D_EFDM using this estimator of μ our natural task is to test the both algorithms. In respect to this, firstly the experiments are performed to validate the accuracy of developed algorithms (MT_2D_CFDM and MT_2D_EFDM) on standard 2D models results then we carried experiments on different 2D earth models for solving 2D Helmholtz equation using both algorithms, MT_2D_CFDM as well as MT_2D_EFDM to observe the efficiency of proposed EFDM in comparison to CFDM.

6.2 Algorithm Testing

It is desirable that an algorithm is exhaustively validated with some analytical solution and established published results. In this context, we first tested the developed algorithms for uniform half space then validation is carried out for some standard 2D earth models.

6.2.1 Homogeneous half space model

In Magnetotelluric source is assumed to be very far away from the surface of the earth. Electromagnetic waves propagate through the surface of the earth to the subsurface as discussed in Chapter 2. For uniform half space, analytical solution is derived in section (2.1.1) and from Equation 2.21 we get, $E(z) = E_o \exp(ikz)$, where E_o is field at surface and z is depth values.

Experiments are performed for uniform half space with resistivity ρ=100 ohm-m (Figure 6.1). Time period of the signal is taken to be T = 0.1 s. The electric fields and apparent resistivities obtained using both developed algorithms MT_2D_EFDM and MT_2D_CFDM are identical with the analytical results at the surface almost everywhere in the horizontal direction (y-direction). The variation of fields with depth (z-direction) is also nearly identical with the analytical results and shown in Figure 6.2 and 6.3.

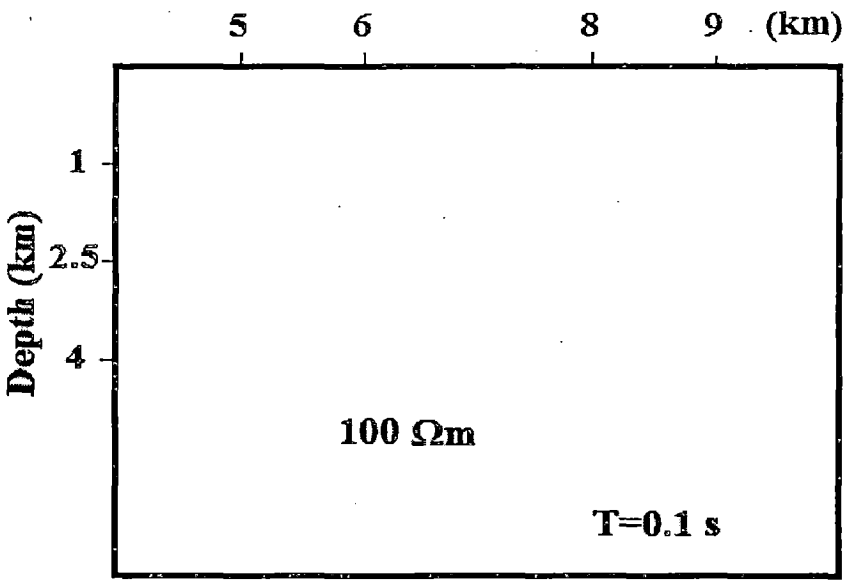

Figure 6.1: Homogeneous half space of resistivity ρ=100 Ωm.

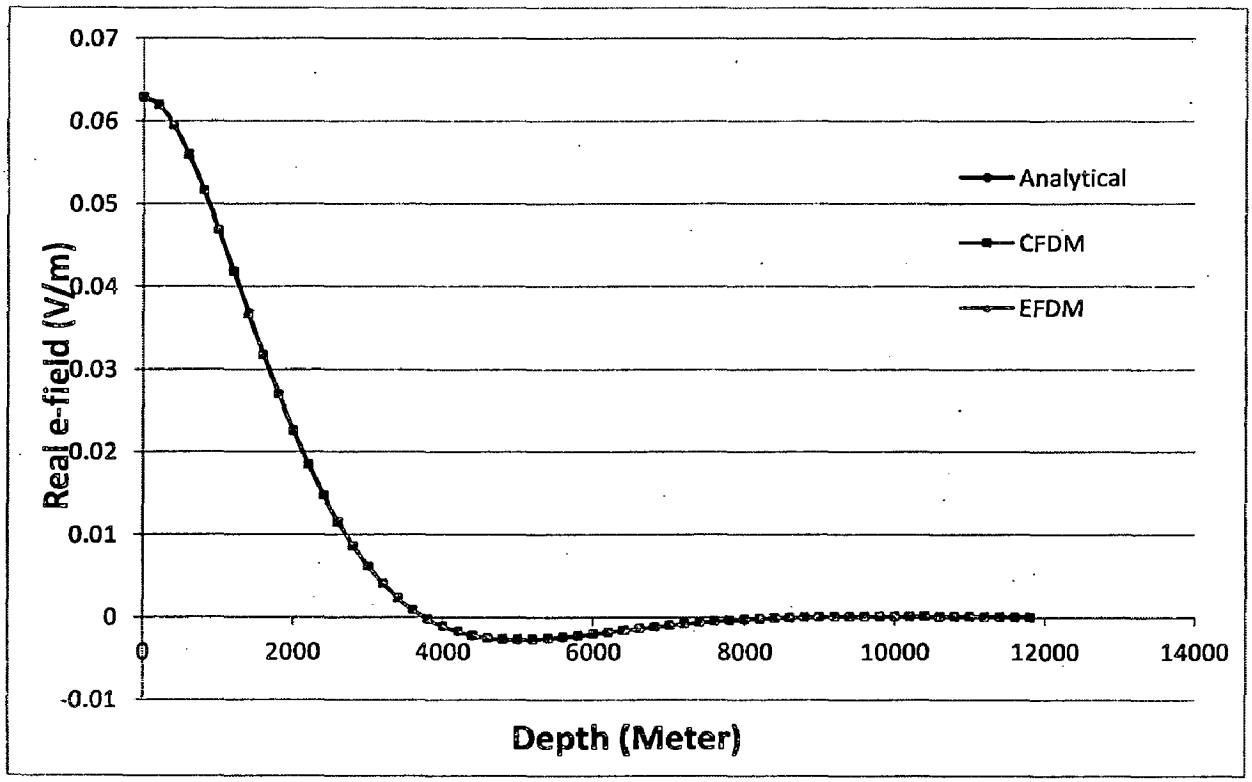

Figure 6.2: Comparison of real component of electric fields obtained using analytical result, CFDM and EFDM for homogeneous half space having resistivity of ρ = 100 Ωm.

It is clear form Figure 6.2 and 6.3 that both the developed algorithms MT_2D_CFDM and MT_2D_EFDM give results nearly similar to analytical results. **Here one point should be noted that these fields are computed using CFDM or EFDM with fine gridding or with large number of nodes in this model.**

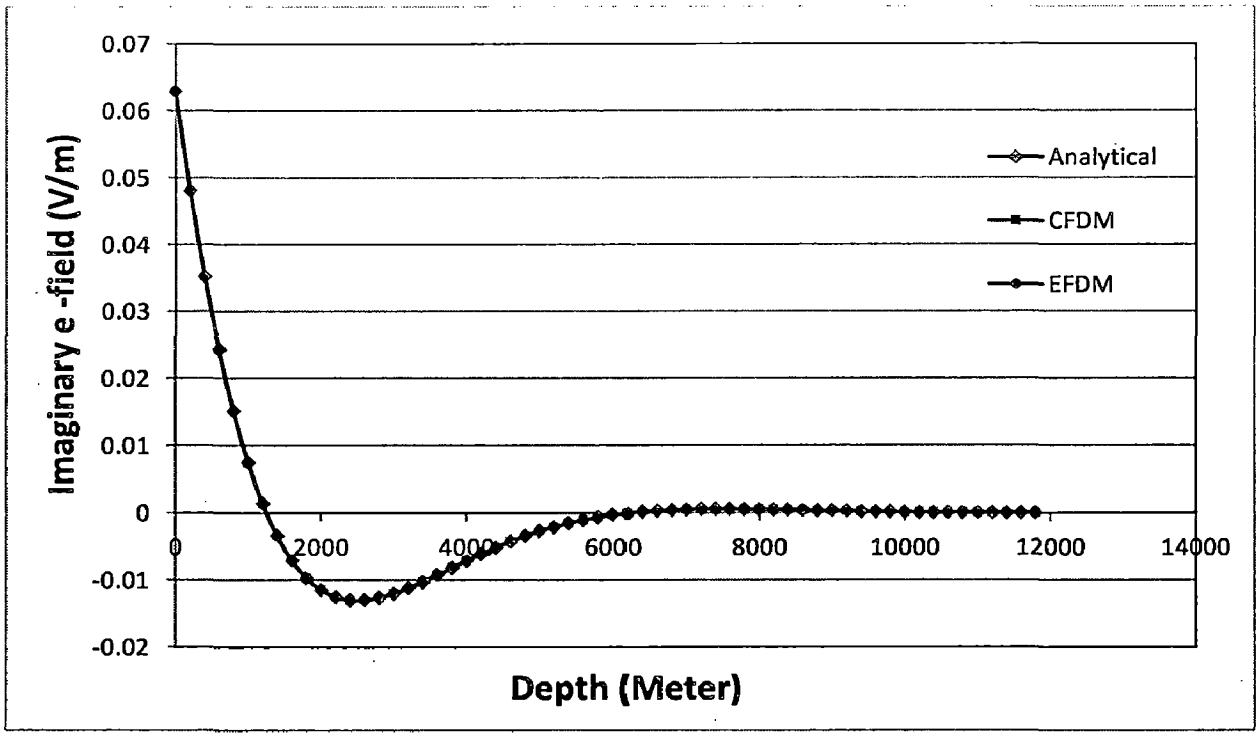

Figure 6.3: Comparison of Imaginary component of electric field obtained using analytical results, CFDM and EFDM for homogeneous half space having resistivity of ρ = 100 Ωm.

The next validation of these algorithms is the reproduction of established published results. In this exercise, two 2D models have been selected from (a) 2D-1 from COMMEMI (Comparison of Modeling Methods for Electro-Magnetic Induction) report by Zhdanov et al. (1997) and (b) Brewitt-Taylor and Weaver (1976) Model. In COMMEMI report the results obtained using different algorithms based on Finite Difference, Finite Element, and Integral Equation methods are given for comparison while in Brewitt-Taylor and Weaver (1976), the results obtained using Finite Difference Method. The comparisons for apparent resistivity values are presented for validation of algorithm.

6.2.2 Model M_1: 2D-1 Model from COMMEMI

Model 2D-1 in the COMMEMI report by Zhdanov et al. (1997) is reproduced in Figure 6.4. It comprises a symmetrical rectangular block embedded in homogeneous half space. The resistivity of the inserted block is 0.5 Ωm while that of the half space is 100 Ωm. The block, placed at a depth of 250 m from the earth surface, has a width of 1 km and thickness of 2 km. The MT responses such as electric field and apparent resistivity are computed for a period of 0.1 s.

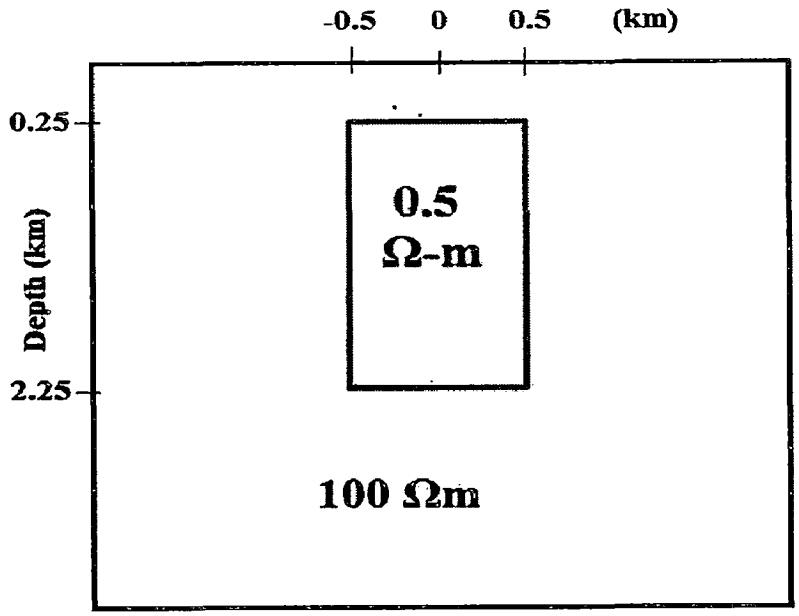

Figure 6.4: Model M_1: 2D-1 of COMMEMI, (distances in km and resistivity in Ωm).

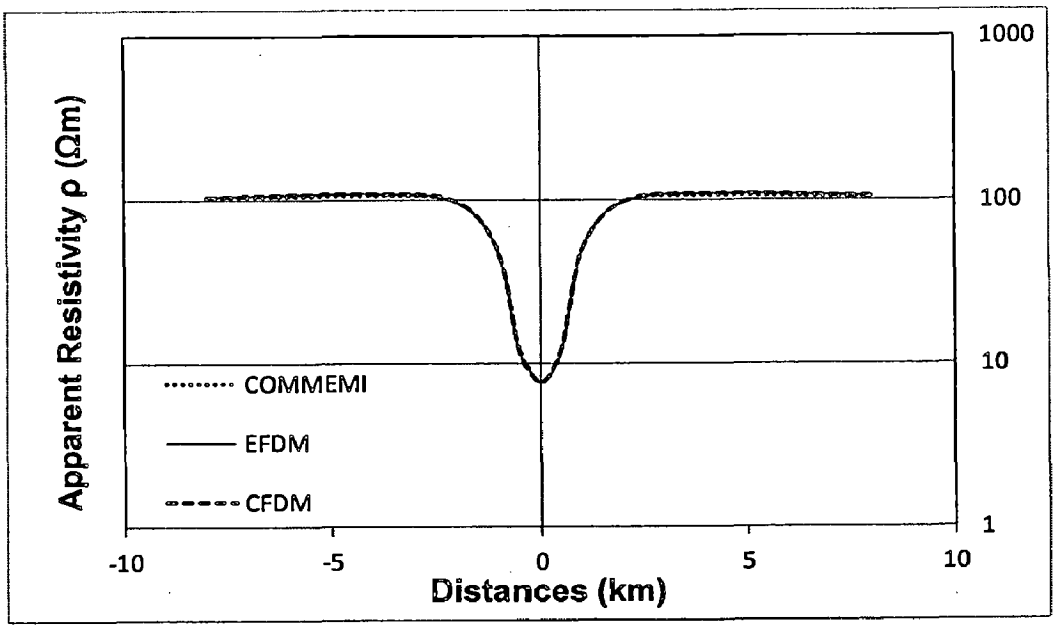

Figure 6.5: Apparent resistivities plot; comparison of COMMEMI (Zhdanov et al., 1997), EFDM and CFDM at 0.1 s with finer gridding.

In Figure 6.5 apparent resistivity values obtained using proposed EFDM and CFDM both with finer gridding are plotted and compared with the average value of apparent resistivity from COMMEMI report. The RMS error between EFDM and COMEMMI is about 0.4 % and CFDM and COMMEMI is about 0.6 % that shows the validation of our algorithms with standard algorithms.

6.2.3 Model M_2: Model from Brewitt-Taylor and Weaver (1976)

Brewitt-Taylor and Weaver (1976) model is reproduced in Figure 6.6. It comprises a rectangular block embedded in homogeneous half space. The resistivity of the inserted block is 0.1 Ωm while that of the half space is 1 Ωm. The block, placed at a depth of 100 m from the earth surface, has a width and thickness of 0.5 km. The MT responses such as electric field and apparent resistivity are computed for a period of 1 s.

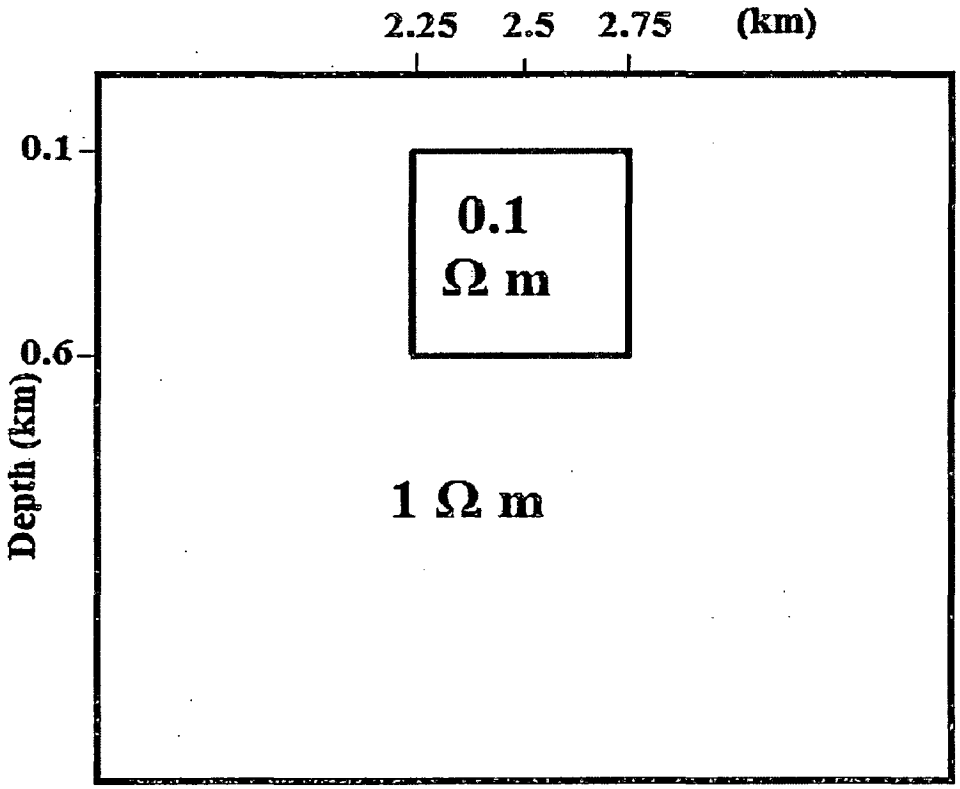

Figure 6.6: Model M_2: Brewitt-Taylor and Weaver (1976) model, (distances in km and resistivity in Ωm).

In Figure 6.7 apparent resistivity values, obtained using proposed EFDM and CFDM using finer gridding, are plotted and compared with the apparent resistivities from Brewitt-Taylor and Weaver (1976). The RMS error between Brewitt-Taylor and Weaver, 1976 results and EFDM or CFDM is about 0.9 % or 1.1 % respectively that again shows the validation of our algorithm with standard algorithms.

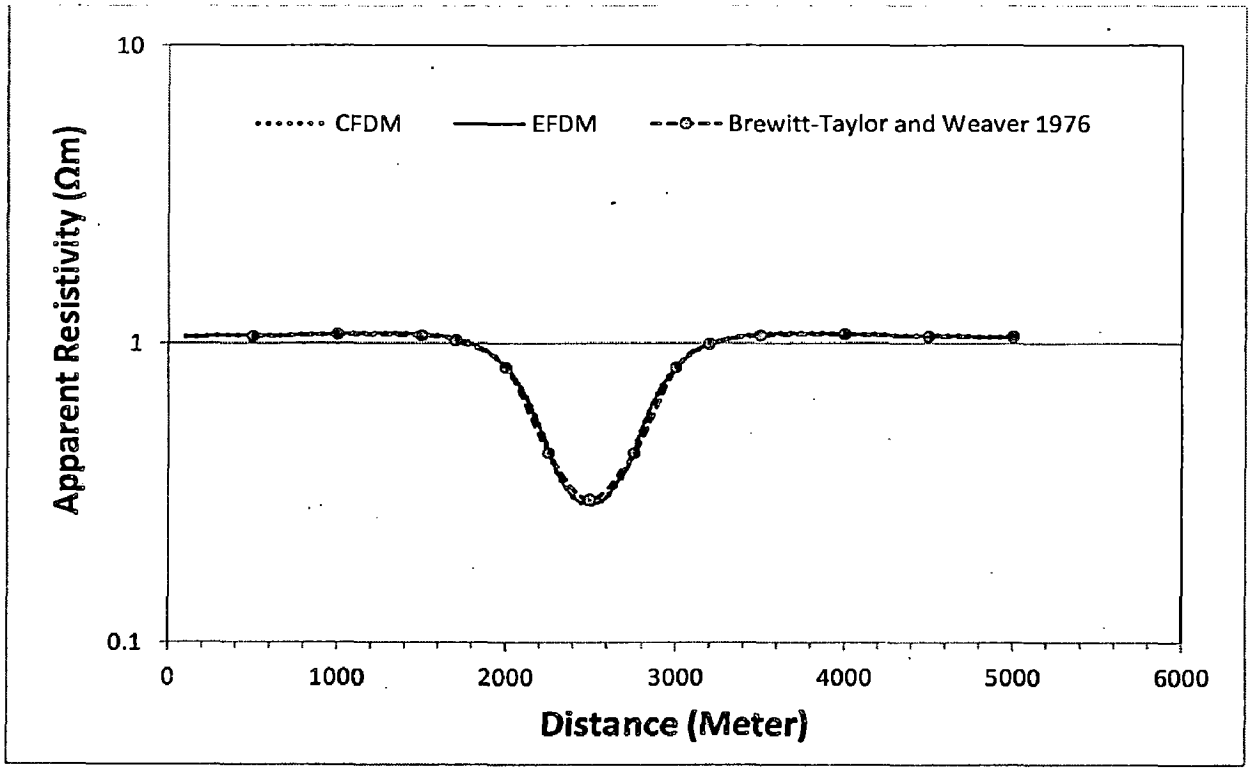

Figure 6.7: Apparent resistivities plot; comparison of Brewitt-Taylor and Weaver (1976), EFDM and CFDM results at 1 s with finer gridding.

6.3 Experiments to establish efficiency of EFDM

Several experiments have been performed on 2D earth models in order to observe the efficiency of proposed EFDM in comparison to CFDM. 2D Helmholtz equation is solved using both CFDM and EFDM for different number of nodes. After computing the field with both algorithms, L_1 norm of relative error $\left[\text{i. e.}, \xi = \sum_n \frac{(|u_{cal} - u_{anl}|)}{n.u_{anl}}\right]$ is computed for different number of nodes. Here u_{cal} is computed field with either CFDM or EFDM and u_{anl} is analytical solution that we obtained using CFDM with very fine discretization or with very large number of nodes (about 5000 nodes). L_1 norm of relative error (ξ) is plotted against different number of nodes used in model for solving 2D Helmholtz equation to observe efficiency of EFDM.

In this context, first the developed algorithm is tested for uniform half space then experiments are carried out for standard 2D earth models.

6.3.1 Homogeneous half space model

In this, same homogeneous half space is considered as in the section 6.2.1 and fields are computed using both MT_2D_CFDM and MT_2D_EFDM algorithms for different number of nodes for signal period of T=0.1s. Plot of relative error against different number of nodes used in homogeneous half space model is shown in Figure 6.8 for both CFDM and EFDM.

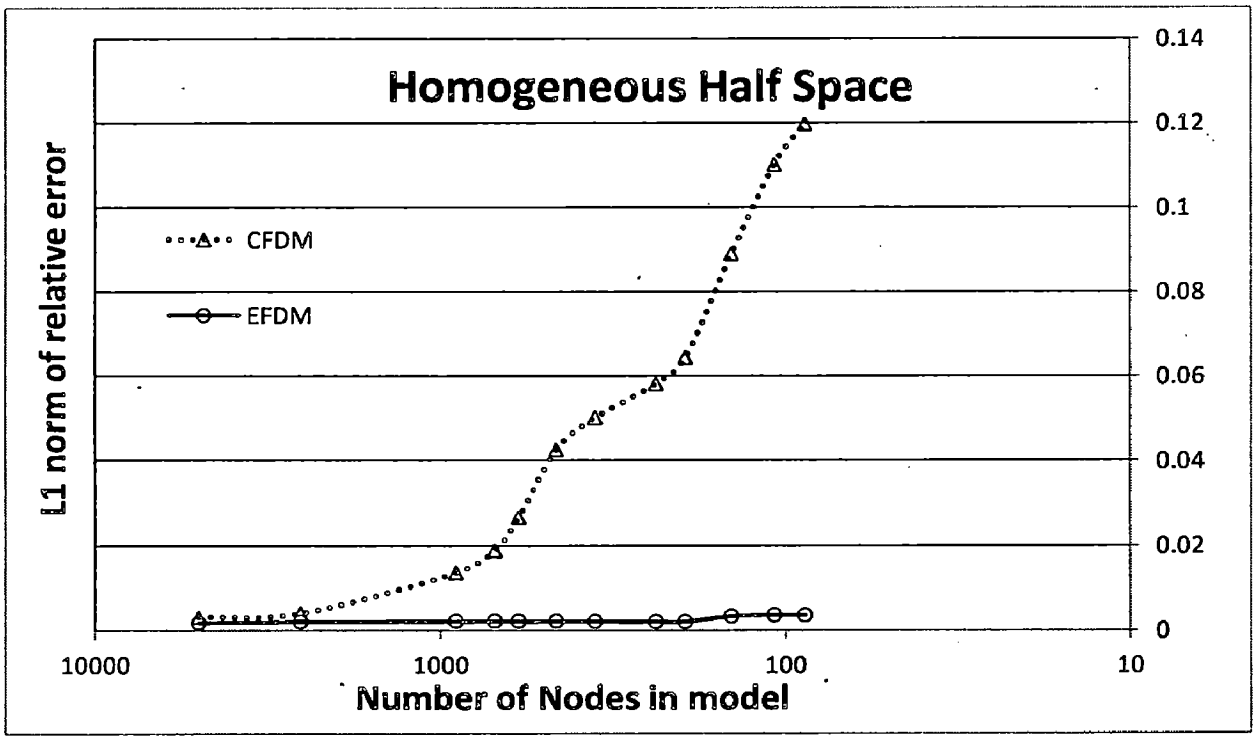

Figure 6.8: Variation of ξ (L_1 norm of relative error) with node spacing for homogeneous half space. Continuous line with circle marker shows error in EFDM and dotted line with triangle marker shows error in CFDM.

Figure 6.8 illustrate that L_1 norm of relative error in EFDM is far less than CFDM, and nearly equals to zero. Therefore, for homogeneous half space, EFDM gives nearly exact analytical solution.

6.3.2 Model M_1: 2D-1 Model from COMMEMI

In this, the same model M_1 is considered as in the section 6.2.2 and fields are computed using both MT_2D_CFDM and MT_2D_EFDM for different number of nodes. Plot of relative error (ξ) against different number of nodes used in model M_1 is shown in Figure 6.9 using both MT_2D_CFDM and MT_2D_EFDM. It is very clear from Figure 6.9 that the relative error in EFDM is much less than error in CFDM hence EFDM gives more accurate result in comparison to CFDM for a given number of nodes. Alternatively, we can use coarser grid in

EFDM to get same accuracy of results as we get with CFDM with finer grid and this is demonstrated in Table 6.1 from Figure 6.9.

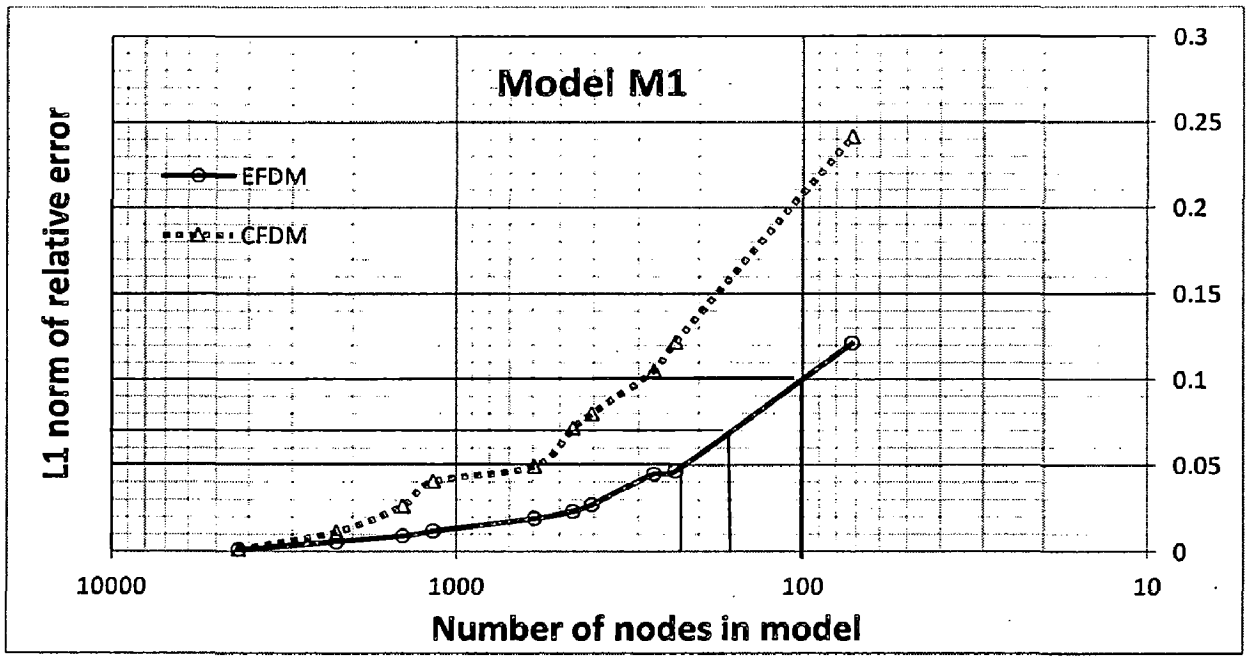

Figure 6.9: Variation of ξ (L_1 norm of relative error) with different number of nodes for model M_1.

Table 6.1: Number of nodes required for same accuracy using both CFDM and EFDM in M_1.

S.N.	Relative error	No. of nodes used in		Reduction of no. of nodes
		CFDM	EFDM	
1.	5%	600	220	63%
2.	7%	480	160	67%
3.	10%	300	100	67%

Table 6.1 represents that about 65% less number of nodes require in EFDM to get same accuracy of results as we obtained using CFDM with a given nodes, illustrating that EFDM requires less time and cost of computations in comparison to CFDM.

6.3.3 Model M_2: Model from Brewitt-Taylor and Weaver (1976)

The same model M_2 is considered as in the section 6.2.3 and fields are computed using both CFDM and EFDM for different number of nodes.

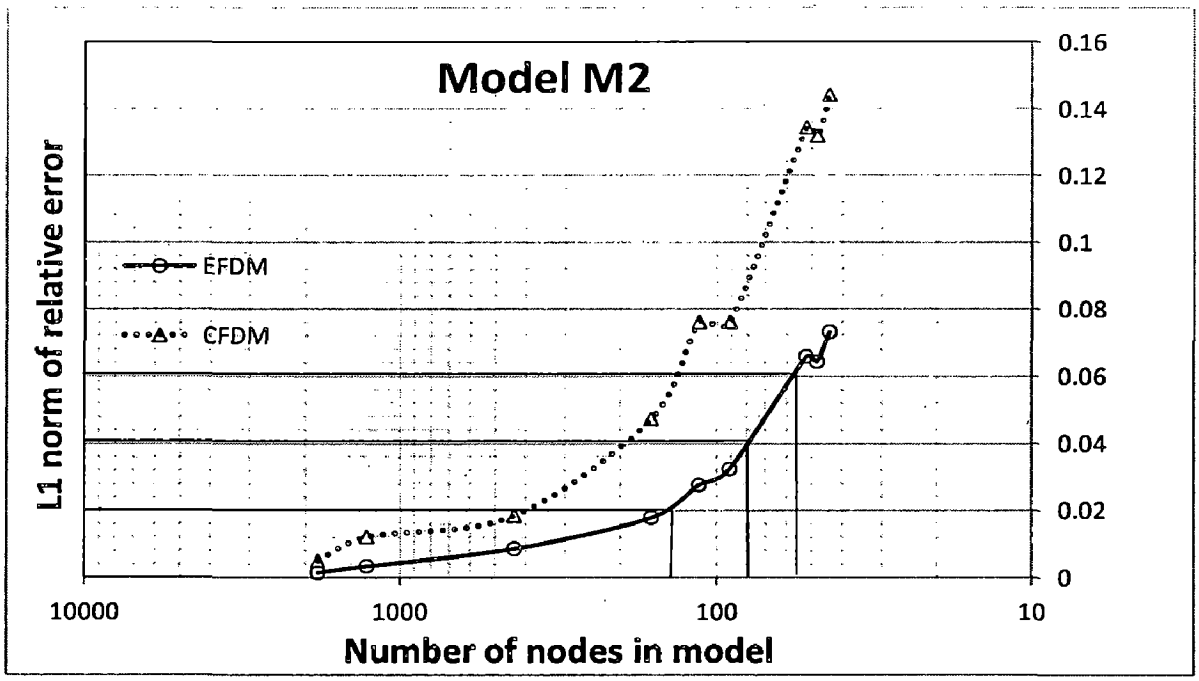

Figure 6.10: Variation of ξ (L_1 norm of relative error) with different number of nodes for model M_2.

It is clear from relative error plot (Figure 6.10) that the relative error in EFDM is less than error in CFDM therefore EFDM gives more accurate result in comparison to CFDM for a given number of nodes. Instead, we can use coarser grid in EFDM to get same accuracy of results as we get with CFDM with finer grid and this is demonstrated in Table 6.2 from Figure 6.10.

Table 6.2: Number of nodes required for same accuracy using both CFDM and EFDM in M_2.

S.N.	Relative error %	No. of nodes used in		Reduction of no. of nodes
		CFDM	EFDM	
1.	2%	400	150	63%
2.	4%	190	80	58%
3.	6%	150	56	63%

Table 6.2 implies that about 61% less number of nodes requires in EFDM to get same accuracy of results as we obtained using CFDM with a given nodes, illustrating that EFDM requires less time and cost of computations in comparison to CFDM.

6.3.4 Model M_3

This test model comprises a symmetrical rectangular block embedded in homogeneous half space. The resistivity of the inserted block is 5 Ωm while that of the half space is 50 Ωm. The block, placed at a depth of 50 m from the earth surface, has a width of 3 km and thickness of 2 km. The MT responses such as electric field and apparent resistivity are computed for a period of 0.1 s. Plot of relative error against different number of nodes for model M_3 is shown in Figure 6.12 using both CFDM and EFDM.

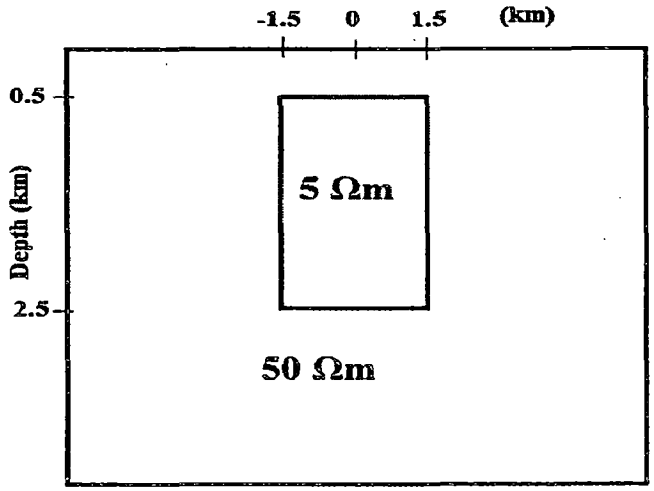

Figure 6.11: Test Model M_3 (distance in km and resistivity in Ωm).

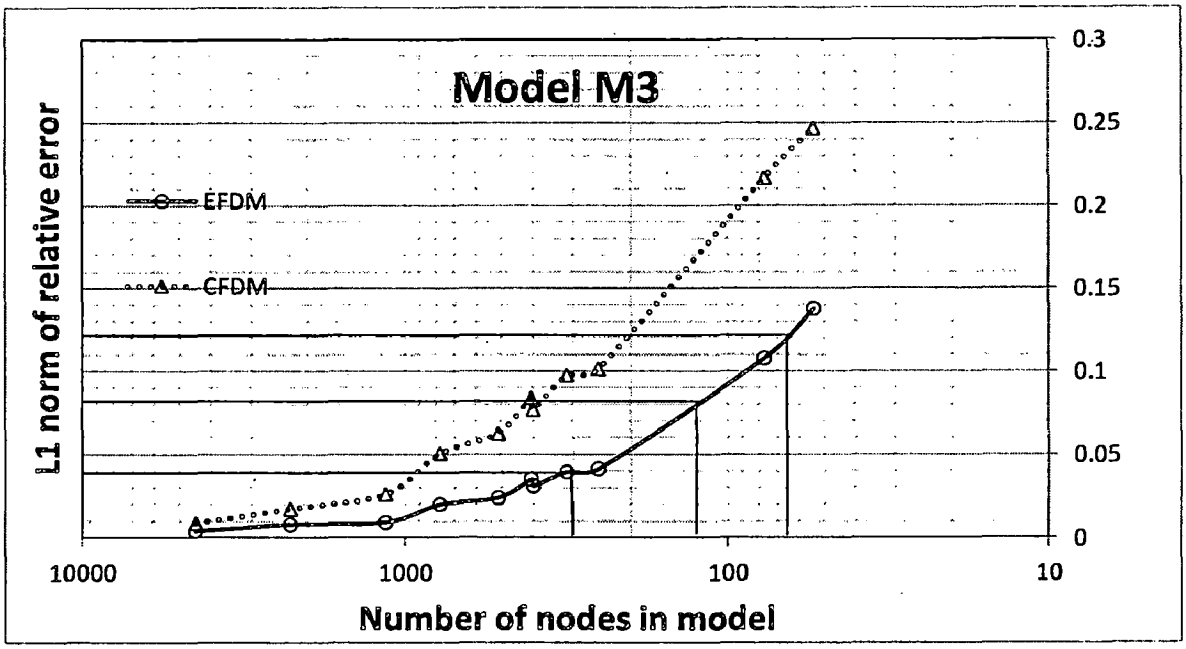

Figure 6.12: Variation of ξ with different number of nodes for model M_3.

Figure 6.12 clearly shows that the relative error in EFDM is less than error in CFDM hence EFDM gives more accurate result in comparison to CFDM for a given number of nodes. In

other way, we can use coarser grid in EFDM to get same accuracy of results as we get with CFDM with finer grid and this is demonstrated in Table 6.3 from Figure 6.12.

Table 6.3: Number of nodes required for same accuracy using both CFDM and EFDM in M_3.

S.N.	Relative error	No. of nodes used in		Reduction of no. of nodes
		CFDM	EFDM	
1.	4%	900	300	67%
2.	8%	400	130	67%
3.	12%	200	66	67%

Table 6.3 clearly shows that about 67% less number of nodes requires in EFDM to get same accuracy of results as we obtained using CFDM with a given nodes, illustrating that EFDM requires less time and cost of computations in comparison to CFDM.

6.3.5 Model M_4

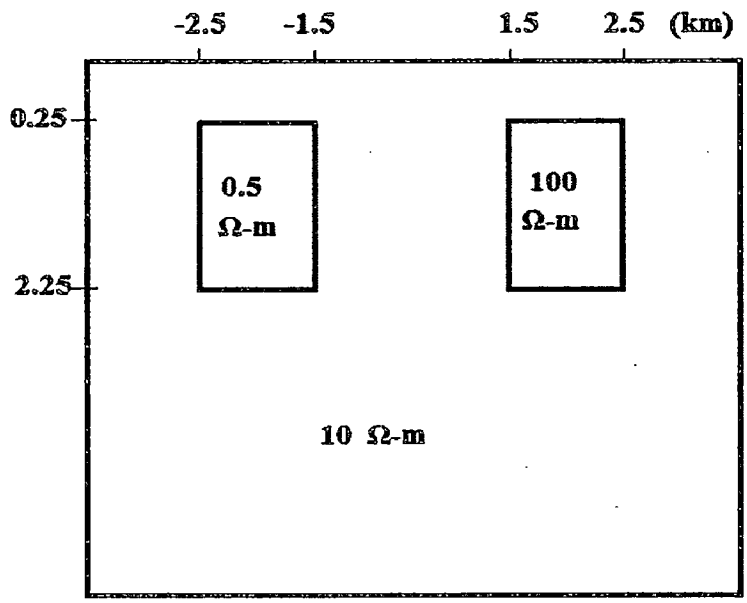

Figure 6.13: Model M_4 (distance in km and resistivity in Ωm).

This model comprises two rectangular blocks embedded in homogeneous half space. The resistivities of the inserted blocks are 0.5 Ωm and 100 Ωm while that of the half space is 10 Ωm. The blocks, placed at a depth of 250 m from the earth surface, have a width of 1 km and

thickness of 2 km each. The MT responses such as electric field and apparent resistivity are computed for a period of 0.1 s. Plot of relative error (ξ) against different number of nodes for model M_4 is shown in Figure 6.14 using both CFDM and EFDM.

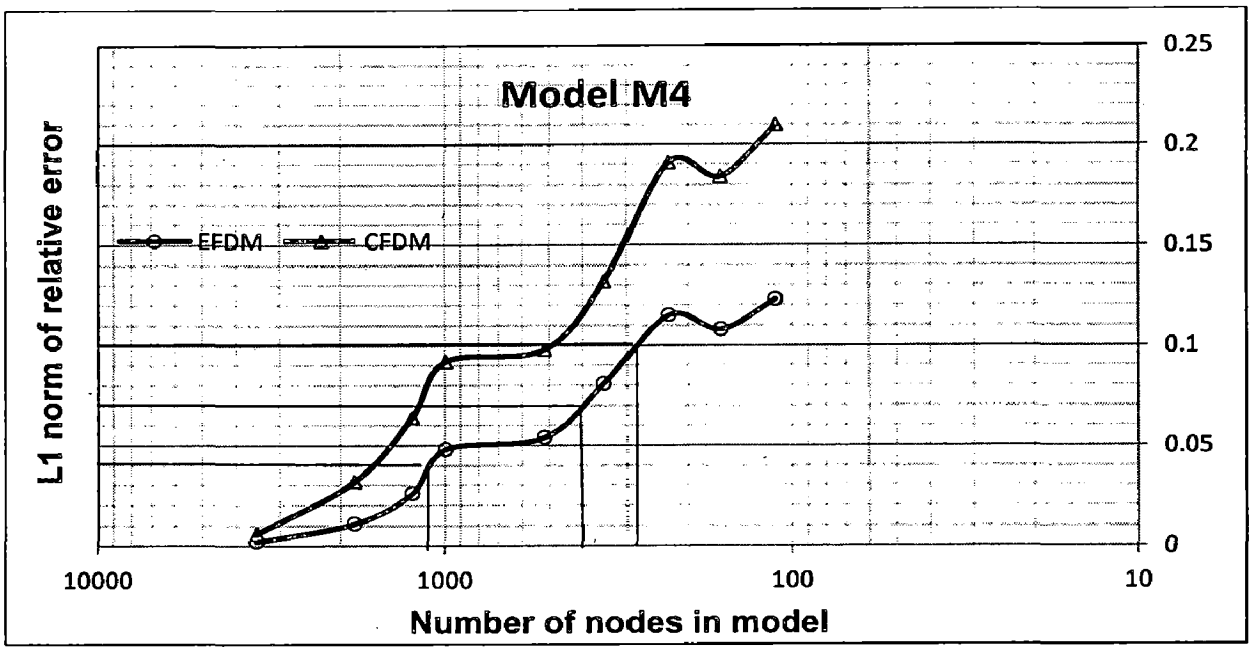

Figure 6.14: Variation of ξ (L_1 norm of relative error) with different number of nodes for model M_4.

Similar to previous models, we can see that relative error in EFDM is much less than error in CFDM hence EFDM gives more accurate result in comparison to CFDM for a given discretization.

Table 6.4: Number of nodes required for same accuracy using both CFDM and EFDM in M_4.

S.N.	Relative error	No. of nodes used in		Reduction of no. of nodes
		CFDM	EFDM	
1.	4%	1700	1100	35%
2.	7%	1200	400	67%
3.	10%	500	280	44%

Table 6.4 clearly illustrate that EFDM required 40-50% less number of nodes to get results having same accuracy as results obtained from CFDM with a given number of nodes, implies that using EFDM we can reduce time and cost of computations in comparison to CFDM.

6.3.6 Model M_5

Again this model has two rectangular blocks embedded in homogeneous half space. The resistivities of the inserted blocks are 2 Ωm and 200 Ωm while that of the half space is 20 Ωm. The blocks, placed at a depth of 1 km from the earth surface, each have a width of 1 km and thicknesses of 1.5 km and 3 km respectively. The MT responses such as electric field and apparent resistivity are computed for a period of 0.1 s. Plot of ξ against different number of nodes for model M_5 is shown in Figure 6.16 using both CFDM and EFDM.

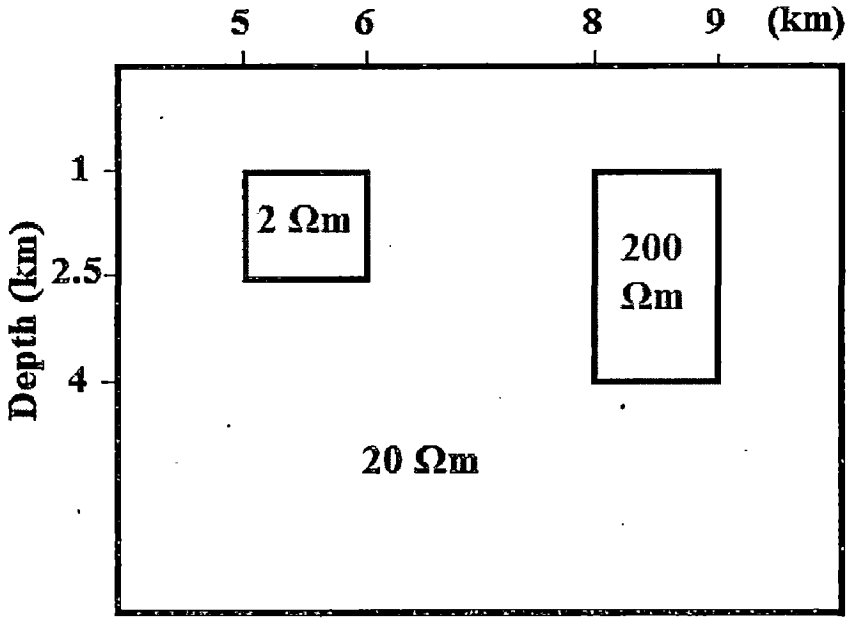

Figure 6.15: Test Model M_5 (distance in km and resistivity in Ωm).

Similar to previous models, we again see that relative error in EFDM is much less than error in CFDM hence EFDM gives more accurate results in comparison to CFDM for a given discretization. Alternatively, we can use coarser grid in EFDM to get same accuracy of results as we get with CFDM with finer grid and this is demonstrated in Table 6.5 from Figure 6.16.

Table 6.5 clearly illustrate that EFDM required 90% less number of nodes to get results having same accuracy as results obtained from CFDM with a given number of nodes, implies that using EFDM we can sufficiently reduce time and cost of computations in comparison to CFDM.

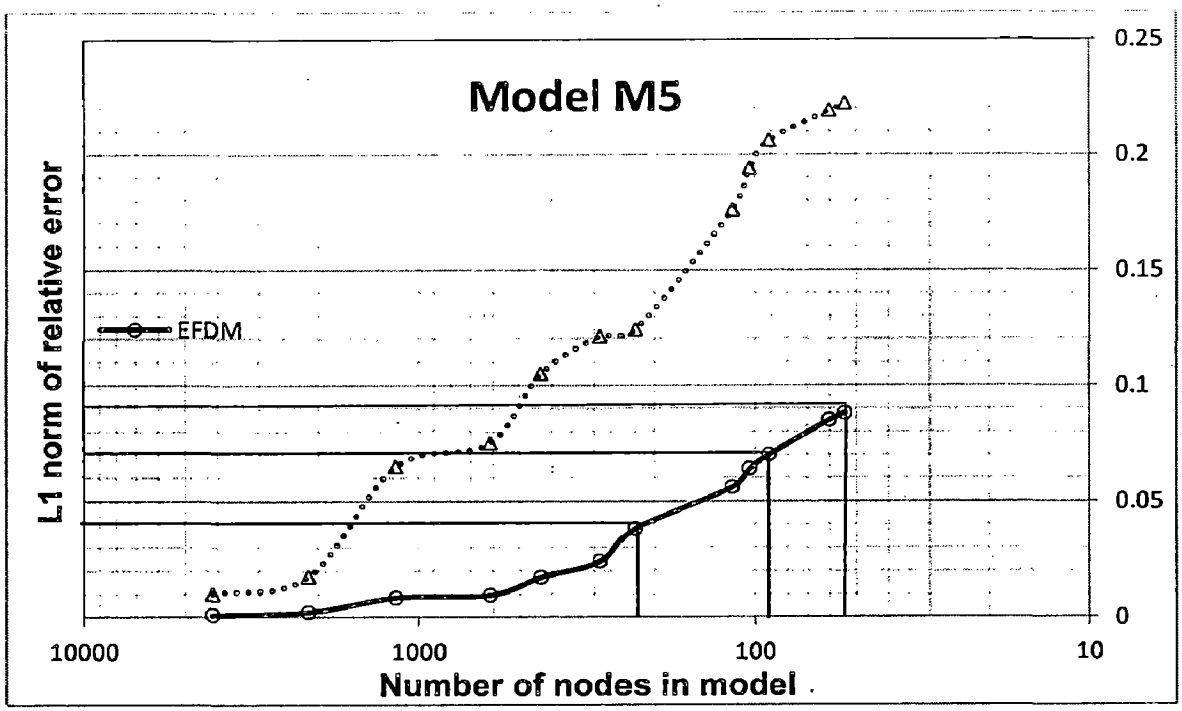

Figure 6.16: Variation of ξ (L_1 norm of relative error) with different number of nodes for model M_5.

Table 6.5: Number of nodes required for same accuracy using both CFDM and EFDM in M_5.

S.N.	Relative error	No. of nodes used in		Reduction of no. of nodes
		CFDM	EFDM	
1.	4%	1600	220	85%
2.	7%	1000	90	90%
3.	9%	500	55	89%

6.3.7 Model M_6

Model M_6 (Figure 6.17 (a)) is similar to M_5 except for a two layered host instead of uniform half space. The resistivities of these two layered are 20 Ω-m and 100 Ω-m. The first layer has thickness of 4 km. The MT responses are computed for a period of 0.1 s. Plot of ξ against different number of nodes for model M_6 is shown in Figure 6.17 (b) using both CFDM and EFDM. The same experiment demonstrate that EFDM requires about 40-70% less number of nodes (Table 6.6) in comparison to nodes required for CFDM to get same accuracy of results, again illustrating that EFDM requires less time and cost of computations in comparison to CFDM.

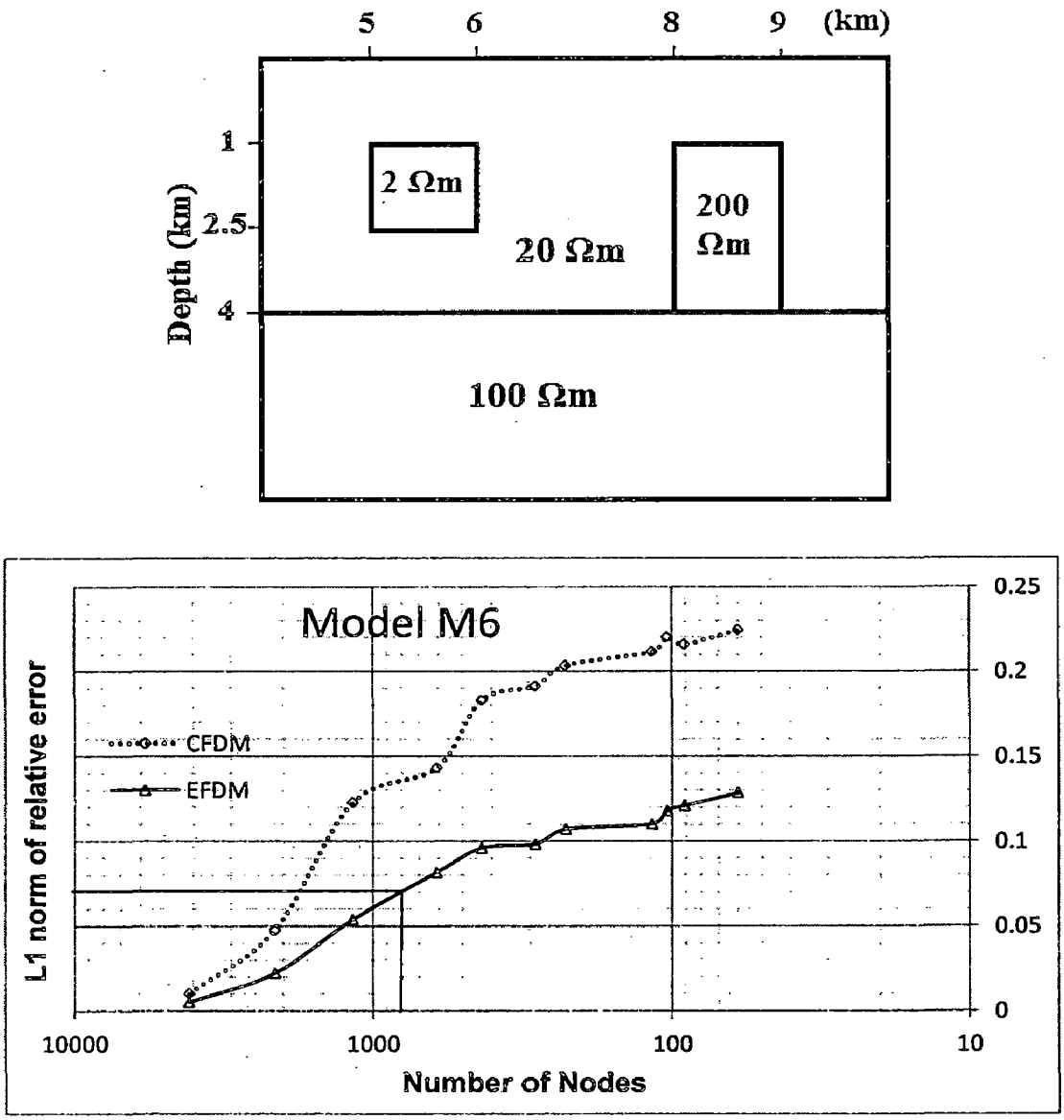

Figure 6.17: (a) Test Model M_6 (distance in km and resistivity in Ωm). (b) Variation of ξ (L_1 norm of relative error) with different number of nodes for model M_6.

Table 6.6: Number of nodes required for same accuracy using both CFDM and EFDM in M_5.

S.N.	Relative error	No. of nodes used in		Reduction of no. of nodes
		CFDM	EFDM	
1.	5%	2100	1200	43%
2.	7%	1800	800	55%
3.	10%	1500	400	73%

From these error plots for different 2D Earth models, we can easily see that relative error in EFDM is less in comparison to CFDM hence EFDM gives more accurate result in comparison to CFDM for a given number of nodes. Above experiments also reveals that, EFDM requires 50-80% less number of nodes in comparison to CFDM to get same accuracy of results, illustrate that we can use coarse grid for EFDM to obtain same accuracy of result as we get using CFDM with fine grid. As a result EFDM sufficiently reduces the time and cost of computation as compared to CFDM.

CHAPTER 7

CONCLUSIONS AND DISCUSSIONS

In this dissertation we have developed two forward modeling algorithms, 2D Classical Finite Difference Method algorithm (MT_2D_CFDM) based on monomials as basis function and 2D Exponential Finite Difference Method algorithm (MT_2D_EFDM) using exponential basis function. The crucial part in EFDM is the selection of optimum value of μ. Using model parameters we defined formula for μ that gives near optimal results. Both the developed numerical algorithm MT_2D_CFDM and MT_2D_EFDM are applied on different 2D earth models for solving 2D Helmholtz equation. From the experiments we observed that proposed EFDM gives more accurate results than CFDM with a given grid. Alternatively, EFDM employs 50-80 % less number of nodes to obtain results identical to CFDM with a given number of nodes. Therefore, using EFDM we can sufficiently reduce time and cost of computation in comparison to CFDM. If we deal with 3D problems, the superiority of proposed EFDM would be much greater than CFDM in respect of time and cost of computations. If we choose same number of nodes in both CFDM and EFDM then we have more accurate forward model responses using EFDM implies that inversion results gives more accurate model using EFDM in comparison to CFDM.

7.1 Limitations of the Algorithms

There are certain limitations of the algorithm identified during testing are as follows,

- In EFDM, only near optimal value of μ is used by model parameters and for very complex models this estimator does not gives much better results.
- At the bottom of the modeling domain, perfectly conducting boundary condition is employed in the algorithm. This constraint forces one to take bottom at sufficient distance so that the tangential electric field will be zero at the domain boundary.
- Presently the algorithm can be used only for the plane wave source.

7.2 Suggestions for future work

This dissertation opens up more interesting prospects for future research work. The work presented so far to compute magnetotelluric response of 2D earth models.

There are things that can be done for future developments of proposed EFDM. These are listed below:

7.2.1 Modification of algorithm for Controlled Source EM

The algorithm can be modified for the computation of responses in case of controlled source EM methods simply by replacing the present primary field response computation subprogram with one corresponding to the given EM source.

7.2.2 Extending to 3D models

From this dissertation work, as EFDM shows more improve result in comparison to CFDM in 2D model, then for 3D models, the improvements will get multiplied and will give a lot better result as compared to existing CFDM results. It is highly probable that EFDM will significantly reduce the number of node points in three dimensions earth modelling therefore EFDM will make matrix size very small as compared to matrix size obtained by CFDM hence the superiority of proposed EFDM would be much greater than CFDM in respect of time and cost of computations.

7.2.3 Application of EFDM for another field of Geophysics

Since other many geophysical fields have oscillatory behaviours therefore apart from Magnetotelluric, the proposed scheme can be tested in other disciplines like Geophysical Fluid Dynamics, Seismology, and Seismic Prospecting etc.

7.2.4 Experiments to obtained optimum μ

In this dissertation the near optimal μ is obtained using model parameters but there can be scope to get better estimator of μ for 2D Earth models. Eigenvalue Analysis of coefficient matrix based on Young's work of Young (1950) or Maximum Entropy Method can be used to get better estimator of μ.

7.2.5 Experiments with self-consistency equation

It is also possible to play with self-consistency equation (Equation 4.18) and to look for the scope of incorporating more exponential terms in basis function to set up EFDM for 2D and 3D earth models.

APPENDIX A.1

SAMPLE INPUT FILE & ALGORITHM PARAMETERS

The complete descriptions about development of algorithms are given in Chapter 5. The generation of input files from the 2D earth model shown in Figure A.1, is explained below.

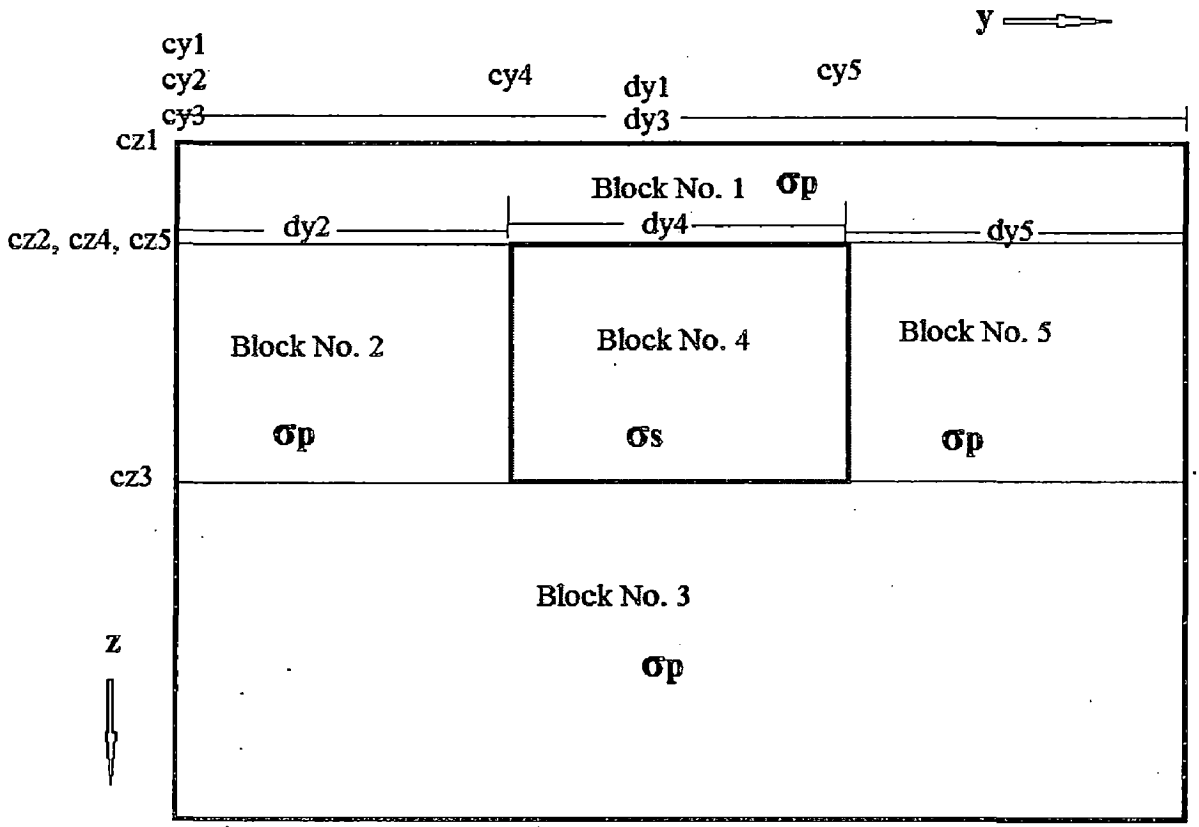

Figure A.1.1: Labelled 2D Earth Model for generation of Input file. Thin line is used to divide whole model into different conductive rectangular blocks.

σ_p= Host conductivity and σ_s= Anomalous body conductivity

Other details of labelling used in this model and input parameters are given in Table A.1.2. The input data and other parameters are also controlled by different counters. The details of these counters along with their values and descriptions are presented in Table A.1. Sample *input* file is presented after the descriptions of these parameters.

Table A.1.1: Description of control parameters.

Parameter	Controls	Value	Descriptions
fcount	Field continuation	0	No field continuation
		1	Field continuation
sbcount	Side boundary condition	0	Neumann boundary condition
		1	Dirichlet boundary condition
		2	Mixed boundary condition
gridcount	Grid generator	0	Uniform grid
		1	Skin depth based grid
		2	Manual grid
ncond	Input data type	0	Data in conductivity
		1	Data in resistivity

Table A.1.2: Description of parameters in *input* file.

Parameters	Descriptions
itmax	Maximum number of iterations for BiCGStab convergence
tol	Tolerance parameter for BiCGStab
scale	Scale for data e.g. if y and z coordinates are in km then scale = 1000 and if in meter scale = 1
nobs	Number of observation points in y or z direction
ynobs	Co-ordinated of observation points in y direction
znobs	Co-ordinated of observation points in z direction
cy	The horizontal location of the left edge of each block
cz	The vertical location of the top left corner of each block
dy	The horizontal width of each block
dz	the vertical depth of each block
yy1, yy2	The horizontal location of the left and right edge of host block
zz1, zz2	The vertical location of the top left corner and bottom left corner host block
blk	Number of anomalous body

nb	Block number of anomalous body
nrperiod	Number of reference frequency used in automatic grid generator
refperiod	Reference period for automatic grid generator
period	Period of signal used in MT model

A.1. Sample Input File

Input.dat

```
Test_Model_M    ! Title of Model

 1          !fcount(=0 or 1)
 1          !sbcount(=0 or 1 or 2)
 2          !gridcount( =0 or 1 or 2)

      10000         !itmax (for BiCGStab)
      1.0e-10       !tol (for BiCGStab)

 1                  !ncond
 1000.0             !scale

        6           !nobs
        0.0,0.5,1.0,2.0,4.0,5.0     !ynobs (km)
        0.0,0.0,0.0,0.0,0.0,0.0     !znobs (km)

     -8.    0.     16.    0.25   100.    ! cy1   cz1   dy1   dz1   ρp
     -8.    0.25   7.5    2.0    100.    ! cy2   cz2   dy2   dz2   ρp
     -8.0   2.25   16.0   9.75   100.    ! cy3   cz3   dy3   dz3   ρp
     -0.5   0.25   1.0    2.0    0.5     ! cy4   cz4   dy4   dz4   ρs
      0.5   0.25   7.5    2.0    100.    ! cy5   cz5   dy5   dz5   ρp
     -8.0   12.0   16.0   2.0    0.001   ! last block taken as highly conducting
     5555   0      0      0      0         !end of data

 -8,8           ! yy-y domain(left right co-ordinate)
 0,12           ! zz-z domain (z co-ordinates of Host)

 1              !blk- number of anomalous body
 4              !nb-block no. of anomalous body

 1,1            !nrperiod,mpr
 0.1            !refperiod

 1              !nperiod
 0.1            ! period
```

APPENDIX A.2

SAMPLE OUTPUT FILES

out_main.dat

```
2D MT _EFDM
  1          ! fcount(=0 or 1)
  1          ! sbcount(=0 or 1 or 2) (side boundary cond)
  2          ! gridcount( =0 or 1 or 2)
   10000          ! itmax (for BiCG)
   1.0e-10        ! tol (for BiCG)

        1          ! ncond
     1000.0        ! scale
        6          ! nobs
0.0, 0.5, 1.0, 2.0, 4.0, 5.0     ! ynobs (km)
0.0, 0.0, 0.0, 0.0, 0.0, 0.0     ! znobs (km)

  -8.      0.       16.      0.25          100.
  -8.      0.25     7.5      2.0           100.
  -8.0     2.25     16.0     9.75          100.
  -0.5     0.25     1.0      2.0           0.5
   0.5     0.25     7.5      2.0           100.
  -8.0     12.0     16.0     2.0           0.001
  5555     0        0        0             0      !end of data

-8,8          ! y domain(left right co-ordinate)
0,12          ! z domain (z co-ordinates of Host)
1             ! number of anomalous body
4             !block no. of anomalous body
```

1,1	!nrperiod,mpr
0.1	!refperiod
1	!nperiod
0.1	! period

i,	b(i),	bh(i)
1	2.000E+03	2.000E+03
2	8.100E+02	1.405E+03
3	3.190E+03	2.000E+03
4	1.275E+03	2.233E+03
5	2.250E+02	7.500E+02
6	2.530E+02	2.390E+02
7	5.600E+01	1.545E+02
8	1.910E+02	1.235E+02
9	2.470E+02	2.190E+02
10	1.970E+02	2.220E+02
11	5.600E+01	1.265E+02
12	5.600E+01	5.600E+01
13	1.194E+03	6.250E+02
14	2.500E+02	7.220E+02
15	2.000E+03	1.125E+03
16	2.000E+03	2.000E+03
17	2.000E+03	2.000E+03
18	0.000E+00	2.000E+03

i,	c(i),	ch(i)
1	2.220E+02	2.220E+02
2	2.800E+01	1.250E+02
3	2.800E+01	2.800E+01
4	3.940E+02	2.110E+02
5	1.268E+03	8.310E+02

6	1.500E+02	7.090E+02
7	4.000E+01	9.500E+01
8	9.000E+01	6.500E+01
9	3.000E+01	6.000E+01
10	1.050E+03	5.400E+02
11	3.300E+02	6.900E+02
12	1.370E+03	8.500E+02
13	1.110E+03	1.240E+03
14	6.900E+02	9.000E+02
15	1.500E+02	4.200E+02
16	9.200E+02	5.350E+02
17	3.300E+02	6.250E+02
18	3.000E+02	3.150E+02
19	1.220E+03	7.600E+02
20	8.000E+01	6.500E+02
21	1.400E+03	7.400E+02
22	3.000E+02	8.500E+02
23	4.000E+02	3.500E+02
24	1.000E+02	2.500E+02
25	0.000E+00	1.000E+02

the counter for res./cond." ncond " = 1

scaling factor " scale" = 1.00E+03

Primary field {efield}

1	6.28319E-02	6.28319E-02
2	6.17191E-02	4.65222E-02
3	6.14375E-02	4.46370E-02
4	6.11283E-02	4.27898E-02
5	5.44540E-02	2.06939E-02
6	2.38317E-02	-1.10320E-02
7	2.06471E-02	-1.20362E-02
8	1.98333E-02	-1.22398E-02

9	1.80592E-02	-1.26077E-02
10	1.74856E-02	-1.27041E-02
11	3.11724E-03	-1.07303E-02
12	6.83870E-04	-9.05583E-03
13	-2.71530E-03	-2.71578E-03
14	-1.90374E-03	-1.68948E-04
15	-1.16445E-03	4.18754E-04
16	-1.01868E-03	4.79219E-04
17	-3.28738E-04	5.38651E-04
18	-1.70008E-04	4.84995E-04
19	-6.19506E-05	4.22983E-04
20	1.16944E-04	1.72885E-04
21	1.18629E-04	1.60055E-04
22	6.19748E-05	2.60809E-05
23	3.94714E-05	1.42766E-052766E-05

out6_result.dat

5346

384

i	z	y	Re(E)	Im(E)	Re(H)	Im(H)	App. Res	Phase
1	0.00E+00	-6.00E+03	6.28E-02	6.28E-02	9.97E-01	-6.00E-02	1.00E+02	4.84E+01
2	0.00E+00	-5.19E+03	6.28E-02	6.28E-02	9.65E-01	-2.86E-02	1.07E+02	4.67E+01
3	0.00E+00	-2.00E+03	6.28E-02	6.28E-02	9.65E-01	-2.86E-02	1.07E+02	4.67E+01
4	0.00E+00	-7.25E+02	6.28E-02	6.28E-02	9.65E-01	-2.86E-02	1.07E+02	4.67E+01
5	0.00E+00	-5.00E+02	6.28E-02	6.28E-02	9.65E-01	-2.86E-02	1.07E+02	4.67E+01
6	0.00E+00	-2.47E+02	6.28E-02	6.28E-02	9.65E-01	-2.86E-02	1.07E+02	4.67E+01
7	0.00E+00	-1.91E+02	6.28E-02	6.28E-02	9.65E-01	-2.86E-02	1.07E+02	4.67E+01
8	0.00E+00	0.00E+00	6.28E-02	6.28E-02	9.65E-01	-2.86E-02	1.07E+02	4.67E+01
9	0.00E+00	2.47E+02	6.28E-02	6.28E-02	9.65E-01	-2.86E-02	1.07E+02	4.67E+01
10	0.00E+00	4.44E+02	6.28E-02	6.28E-02	9.65E-01	-2.86E-02	1.07E+02	4.67E+01
11	0.00E+00	5.00E+02	6.28E-02	6.28E-02	9.65E-01	-2.86E-02	1.07E+02	4.67E+01

12	0.00E+00	5.56E+02	6.28E-02	6.28E-02	9.65E-01	-2.86E-02	1.07E+02	4.67E+01
13	0.00E+00	1.75E+03	6.28E-02	6.28E-02	9.65E-01	-2.86E-02	1.07E+02	4.67E+01
14	0.00E+00	2.00E+03	6.28E-02	6.28E-02	9.65E-01	-2.86E-02	1.07E+02	4.67E+01
15	0.00E+00	4.00E+03	6.28E-02	6.28E-02	9.65E-01	-2.86E-02	1.07E+02	4.67E+01
16	0.00E+00	6.00E+03	6.28E-02	6.28E-02	9.71E-01	-2.90E-02	1.06E+02	4.67E+01
17	2.22E+02	-6.00E+03	6.17E-02	4.65E-02	9.22E-01	-7.06E-02	8.85E+01	4.14E+01
18	2.22E+02	-5.19E+03	6.17E-02	4.65E-02	9.22E-01	-7.06E-02	8.85E+01	4.14E+01
19	2.22E+02	-2.00E+03	6.17E-02	4.65E-02	9.22E-01	-7.06E-02	8.85E+01	4.14E+01
20	2.22E+02	-7.25E+02	6.17E-02	4.65E-02	9.22E-01	-7.06E-02	8.85E+01	4.14E+01
21	2.22E+02	-5.00E+02	6.17E-02	4.65E-02	9.22E-01	-7.06E-02	8.85E+01	4.14E+01
22	2.22E+02	-2.47E+02	6.17E-02	4.65E-02	9.22E-01	-7.06E-02	8.85E+01	4.14E+01
23	2.22E+02	-1.91E+02	6.17E-02	4.65E-02	9.22E-01	-7.06E-02	8.85E+01	4.14E+01
24	2.22E+02	0.00E+00	6.17E-02	4.65E-02	9.22E-01	-7.06E-02	8.85E+01	4.14E+01
25	2.22E+02	2.47E+02	6.17E-02	4.65E-02	9.22E-01	-7.06E-02	8.85E+01	4.14E+01
26	2.22E+02	4.44E+02	6.17E-02	4.65E-02	9.22E-01	-7.06E-02	8.85E+01	4.14E+01
27	2.22E+02	5.00E+02	6.17E-02	4.65E-02	9.22E-01	-7.06E-02	8.85E+01	4.14E+01
28	2.22E+02	5.56E+02	6.17E-02	4.65E-02	9.22E-01	-7.06E-02	8.85E+01	4.14E+01
29	2.22E+02	1.75E+03	6.17E-02	4.65E-02	9.22E-01	-7.06E-02	8.85E+01	4.14E+01
30	2.22E+02	2.00E+03	6.17E-02	4.65E-02	9.22E-01	-7.06E-02	8.85E+01	4.14E+01
31	2.22E+02	4.00E+03	6.17E-02	4.65E-02	9.22E-01	-7.06E-02	8.85E+01	4.14E+01
32	2.22E+02	6.00E+03	6.17E-02	4.65E-02	9.22E-01	-7.06E-02	8.85E+01	4.14E+01
33	2.50E+02	-6.00E+03	6.14E-02	4.46E-02	8.44E-01	-1.34E-01	1.00E+02	4.50E+01
34	2.50E+02	-5.19E+03	6.14E-02	4.46E-02	8.44E-01	-1.34E-01	1.00E+02	4.50E+01
35	2.50E+02	-2.00E+03	6.14E-02	4.46E-02	8.44E-01	-1.34E-01	1.00E+02	4.50E+01
36	2.50E+02	-7.25E+02	6.14E-02	4.46E-02	8.44E-01	-1.34E-01	1.00E+02	4.50E+01
37	2.50E+02	-5.00E+02	6.14E-02	4.46E-02	8.44E-01	-1.34E-01	1.00E+02	4.50E+01
38	2.50E+02	-2.47E+02	6.14E-02	4.46E-02	8.44E-01	-1.34E-01	1.00E+02	4.50E+01
39	2.50E+02	-1.91E+02	6.14E-02	4.46E-02	8.44E-01	-1.34E-01	1.00E+02	4.50E+01
40	2.50E+02	0.00E+00	6.14E-02	4.46E-02	8.44E-01	-1.34E-01	1.00E+02	4.50E+01
41	2.50E+02	2.47E+02	6.14E-02	4.46E-02	8.44E-01	-1.34E-01	1.00E+02	4.50E+01
42	2.50E+02	4.44E+02	6.14E-02	4.46E-02	8.44E-01	-1.34E-01	1.00E+02	4.50E+01

43	2.50E+02	5.00E+02	6.14E-02	4.46E-02	8.44E-01	-1.34E-01	1.00E+02	4.50E+01
44	2.50E+02	5.56E+02	6.14E-02	4.46E-02	8.44E-01	-1.34E-01	1.00E+02	4.50E+01
45	2.50E+02	1.75E+03	6.14E-02	4.46E-02	8.44E-01	-1.34E-01	1.00E+02	4.50E+01
46	2.50E+02	2.00E+03	6.14E-02	4.46E-02	8.44E-01	-1.34E-01	1.00E+02	4.50E+01
47	2.50E+02	4.00E+03	6.14E-02	4.46E-02	8.44E-01	-1.34E-01	1.00E+02	4.50E+01
48	2.50E+02	6.00E+03	6.14E-02	4.46E-02	8.44E-01	-1.34E-01	1.00E+02	4.50E+01
49	2.78E+02	-6.00E+03	6.11E-02	4.28E-02	7.19E-01	-2.10E-01	1.26E+02	5.13E+01
50	2.78E+02	-5.19E+03	6.11E-02	4.28E-02	7.19E-01	-2.10E-01	1.26E+02	5.13E+01
51	2.78E+02	-2.00E+03	6.11E-02	4.28E-02	7.19E-01	-2.10E-01	1.26E+02	5.13E+01
52	2.78E+02	-7.25E+02	6.11E-02	4.28E-02	7.19E-01	-2.10E-01	1.26E+02	5.13E+01
53	2.78E+02	-5.00E+02	6.11E-02	4.28E-02	7.19E-01	-2.10E-01	1.26E+02	5.13E+01
54	2.78E+02	-2.47E+02	6.11E-02	4.28E-02	7.19E-01	-2.10E-01	1.26E+02	5.13E+01
55	2.78E+02	-1.91E+02	6.11E-02	4.28E-02	7.19E-01	-2.10E-01	1.26E+02	5.13E+01
56	2.78E+02	0.00E+00	6.11E-02	4.28E-02	7.19E-01	-2.10E-01	1.26E+02	5.13E+01
57	2.78E+02	2.47E+02	6.11E-02	4.28E-02	7.19E-01	-2.10E-01	1.26E+02	5.13E+01
58	2.78E+02	4.44E+02	6.11E-02	4.28E-02	7.19E-01	-2.10E-01	1.26E+02	5.13E+01
59	2.78E+02	5.00E+02	6.11E-02	4.28E-02	7.19E-01	-2.10E-01	1.26E+02	5.13E+01
60	2.78E+02	5.56E+02	6.11E-02	4.28E-02	7.19E-01	-2.10E-01	1.26E+02	5.13E+01
61	2.78E+02	1.75E+03	6.11E-02	4.28E-02	7.19E-01	-2.10E-01	1.26E+02	5.13E+01
62	2.78E+02	2.00E+03	6.11E-02	4.28E-02	7.19E-01	-2.10E-01	1.26E+02	5.13E+01
63	2.78E+02	4.00E+03	6.11E-02	4.28E-02	7.19E-01	-2.10E-01	1.26E+02	5.13E+01
64	2.78E+02	6.00E+03	6.11E-02	4.28E-02	7.19E-01	-2.10E-01	1.26E+02	5.13E+01
65	6.72E+02	-6.00E+03	5.45E-02	2.07E-02	4.10E-01	-2.84E-01	1.73E+02	5.55E+01
66	6.72E+02	-5.19E+03	5.45E-02	2.07E-02	4.10E-01	-2.84E-01	1.73E+02	5.55E+01
67	6.72E+02	-2.00E+03	5.45E-02	2.07E-02	4.10E-01	-2.84E-01	1.73E+02	5.55E+01
68	6.72E+02	-7.25E+02	5.45E-02	2.07E-02	4.10E-01	-2.84E-01	1.73E+02	5.55E+01
69	6.72E+02	-5.00E+02	5.45E-02	2.07E-02	4.10E-01	-2.84E-01	1.73E+02	5.55E+01
70	6.72E+02	-2.47E+02	5.45E-02	2.07E-02	4.10E-01	-2.84E-01	1.73E+02	5.55E+01
71	6.72E+02	-1.91E+02	5.45E-02	2.07E-02	4.10E-01	-2.84E-01	1.73E+02	5.55E+01
72	6.72E+02	0.00E+00	5.45E-02	2.07E-02	4.10E-01	-2.84E-01	1.73E+02	5.55E+01
73	6.72E+02	2.47E+02	5.45E-02	2.07E-02	4.10E-01	-2.84E-01	1.73E+02	5.55E+01

74	6.72E+02	4.44E+02	5.45E-02	2.07E-02	4.10E-01	-2.84E-01	1.73E+02	5.55E+01
75	6.72E+02	5.00E+02	5.45E-02	2.07E-02	4.10E-01	-2.84E-01	1.73E+02	5.55E+01
76	6.72E+02	5.56E+02	5.45E-02	2.07E-02	4.10E-01	-2.84E-01	1.73E+02	5.55E+01
77	6.72E+02	1.75E+03	5.45E-02	2.07E-02	4.10E-01	-2.84E-01	1.73E+02	5.55E+01
78	6.72E+02	2.00E+03	5.45E-02	2.07E-02	4.10E-01	-2.84E-01	1.73E+02	5.55E+01
79	6.72E+02	4.00E+03	5.45E-02	2.07E-02	4.10E-01	-2.84E-01	1.73E+02	5.55E+01
80	6.72E+02	6.00E+03	5.45E-02	2.07E-02	4.10E-01	-2.84E-01	1.73E+02	5.55E+01
81	1.94E+03	-6.00E+03	2.38E-02	-1.10E-02	2.92E-01	-3.02E-01	4.94E+01	2.11E+01
82	1.94E+03	-5.19E+03	2.38E-02	-1.10E-02	2.92E-01	-3.02E-01	4.94E+01	2.11E+01
83	1.94E+03	-2.00E+03	2.38E-02	-1.10E-02	2.92E-01	-3.02E-01	4.94E+01	2.11E+01
84	1.94E+03	-7.25E+02	2.38E-02	-1.10E-02	2.92E-01	-3.02E-01	4.94E+01	2.11E+01
85	1.94E+03	-5.00E+02	2.38E-02	-1.10E-02	2.92E-01	-3.02E-01	4.94E+01	2.11E+01
86	1.94E+03	-2.47E+02	2.38E-02	-1.10E-02	2.92E-01	-3.02E-01	4.94E+01	2.11E+01
87	1.94E+03	-1.91E+02	2.38E-02	-1.10E-02	2.92E-01	-3.02E-01	4.94E+01	2.11E+01
88	1.94E+03	0.00E+00	2.38E-02	-1.10E-02	2.92E-01	-3.02E-01	4.94E+01	2.11E+01
89	1.94E+03	2.47E+02	2.38E-02	-1.10E-02	2.92E-01	-3.02E-01	4.94E+01	2.11E+01
90	1.94E+03	4.44E+02	2.38E-02	-1.10E-02	2.92E-01	-3.02E-01	4.94E+01	2.11E+01
91	1.94E+03	5.00E+02	2.38E-02	-1.10E-02	2.92E-01	-3.02E-01	4.94E+01	2.11E+01
92	1.94E+03	5.56E+02	2.38E-02	-1.10E-02	2.92E-01	-3.02E-01	4.94E+01	2.11E+01
93	1.94E+03	1.75E+03	2.38E-02	-1.10E-02	2.92E-01	-3.02E-01	4.94E+01	2.11E+01
94	1.94E+03	2.00E+03	2.38E-02	-1.10E-02	2.92E-01	-3.02E-01	4.94E+01	2.11E+01
95	1.94E+03	4.00E+03	2.38E-02	-1.10E-02	2.92E-01	-3.02E-01	4.94E+01	2.11E+01
96	1.94E+03	6.00E+03	2.38E-02	-1.10E-02	2.92E-01	-3.02E-01	4.94E+01	2.11E+01
97	2.09E+03	-6.00E+03	2.06E-02	-1.20E-02	8.05E-02	-2.67E-01	9.33E+01	4.30E+01

Contd. till 384th node.....

383	1.19E+04	4.00E+03	7.98E-06	2.60E-06	3.30E-04	-1.01E-03	7.90E-01	-9.00E+01
384	1.19E+04	6.00E+03	7.98E-06	2.60E-06	3.30E-04	-1.01E-03	7.90E-01	-9.00E+01

APPENDIX A.3

BiCG Method

Basic steps of Bi-conjugate gradient method to solve matrix equation Ax=b

Consider: Ax = b

Start with: x_0 = an initial estimate of solution

Residual: $r_0 = b - Ax_0$

Bi-residual: $\hat{r}_0 = r_0^*$

Initial search vector: $p_0 = r_0$

Bi-search vector: $\hat{p}_0 = p_0^*$

For iterations i = 0, 1, 2 ,3, ...

Step length coefficients

$$\alpha_i = \frac{(\hat{r}_i, r_i)}{(\hat{p}_i, Ap_i)}$$

New estimate: $x_{i+1} = x_i + \alpha_i p_i$

New residual: $r_{i+1} = r_i - \alpha_i A p_i$

Bi-residual: $\hat{r}_{i+1} = \hat{r}_i - \alpha^*{}_i A^H \hat{p}_i$

Bi-conjugate coefficient:

$$\beta_i = \frac{(A^H \hat{p}_i, r_{i+1})}{(\hat{p}_i, Ap_i)}$$

New search vector: $p_{i+1} = r_{i+1} + \beta_i p_i$

Bi-search vector: $\hat{p}_{i+1} = \hat{r}_{i+1} + \beta^*{}_i \hat{p}_i$

Continue until $r_{i+1} = 0$

In above steps, H indicates Hermitian conjugate, the inner product (x,y) = $x^H y$ and * denotes the complex conjugate.

REFERENCES

Adam, A., 1997. Magnetotelluric phase anisotropy above extensional structures of the Neogene Pannonian Basin. J. Geomag. Geoelec., 49, 1549-1557.

Berdichevsky, M. N., and Zhdanov, M. S., 1984. Advanced theory of deep geomagnetic sounding. Elsevier, Amsterdam, pp. 408.

Brewitt-Taylor, C. R., and Weaver, J. T., 1976. On the finite difference solution of two dimensional induction problems; Geophys. J. R. Atsr. Soc., 47, 375-396.

Born, M., and Wolf, E., 2005. Principles of optics, 7th edition. Cambridge University Press, UK, pp. 952.

Forsythe, G. E. and Wasow, W. A., 1964. Finite difference method for partial differential equations. Wiley, New York, pp. 444.

Fox, L., and Ingerov, O., 2007. Natural source EM for offshore hydrocarbon detection offers potential cost savings. First Break, 25, 87-96.

Grant, F. S., and West, G. F., 1965. Interpretation theory in applied geophysics. McGraw-HiliBook Company, New York, pp. 584.

Gupta, P. K., Niwas, S. and Rastogi A., 1999. EM2INV – A finite difference based algorithm for two-dimensional inversion of geoelectromagnetic data; Earth Planet. Sci., **108**, 233–253.

Harinarayana, T., Murthy, D. N., Eknath Rao, S. P., Manoj, C., Veeraswamy, K., Naganjaneyulu, K., Abdul Azeez, K. K., Sastry, R. S., and Virupakshi, G., 2002. Magnetotelluric field investigations in Puga geothermal region, Jammu and Kashmir, India: 1-D modeling results. Geotherm. Resour. Counc. Trans., 26, 393-397.

Hildebrand, F. B., 1974. Introduction to numerical analysis, Tata-McGraw Hill, New Delhi, pp. 669.

Hoover, D. B., Long, C. L., and Senterfit, R. M., 1978. Some results from audiomagnetotellurics investigations in geothermal areas. Geophys., **43**, 1501-1514.

Israil, M., Tyagi, D. K., Gupta, P. K., and Niwas, S., 2008. Magnetotelluric investigations for imaging electrical structure of Garhwal Himalayan corridor Uttarakhand, India. J. Earth. Syst. Sci., **117**, 189-200.

Ixaru, L. Gr., 1997. Operations on oscillatory functions; Compute. Phys. Commun., **105**, 1-19.

Ixaru, L. Gr., and Berghe, G. V., 2004. Exponential fitting; Kluwer Academic Publishers, Dordrecht, pp.1-150.

Jackson, J. D., 1975. Classical electrodynamics. John Wiley and Sons, New York.

Johansen, S. E., Amundsen, H. E. F., Røsten, T., Ellingsrud, S., Eidesmo, T., and Bhuyian, A. H., 2005. Subsurface hydrocarbons detected by electromagnetic sounding. First Break, **23**, 31-36.

Jones, F. W. and Pascoe, L. J., 1971. A general computer program to determine the perturbation of alternating electric currents in a two-dimensional model of a region of uniform conductivity with an embedded inhomogeneity; Geophys. J. R. Astr. Soc., **24**, 3–30.

Kaufman, A. A, and Keller, G. V., 1981. The magnetotelluric sounding method. Elsevier, Amsterdam.

Kong, F. N., Westerdahl, H., Ellingsrud, S., Eidesmo, T., and Johansen, J., 2002. 'Seabed logging': A possible direct hydrocarbon indicator for deep sea prospects using EM energy. Oil and Gas Journal, **100**, 30-38.

Kumar, K., 2009. 3D Simulation of magnetotelluric data using finite difference eigenmode method; Ph. D thesis. Indian Institute of Technology-Roorkee, India.

Lee, T. J., Song, Y., and Uchida, T., 2007. Three-dimensional magnetotelluric surveys for geothermal development in Pohang, Korea. Expol. Geophys., **38**, 89-97.

MacGregor, L., and Sinha, S., 2000. Use of marine controlled-source electromagnetic sounding for sub-basalt exploration. Geophys. Prosp., **48**, 1091-1106.

Mitchell, A. R., and Griffiths, D. F., 1980. The finite difference method in partial differential equations. Wiley-Interscience publication, Chichester, Wiley.

Mitra, R., 1973. Computer techniques for electromagnetics. Pergamon, New York.

Mitra, R., 1975. Numerical and asymptotic techniques in electromagnetics. Springer-Verlag, New York.

Mitsuhata, Y. and Uchida, T., 2004. Three-dimensional magnetotelluric modeling using the T-Ω finite element method; Geophys., **69**, 108–119.

Morgan, M. A., (Ed.), 1990. Finite element and finite difference methods in electromagnetic scattering. Elsevier, New York.

Morse, P. M., and Feshbach, H., 1953. Methods of theoretical physics. McGraw-Hill Book Co., Inc., Tokyo.

Nabighian, M. N. (Ed.), 1988. Electromagnetic methods in applied geophysics, Vol. I, Theory. Soc. Expl. Geophys., Tulsa.

Nabighian, M. N. (Ed.), 1991. Electromagnetic methods in applied geophysics, Vol. II, Applications. Soc. Expl. Geophys., Tulsa.

Nabighian, M. N., 2000. Electromagnetic Methods in Applied Geophysics-Theory, Volume 1; Soc. Expl. Geophys., Tulsa, pp. 1-50.

Pellerin, L., Johnston, J. M., and Hohmann, G. W., 1996. A numerical evaluation of electromagnetic methods in geothermal exploration. Geophys., **61**, 121-130.

Petrick, W. R., 2005. A new passive technique to monitor and discover agricultural groundwater resources. Industrial Imaging Co., Inc., Salt Lake city, UT 84103.

Porstendorfer, G., 1975. Principles of magnetotelluric prospecthig. Bomtraeger, Berlin.

Pous, J., Ledo, J., Marcuello, A., and Daignières, M., 2007. Electrical resistivity model of the crust and upper mantle from a magnetotelluric survey through the central Pyrenees. Geophys. J. Int., **121**, 750-762.

Press, W. H., Teukolsky, S. A., Vetterling W. T. and Flannery, B. P., 1993. Numerical recipes in FORTRAN: The art of scientific computing, second edition; in arrangement with Cambridge Univ. Press, Foundation Books, New Delhi, pp. 765-790.

Rao, I. B. R. R., Chary, M. V., and Mathur, R. R., 2003. EM studies over suspected seismic zones in peninsular India, Mem. Geol. Soc. .India, **54**, 23-42.

Rao, I. B. R. R., Nagendra, R., Rao, S. L. N., and Venkatramaiah , J., 2008. Very low frequency electromagnetic prospecting method-A few field applications in India. J. Earth Syst. Sci., **92**, 165-177.

Rastogi, A., 1997. A finite difference algorithm for two dimensional inversions of geoelectromagnetic data. Ph.D thesis, Indian Institute of Technology Roorkee, India.

Ray, S., 2011. Simulation of electromagnetic response of layered earth using exponential finite difference method; Master's thesis, Indian Institute of Technology-Roorkee, India.

Rikitake, T., 1966. Electromagnetism and the earth's interior. Elsevier, Amsterdam, pp. 308.

Smythe, W. R., 1950. Static and dynamic electricity. McGraw-Hill Book Co., Inc., Tokyo, pp. 616.

Stuntebeck, C., 2003. Three-dimensional electromagnetic modeling by free-decay mode superposition; Ph.D. Thesis, Technical University of Braunschweig, Germany.

Taflove, A., 1995. Computational electrodynamics: The finite-differentiation time-domain method. Artech House, Inc., Morwood, pp. 599.

Tyagi, D. K., 2007. 2D modeling and inversion of magnetotelluric data acquired in Garhwal Himalaya. Ph.D. thesis, Indian institute of Technology Roorkee, India.

Wait, J. R., 1982. Geo-Electromagnetism. Academic Press Inc., New York.

Wannamaker, P. E., 1991. Advances in three-dimensional magnetotelluric modeling using integral equations; Geophys., **56**, 1716 – 1728.

Ward, S. H., 1967. Electromagnetic theory for geophysical application. In: Mining Geophysics, Vol. II, Chap II, Part A, Soc. Expl. Geophys., Tulsa, Oklahoma, 10- 196.

Weaver, J. T., 1994. Mathematical methods for geo-electromagnetic induction; Research Studies Press Ltd., Taunton, Somerset, England.

Weaver, J. T. and Brewitt-Taylor, C. R., 1978. Improved boundary condition for the numerical solution of E-polarization problems in geomagnetic induction; Geophys. J. R. Astr. Soc., **54**, 309-317.

Wei, W., Martyn, U., Alan, J., John, B., Tan, H., Doug, N., Chen, L., Li, S., Kurt, S., Paul, B., Jin, S., Deng, M., Juanjo, L., David, K., and Brian, R., 2001. Detection of widespread fluids in the Tibetan crust by magnetotelluric studies. Sci., **292**, 716- 718.

Weitemeyer, K. A., Constable, S. C., Key, K. W., and Behrens, J. P., 2006. First results from a marine controlled-source electromagnetic survey to detect gas hydrates offshore Oregon. Geophys. Res. Lett., 33, L03304.

Young, D. M., 1950. Iterative methods for solving partial difference equations of elliptic type; Ph.D. thesis, Harvard University. Cambridge-USA.

Zhdanov, M. S., Varentsov, I. M., Weaver, J. T., Golubev, N. G., and Krylov, V. A., 1997. Methods for modeling electromagnetic fields results from COMMEMI – the international project on the comparison of modeling methods for electromagnetic induction; J. App. Geophys., 37, 133-271.

Zhou, P. B., 1993. Numerical analysis of electromagnetic fields. Springer-Verlag, pp. 406.